

Preparation for Implementation of the Mechanistic-Empirical Pavement Design Guide in Michigan

Part 1: HMA Mixture Characterization

ORBP Reference Number: ORBP OR10-022

FINAL REPORT RC-1593
The Michigan Department of Transportation
Office of Research and Best Practices
425 West Ottawa
Lansing, MI-48933

By

M. Emin Kutay, Ph.D., P.E.,
Co-Principal Investigator (Co-PI)
Assistant Professor

&

Anas Jamrah
Research Assistant

**Department of Civil & Environmental Engineering
Michigan State University**

March 2013

Technical Report Documentation Page

1. Report No. RC-1593		2. Government Accession No.		3. Recipient's Catalog No.	
4. Title and Subtitle Preparation for Implementation of the Mechanistic-Empirical Pavement Design Guide in Michigan: <i>Part 1-HMA Mixture Characterization</i>				5. Report Date March 31 st , 2013	
				6. Performing Organization Code	
7. Author(s) M. Emin Kutay and Anas Jamrah				8. Performing Organization Report No. ORBP OR10-022	
9. Performing Organization Name and Address Michigan State University 428 S. Shaw Ln., Rm. 3546 Engineering Building, East Lansing, MI 48824				10. Work Unit No. (TRAIS)	
				11. Contract or Grant No. ORBP OR10-022	
12. Sponsoring Agency Name and Address Michigan Department of Transportation Murray Van Wagoner Building 425 West Ottawa, P.O. Box 30050 Lansing, MI 48909				13. Type of Report and Period Covered Final Report 10/1/2011 – 12/31/2012	
				14. Sponsoring Agency Code	
15. Supplementary Notes					
16. Abstract This is the final report of the Part 1 (HMA Mixture Characterization) of the "Preparation for Implementation of the Mechanistic-Empirical Pavement Design Guide in Michigan" project. The main objectives of the Part 1 were (i) to conduct a literature search to determine the existing and past research on HMA mixture characterization for M-E PDG, (ii) review MDOT's HMA testing program, and (iii) laboratory testing of samples collected. Scope of the literature review included the past and on-going research on HMA characterization as a preparation for the M-E PDG (or DARWin-ME) as well as predictive models for some of the key inputs such as the Complex (Dynamic) Modulus ($ E^* $) mastercurve. Several regression-based $ E^* $ models were evaluated and calibrated for local asphalt mixtures in Michigan. In addition, an Artificial Neural Network (ANN) model has been developed for better prediction of $ E^* $ from asphalt volumetrics. The research team reviewed the current HMA test data available as part of the MDOT testing program and compared it with the test data required by the M-E PDG. In addition, an extensive laboratory testing program was conducted to characterize asphalt mixtures commonly used in Michigan for the Complex (Dynamic) Modulus $ E^* $, Complex Shear Modulus ($ G^* $) of binders and Indirect Tension Strength (IDT) at low temperatures. A standalone software, called DYNAMOD, was developed to serve as a database for all the material testing performed in this project. The DYNAMOD will allow engineers to easily reach the material testing data and generate input files that can directly be imported by the M-E PDG (or DARWin-ME).					
17. Key Word Hot mix asphalt, dynamic modulus, dynamic shear modulus, warm mix asphalt, flexible pavement, indirect tensile strength, creep compliance, DARWin-ME, M-E PDG			18. Distribution Statement No restrictions. This document is available to the public through the Michigan Department of Transportation		
19. Security Classif. (of this report) Unclassified		20. Security Classif. (of this page) Unclassified		21. No. of Pages 120	22. Price n/a

TABLE OF CONTENTS

LIST OF TABLES.....	6
LIST OF FIGURES.....	7
EXECUTIVE SUMMARY	10
INTRODUCTION.....	12
SCOPE AND OBJECTIVE.....	15
METHODOLOGY	16
DYNAMIC MODULUS ($ E^* $) MASTER CURVE OF ASPHALT MIXTURES	17
<i>Background on E^* Test</i>	<i>17</i>
<i>Relevance of E^* to DARWin-ME.....</i>	<i>19</i>
<i>Development of E^* Master Curve</i>	<i>21</i>
<i>Effect of E^* Master Curve on Fatigue and Rutting Predictions in DarWin-ME.....</i>	<i>23</i>
<i>Details of Laboratory E^* Tests.....</i>	<i>25</i>
DYNAMIC SHEAR MODULUS ($ G^* $) MASTER CURVE OF ASPHALT BINDERS.....	26
CREEP COMPLIANCE (D(T)) AND INDIRECT TENSILE STRENGTH OF MIXTURES	27
DISCUSSION OF RESULTS.....	30
TASK 1-1: “LITERATURE SEARCH TO DETERMINE WHAT EXISTING OR ON-GOING RESEARCH IS BEING DONE ON ASPHALT MIXTURE CHARACTERIZATION FOR M-E PDG”	30
<i>Flintsch et al. 2008 (“Asphalt materials characterization in support of the mechanistic- empirical pavement design guide implementation efforts in Virginia”)</i>	<i>30</i>
<i>Mohammad et al. (2007) (“Characterization of Louisiana Asphalt Mixtures Using Simple Performance Tests”)</i>	<i>32</i>
<i>Clyne et al. (2003) (“Dynamic and Resilient Modulus of MN DOT Asphalt Mixtures.”)</i>	<i>32</i>
<i>Birgisson et al. (2005) (“Evaluation of Predicted Dynamic Modulus for Florida Mixtures”)</i> ...	<i>33</i>

<i>Literature on E* Predictive Equations and Models</i>	35
TASK 1-2: “REVIEW MDOT'S HMA TESTING PROGRAM”	37
TASK 1-3: “IN CONSULTATION WITH THE RESEARCH ADVISORY PANEL (RAP), CHOOSE CONSTRUCTION PROJECTS THAT WILL ALLOW SAMPLING OF MIXTURES IN THE MATRIX DEVELOPED BY THE PRINCIPLE INVESTIGATOR”	39
TASK 1-4: “LABORATORY TESTING OF SAMPLES COLLECTED”	39
<i>Summary of E* values based on MDOT mix designation for each region</i>	43
<i>Comparison of variation in E* mastercurves based on MDOT mix designation</i>	43
<i>Summary of G* and phase angle of the binders</i>	48
<i>Summary of IDT Strength and D(t) values</i>	50
EVALUATION AND CALIBRATION OF THE WITCZAK’S EQUATION FOR MICHIGAN MIXTURES.....	52
VALIDATION OF THE CALIBRATED MODIFIED WITCZAK E* PREDICTIVE MODEL FOR MDOT MIXTURES	56
EVALUATION OF THE ANNACAP SOFTWARE FOR PREDICTING E* OF MDOT MIXTURES	57
DEVELOPMENT AND VALIDATION OF A NEW ANN-BASED E* PREDICTIVE MODEL TRAINED FOR MICHIGAN MIXTURES	58
<i>Structure of the ANN</i>	60
<i>Training the ANN</i>	62
DEVELOPMENT OF THE DYNAMOD SOFTWARE	65
CONCLUSIONS	68
RECOMMENDATIONS FOR FURTHER RESEARCH	70
RECCOMENDATIONS FOR IMPLEMENTATION	73
REFERENCES	75
APPENDIX A: DYNAMIC MODULUS (E*) PREDICTIVE EQUATIONS	80

ORIGINAL WITCZAK MODEL (ANDREI ET AL. 1999) - OW	80
MODIFIED WITCZAK MODEL (BARI 2005) - MW	80
HIRSCH MODEL (CHRISTENSEN ET AL. 2003) - HM	81
APPENDIX B: RELATIONSHIP BETWEEN ASPHALT BINDER GRADE AND VISCOSITY PARAMETERS.	83
APPENDIX C: A LIST OF ASPHALT MIXTURE SAMPLES PREPARED AND TESTED BETWEEN 10/ 1/11 & 12/31/12	84
APPENDIX D: E* MASTERCURVES OF THE MIXTURES GROUPED BASED ON THE MDOT MIX DESIGNATION	92
APPENDIX E: G* MASTER CURVES GROUPED BASED ON THE PG	100
APPENDIX F: DYNAMOD SOFTWARE TUTORIAL	105
STEP 1: CHOOSE A DATABASE	105
STEP 2: SELECT A REGION.....	106
E* DATABASE:.....	107
<i>Step 1: Select Mixture and View Corresponding Excel File.....</i>	<i>107</i>
<i>Step 2: Export Data as DARWin-ME Input.....</i>	<i>109</i>
<i>Step 3: E* Prediction.....</i>	<i>112</i>
G* DATABASE:	116
<i>Step 1: Select Asphalt Binder and View Corresponding Excel File</i>	<i>116</i>
<i>Step 2: Export Data as DARWin-ME Input.....</i>	<i>117</i>
D(T) & IDT STRENGTH DATABASE:.....	119

LIST OF TABLES

Table 1: Typical $ E^* $ results (in psi) at different temperatures and frequencies.....	19
Table 2: A and VTS values reported in Birgisson et al. (2005).....	34
Table 3: Parameters used in different $ E^* $ predictive models.....	35
Table 4: Level 1 analysis material inputs.	38
Table 5: Level 2 analysis material inputs.	38
Table 6: Level 3 analysis material inputs.	38
Table 7: $ E^* $ master curve coefficients obtained from laboratory measurements	41
Table 8: Summary of $ E^* $ values for different asphalt mixture types in North, Grand, Bay, Southwest and University Regions	44
Table 9: Summary of $ E^* $ values for different asphalt mixture types in Metro Region	45
Table 10: Summary of $ E^* $ values for different asphalt mixture types in Superior Region ...	46
Table 11: $ G^* $ master curve coefficients obtained from laboratory measurements.....	49
Table 12: IDT Strength values of all mixtures.....	50
Table 13: A typical D(t) data for an asphalt mixture (49B).....	52
Table 14: Comparison between coefficients used in the original and optimized models.....	56

LIST OF FIGURES

Figure 1: Illustration of a typical cyclic uniaxial load applied to a cylindrical asphalt sample and the resulting cyclic strain at temperature (T) = -10°C, frequency (f) = 10Hz. Note: $f = 1/\Delta t$ and one microstrain = 10^{-6} strain in the figure.	18
Figure 2: Illustration of an $ E^* $ test run at T = 21°C (69.8°F) and f = 10Hz.....	18
Figure 3: Illustration of DARWin-ME analysis periods.....	20
Figure 4: Illustration of shifting $ E^* $ data at different temperatures to obtain the $ E^* $ master curve: (a) Unshifted (original) $ E^* $ versus frequency graphs, (b) shifted $ E^* $ versus reduced frequency graph.	22
Figure 5: Shift factor (a(T)) coefficients at different temperatures for an asphalt mixture.	23
Figure 6: Illustration of an example computation of $ E^* $ at any T and f from given sigmoid and shift factor polynomial coefficients.	24
Figure 7: Illustration of two typical $ E^* $ mastercurves and expected fatigue and rutting performance trends for these $ E^* $ curves.	25
Figure 8: Asphalt Mixture Performance Tester (AMPT)	26
Figure 9: Illustration of dynamic shear rheometer (DSR)	28
Figure 10: Indirect tensile (IDT) strength test loading scheme and a picture of an asphalt sample after the test.	29

Figure 11: Dynamic Modulus mastercurves of all tested asphalt mixture specimens. The plot in log-log scale is to show the differences in low frequency/high temperature, and the linear-log scale is to show the differences in high frequency/low temperature). 40

Figure 12: $|E^*|$ mastercurves of four 3E3 mixtures, 3 of which (26* mixes) are from same region. NGBSU = North, Grand, Bay, Southwest and University Regions. 47

Figure 13: $|G^*|$ Master curves of four different PG64-28 binders. NGBSU = North, Grand, Bay, Southwest and University Regions..... 48

Figure 14: The modified Witczak’s equation developed as part of the NCHRP 1-40D. The plot shows the predicted versus measured values before calibration for MDOT mixtures. $S_e/S_y = 0.5084$, $R^2 = 0.7881$ (linear-linear plot), and $S_e/S_y = 0.446$, $R^2 = 0.8369$ (log-log plot). 54

Figure 15: The modified Witczak’s equation developed as part of the NCHRP 1-40D. The plot shows the predicted versus measured values after calibration for MDOT mixtures. $S_e/S_y = 0.3029$, $R^2 = 0.9248$ (linear-linear plot), and $S_e/S_y = 0.2053$, $R^2 = 0.965$ (log-log plot).... 55

Figure 16: The modified Witczak’s equation developed as part of the NCHRP 1-40D. The plot shows the predicted versus measured values for MDOT mixtures using the calibrated coefficients. $S_e/S_y = 0.3749$, $R^2 = 0.885$ (log-log plot)..... 57

Figure 17: Predicted versus measured values for MDOT mixtures using the ANNACAP software: (a) Linear-Linear plot, (b) Log-Log plot..... 58

Figure 18: Structure of the ANN model. 60

Figure 19: Errors versus the epochs in the ANN model developed in this project..... 63

Figure 20: Predicted versus measured $|E^*|$ values for Training, Validation and Testing datasets as well as all the data (for mixtures used during development of the model)..... 64

Figure 21: Predicted versus measured values for MDOT mixtures using the MSU-ANN model for mixtures not used during development of the model 65

Figure 22: Snapshot of the $|E^*|$ database in the DYNAMOD software developed by the research team 66

Figure 23: Snapshot of the $|G^*|$ database in the DYNAMOD software developed by the research team 67

Figure 24: Snapshot of the IDT database in the DYNAMOD software developed by the research team 67

Figure 25: WMA versus HMA for the same type of MDOT mixture (3E30)..... 71

Figure 26: WMA versus HMA for the same type of MDOT mixture (LVSP)..... 71

EXECUTIVE SUMMARY

This is the final report of the Part 1 (HMA Mixture Characterization) of the “Preparation for Implementation of the Mechanistic-Empirical Pavement Design Guide in Michigan” project. The main objectives of the Part 1 were (i) to conduct a literature search to determine the existing and past research on HMA mixture characterization for M-E PDG, (ii) review MDOT's HMA testing program, and (iii) laboratory testing of samples collected. Scope of the literature review included the past and on-going research on HMA characterization as a preparation for the M-E PDG (or DARWin-ME) as well as predictive models for some of the key inputs such as the Complex (Dynamic) Modulus ($|E^*|$) mastercurve. Several regression-based $|E^*|$ models were evaluated and calibrated for local asphalt mixtures in Michigan. In addition, an Artificial Neural Network (ANN) model has been developed for better prediction of $|E^*|$ from asphalt volumetrics. The research team reviewed the current HMA test data available as part of the MDOT testing program and compared it with the test data required by the M-E PDG. In addition, an extensive laboratory testing program was conducted to characterize asphalt mixtures commonly used in Michigan for the Complex (Dynamic) Modulus $|E^*|$, Complex Shear Modulus ($|G^*|$) of binders and Indirect Tension Strength (IDT) at low temperatures. A standalone software, called DYNAMOD, was developed to serve as a database for all the material testing performed in this project. The DYNAMOD will allow engineers to easily reach the material testing data and generate input files that can directly be imported by the M-E PDG (or DARWin-ME).

Typically, at design stage, asphalt mixtures are selected based on the MDOT mix designation (e.g., 4E1, 3E03 etc.) and binder PG (e.g., PG70-22). If the selected MDOT mix designation and the binder PG have been tested as part of this research, the laboratory data in

the DYNAMOD software should be exported and used in DARWin-ME analysis as Level 1 input. If there are more than one mixture tested for a given MDOT mix designation, it is recommended to choose an $|E^*|$ that will result in the least conservative predictions of fatigue cracking and rutting.

If measured $|E^*|$ data is not available in the DYNAMOD software for the given MDOT designation and PG, it is recommended that the designer should use either locally calibrated Modified Witczak or the ANN model to predict the $|E^*|$ and use as Level 1 input in DARWin-ME. Both of these models are available in the DYNAMOD software. The ANN model, in general, is more accurate than the locally calibrated Modified Witczak model.

There are no predictive equations for $|G^*|$ master curve, therefore, this parameter needs to be measured in the laboratory if the data is not available in the DYNAMOD database. The same is true for the IDT strength as well as the $D(t)$ values. If testing is not possible, the closest green shaded mixture in the DYNAMOD may be selected and used in DARWin-ME as Level 1 material input.

INTRODUCTION

The DARWin-ME, an AASHTOWare® pavement design software that is based on the AASHTO's Mechanistic-Empirical Pavement Design Guide (M-E PDG), allows engineers to perform the design based on prediction of distresses over time. The software utilizes semi-mechanistic and semi-empirical models to predict the distresses such as fatigue cracking, rutting and thermal cracking in asphalt pavements. A number of different material inputs are required by the DARWin-ME, and accurate measurement of these inputs (especially the mixture $|E^*|$ and the binder $|G^*|$) is crucial for the accuracy of the DARWin-ME distress predictions. Many State Departments of Transportation (DOTs) (including the Michigan Department of Transportation (MDOT)) do not have a testing program to measure certain key inputs required by the DARWin-ME. The Part 1 of this project addresses the need for generating a catalog of input variables for typical asphalt mixtures used in Michigan (MI).

In flexible (asphalt) pavement design, the most important and hard-to-obtain material inputs for the Level 1 analysis are: (i) complex (dynamic) modulus ($|E^*|$) master curve of asphalt mixture, (ii) complex (dynamic) shear modulus ($|G^*|$) master curve of asphalt binder, (iii) Indirect Tensile (IDT) Strength and creep compliance ($D(t)$) of the asphalt mixture. The $|E^*|$ master curve is a unique material property that captures the dependency of the asphalt mixture on temperature and loading rate at low strain level. Past research indicated that, even though $|E^*|$ represents the linear viscoelastic property of asphalt mixture at low strain levels, it is related to the pavement performance, specifically the rutting and fatigue cracking. This is because relatively large $|E^*|$ values at high temperatures (and slow loading rates) leads to rut-resistant mixtures, whereas relatively low $|E^*|$ values at intermediate and low

temperatures (and fast loading rates) leads to fatigue-resistant asphalt mixtures. The $|G^*|$ master curve, which defines the linear viscoelastic property of an asphalt binder, is required by both Level 1 and Level 2 analyses of DARWin-ME. In Level 1 analysis, $|G^*|$ is primarily used in asphalt aging models, whereas in Level 2, it is used in both aging models and in predicting the $|E^*|$ master curve of the asphalt mixture using Witzak's predictive equation. It is noted that Witzak's equation predicts the $|E^*|$ of the mixture from the binder $|G^*|$ as well as mixture volumetrics such as the aggregate gradation, binder content etc. Level 3 analysis in DARWin-ME does not require testing of $|E^*|$ and $|G^*|$ and uses typical values based on the binder performance grade (PG). However, in all levels (Levels 1, 2 and 3), thermal cracking prediction model requires the IDT strength as well as $D(t)$ values.

The overall goal of this project is to prepare the MDOT for implementation of DARWin-ME pavement design software. In order to achieve this goal, this project has been divided into three major (semi-independent) parts:

Part 1: HMA Mixture Characterization

Part 2: Evaluation of Rehabilitation Fixes

Part 3: Local Calibration and Validation of the M-E PDG Performance Models for Michigan Conditions

This report is the final report of the *Part 1: HMA Mixture Characterization*, which is composed of the following four basic tasks:

TASK 1-1: Literature search to determine what existing or on-going research is being done on asphalt mixture characterization for M-E PDG.

TASK 1-2: Review MDOT's asphalt mixture testing program.

TASK 1-3: In consultation with the Research Advisory Panel (RAP), choose construction projects that will allow sampling of mixtures in the matrix developed by the principle investigator.

TASK 1-4: Laboratory testing of samples collected.

All of these tasks have been completed and the results are presented in the sections below.

SCOPE AND OBJECTIVE

The main objectives of the *Part 1: HMA Mixture Characterization* are to (i) conduct a literature search to determine the existing and past research on asphalt mixture characterization for M-E PDG, (ii) review MDOT's asphalt mixture testing program, and (iii) laboratory testing of samples collected by MDOT, which includes tests to determine asphalt mixture $|E^*|$ mastercurve, asphalt binder $|G^*|$ mastercurve and asphalt mixture indirect tensile strength (IDT) of typical asphalt mixtures and binders used in Michigan.

METHODOLOGY

As part of Task 1-1, the research team conducted a literature review and summarized the findings that are closely related to this project in the “Discussion of Results” section. Task 1-2 included review of the MDOT’s asphalt mixture testing program. The research team communicated with MDOT engineers to determine the types of available data collected by MDOT and the ones that are not available but required by the DARWin-ME software. Under Task 1-3, the research team continuously communicated with the MDOT project manager regarding the selection of asphalt pavement construction projects and asphalt sampling.

The Task 1-4, which constituted the majority of this part of the project, included material testing to determine the following parameters:

- Asphalt mixture $|E^*|$ master curve
- Asphalt binder $|G^*|$ master curve
- Asphalt mixture indirect tensile strength (IDT) at -10°C
- Asphalt mixture creep compliance master curve

All asphalt mixture and binder tests were conducted at the AASHTO certified Advanced Asphalt Characterization Laboratory (AACL) located at the Michigan State University (MSU) campus. A brief description of the test methodologies and parameters obtained are provided below.

Dynamic Modulus ($|E^*|$) Master Curve of Asphalt Mixtures

Background on $|E^*|$ Test

The dynamic modulus ($|E^*|$) test is conducted by applying a compressive haversine stress to a cylindrical 100 mm diameter, 150 mm tall sample. The resulting strain is measured by mounting a set of LVDTs (Linear Variable Differential Transformer) on the specimen. A haversine is actually a sinusoidal function where the minimum value is zero and maximum value is twice the amplitude. When an asphalt sample is subjected to a cyclic haversine stress, the resulting strain response will also be haversine as shown in Figure 1. The $|E^*|$ is defined as:

$$|E^*| = \frac{\sigma_{peak}}{\varepsilon_{peak}} \quad [1]$$

where σ_{peak} and ε_{peak} are the peak stress and strain, respectively.

In Figure 1, the $\sigma_{peak} = 100 \text{psi}$ and $\varepsilon_{peak} = 37.7 \times 10^{-6}$, as a result, the dynamic modulus is $|E^*| = \frac{100 \text{psi}}{37.7 \times 10^{-6}} = 2,652,519 \text{psi}$. This $|E^*|$ corresponds to the testing temperature of $T = -10^\circ\text{C}$ (14°F) and load frequency of $f = 1/0.1 = 10 \text{Hz}$. Asphalt mixtures have different $|E^*|$ values at different temperatures (T) and loading frequencies (f). The $|E^*|$ increases with increasing frequency and decreases with increasing temperature. Figure 2 shows the result of another $|E^*|$ test run at $T = 21^\circ\text{C}$ (69.8°F) and $f = 10 \text{Hz}$. In this case, the $\sigma_{peak} = 100 \text{psi}$ and $\varepsilon_{peak} = 92 \times 10^{-6}$, as a result, $|E^*| = \frac{100 \text{psi}}{92 \times 10^{-6}} = 1,086,956 \text{psi}$. The only difference between the test in Figure 1 and the test in Figure 2 is the temperature. Because of an increase in temperature from -10°C to 21°C , the $|E^*|$ decreased from 2,652,519 psi to 1,089,956 psi.

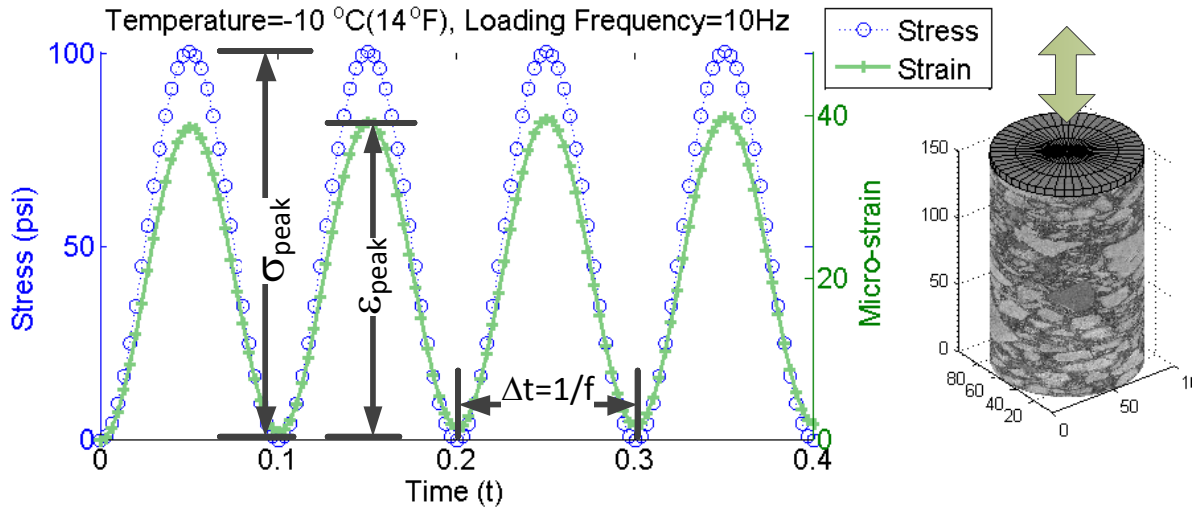


Figure 1: Illustration of a typical cyclic uniaxial load applied to a cylindrical asphalt sample and the resulting cyclic strain at temperature (T) = -10°C, frequency (f) = 10Hz. Note: $f = 1/\Delta t$ and one microstrain = 10^{-6} strain in the figure.

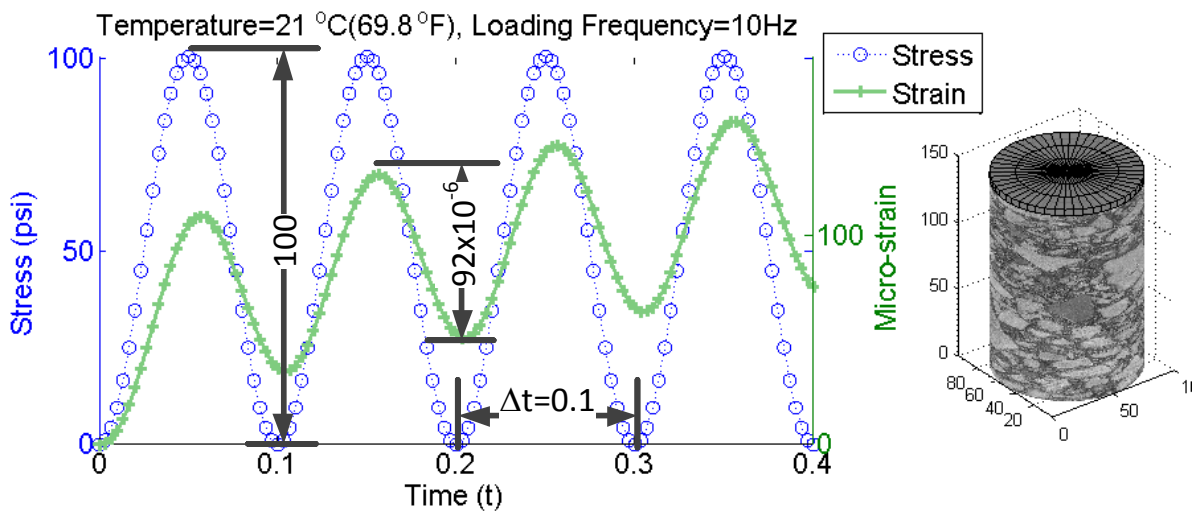


Figure 2: Illustration of an $|E^*|$ test run at T = 21°C (69.8°F) and f = 10Hz.

Table 1 shows typical values of measured $|E^*|$ at different temperatures and frequencies. As shown, the $|E^*|$ decreases from left to right (as the frequency decreases) and also decreases from top to bottom (as the temperature increases). It should be noted that the $|E^*|$ represents the linear viscoelastic behavior of asphalt mixtures and only applicable to strain levels less than 100-120 microstrain, which is known as the endurance limit. At higher strain levels, plastic deformation and microcracking initiates and propagates. Plastic

deformation occurs at high temperatures (40-70°C), whereas microcracking initiates at intermediate (10-25°C) and low (less than 0°C) temperatures.

Table 1: Typical $|E^*|$ results (in psi) at different temperatures and frequencies.

$f =$ T	25.0 (Hz)	10.0 (Hz)	5.0 (Hz)	1.0 (Hz)	0.5 (Hz)	0.1 (Hz)
-10°C (14°F)	2,843,832	2,645,138	2,483,212	2,107,692	1,926,125	1,521,432
4°C (39.2°F)	1,798,597	1,586,551	1,432,221	1,104,741	977,068	715,868
21°C (69.8°F)	814,804	661,055	557,765	363,522	302,612	186,889
37°C (98.6°F)	305,443	234,107	187,083	110,073	90,392	56,923
54°C (129.2°F)	103,406	76,047	59,105	36,947	32,845	25,491

Relevance of $|E^*|$ to DARWin-ME

The $|E^*|$ is one of the main parameters used in bottom-up, top-down fatigue cracking models as well as in the rutting model in DARWin-ME. The DARWin-ME divides the pavement structure into sublayers and divides the analysis period (i.e., the performance prediction period) into 1 month intervals (see Figure 3). Then for each period:

- 1) The Enhanced Integrated Climatic Model (EICM) predicts the temperature variation with depth for each sublayer.
- 2) An equivalent frequency is chosen based on the traffic speed, type of road facility (interstate, urban street etc.) and depth of each sublayer.
- 3) From the temperature and frequency (steps 1 and 2 above), an $|E^*|$ is selected/computed and used as elastic modulus $E = |E^*|$ in a layered elastic pavement model called JULEA.
- 4) In the bottom-up fatigue cracking model, JULEA predicts the tensile strain at the base of the asphalt and uses it in an MS-1 model to predict the number of cycles to failure

(N_f) for the given analysis period. Then this N_f is used in Miner's damage accumulation law to predict the damage because of bottom-up fatigue cracking.

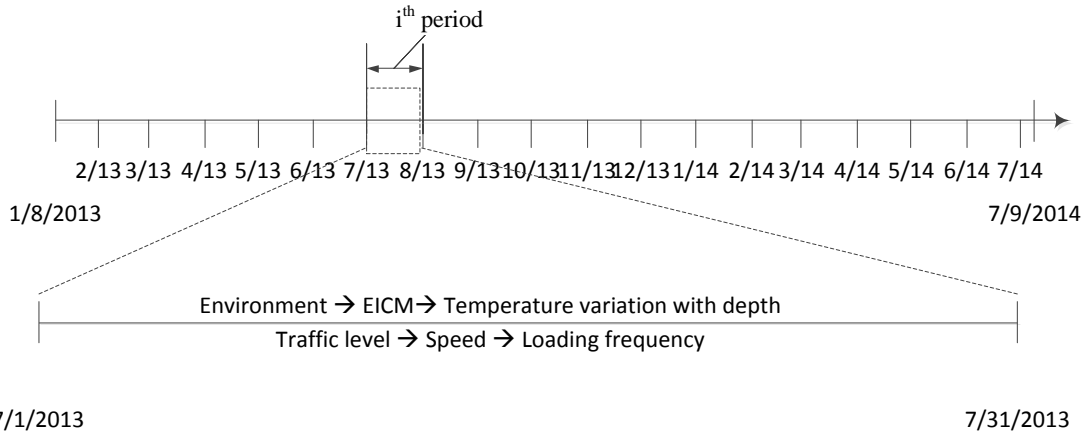


Figure 3: Illustration of DARWin-ME analysis periods.

- 5) In the top-down fatigue cracking model, JULEA predicts the tensile strain at the edge of the tire and uses it in another MS-1 type empirical model to predict the number of cycles to failure (N_f) for the given analysis period. Then this N_f is used in Miner's damage accumulation law to predict the damage because of top-down fatigue cracking.
- 6) In the rutting model, the resilient strain of the material is predicted by JULEA and used in the empirical rutting model, along with the temperature and number of load repetitions.

The detailed description of JULEA, MS-1, Miner's law and rutting models mentioned above can be found in the DARWin-ME (or MEPDG) documentation, therefore, they will not be repeated here for brevity. One important relevant issue is the computation of the $|E^*|$ value in step 3 above for any given temperature and frequency. The DARWin-ME does not interpolate using the $|E^*|$ table input (which is similar to Table 1). Instead, it uses

the time-temperature superposition (TTS) principle to develop the $|E^*|$ master curve, which results in a sigmoid shaped curve where $|E^*|$ at any temperature and frequency combination can be computed. The next section describes how to develop an $|E^*|$ master curve and how it can be used to compute $|E^*|$ at a given temperature and frequency.

Development of $|E^*|$ Master Curve

Once $|E^*|$ values are measured at different temperatures (T) and loading frequencies (f), the $|E^*|$ master curve is obtained using the time-temperature superposition (TTS) principle (Kim 2009). Figure 4a shows a graph of $|E^*|$ values at different temperatures and frequencies that is generated from raw $|E^*|$ data similar to the one shown in Table 1. Based on the TTS principle, a single $|E^*|$ master curve can be obtained by shifting the $|E^*|$ data obtained at different temperatures horizontally as shown in Figure 4b. Once shifted, the parameter in x-axis is called reduced frequency (f_R), which is defined as follows:

$$f_R = f a_T(T) \quad [2]$$

where f is the frequency of the load and $a_T(T)$ is the shift factor coefficient for a given temperature T. As shown Figure 4b, the shift factor coefficient ($a_T(T)$), i.e., the amount of horizontal shift for each temperature is different. During shifting process, the shift factors at each temperature are varied until a good sigmoid fit to the $|E^*|$ data of all temperatures is obtained. Typically the following sigmoid function is used:

$$\log(|E^*|) = b_1 + \frac{b_2}{1 + \exp(-b_3 - b_4 \log(f_R))} \quad [3]$$

where b_1 , b_2 , b_3 and b_4 are the sigmoid coefficients, f_R is the reduced frequency.

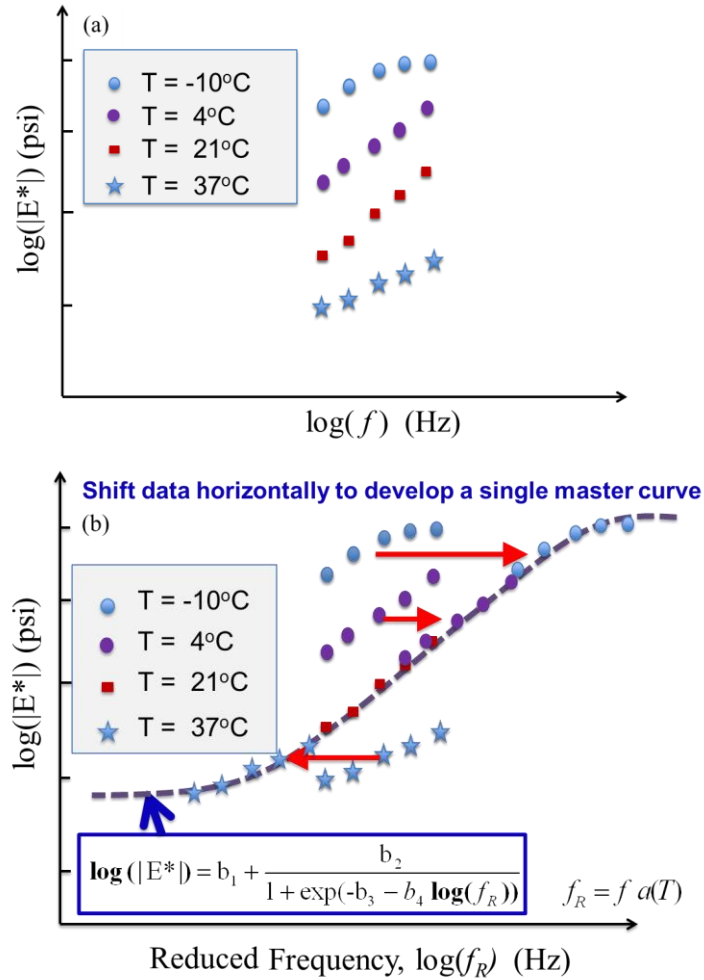


Figure 4: Illustration of shifting $|E^*|$ data at different temperatures to obtain the $|E^*|$ master curve: (a) Unshifted (original) $|E^*|$ versus frequency graphs, (b) shifted $|E^*|$ versus reduced frequency graph.

It is noted that while generation of the master curve, $|E^*|$ data at one of the temperatures is not shifted and this temperature is called reference temperature (T_{ref}). This means that shift factor coefficient for T_{ref} is equal to unity (i.e., $a_T(T=T_{\text{ref}}) = 1$). After the shifting is completed and the shift factor coefficients ($a_T(T)$) are determined, they are plotted against each temperature (T) as shown in Figure 5. Then a second order polynomial is fitted to the data as shown in Figure 5b to obtain the polynomial coefficients a_1 and a_2 in the following equation:

$$a_T(T) = 10^{a_1(T^2 - T_{ref}^2) + a_2(T - T_{ref})} \quad [4]$$

where T_{ref} is the reference temperature.

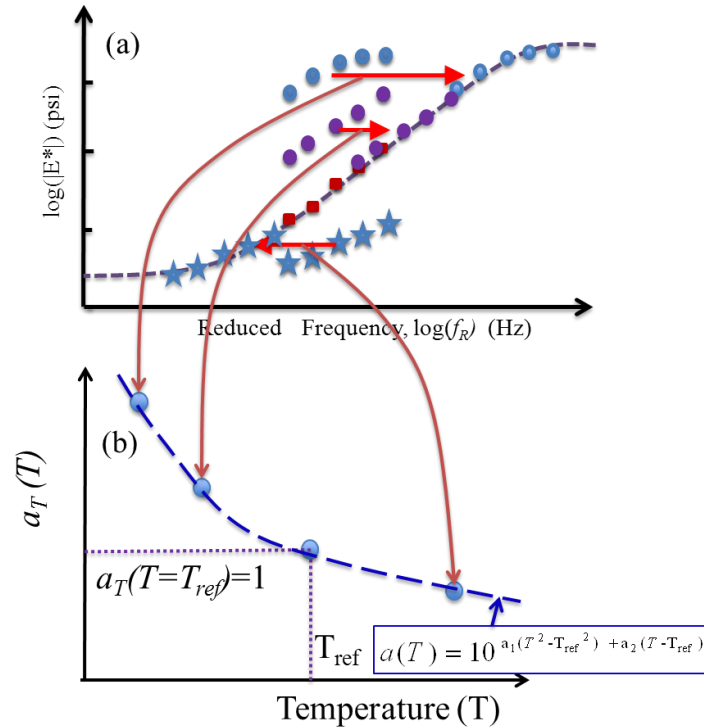


Figure 5: Shift factor ($a(T)$) coefficients at different temperatures for an asphalt mixture.

Development of $|E^*|$ master curve is very useful because once $b_1, b_2, b_3, b_4, a_1, a_2$ and T_{ref} are known, $|E^*|$ at any temperature (T) and frequency (f) can be computed. Figure 6 illustrates an example computation of $|E^*|$ at any T and f from given sigmoid coefficients (i.e., b_1, b_2, b_3 and b_4) and shift factor polynomial coefficients (i.e., a_1, a_2 and T_{ref}).

Effect of $|E^*|$ Master Curve on Fatigue and Rutting Predictions in DarWin-ME

Figure 7 illustrates two typical $|E^*|$ master curves labeled as Mix-A and Mix-B. In a $|E^*|$ master curve graph, the left side of the graph corresponds to high temperature and low frequency, whereas the right side of the graph corresponds to low temperature and high

frequency, as illustrated in Figure 7. Typically, better fatigue resistance is expected if the $|E^*|$ curve is relatively low on the right side of the curve. Conversely, better rutting resistance is expected if the $|E^*|$ curve is relatively high in the left side of the curve. In Figure 7, Mix-A is typically expected to perform better in both rutting and fatigue resistance as compared to Mix-B. The middle of the $|E^*|$ master curve, for most mixtures, corresponds to 21°C (~70°F) at 0.1 Hz. Therefore, relatively low temperatures (right side of the vertical dashed line in the middle of the curves in Figure 7) corresponds to temperatures less than 70°F, and the left side is the temperatures higher than 70°F. It should be noted that this mid point (i.e., median temperature) can be slightly different for different mixtures.

Question: What is $|E^*|$ at $T = 17.5^\circ\text{C}$ and $f=8.4\text{Hz}$, given the following coefficients: $a_1 = 4.61\text{E-}04$, $a_2 = -0.135$, $b_1=1.07$, $b_2=3.42$, $b_3=1.32$, $b_4 = 0.43$ and $T_{\text{ref}} = 21^\circ\text{C}$? Note that the sigmoid coefficients will result in $|E^*|$ in MPa.

Solution:

→ Step 1: Calculate shift factor coefficient for $T = 17.5\text{C}$:

$$a_T(17.5) = 10^{a_1(T^2 - T_{\text{ref}}^2) + a_2(T - T_{\text{ref}})} = 10^{4.61\text{E-}04(17.5^2 - 21^2) + (-0.135)(17.5 - 21)} = 2.57$$

→ Step 2: Calculate the reduced frequency:

$$f_R = f * a_T(T=17.5) = 8.4 * 2.57 = 21.6 \text{ Hz}$$

→ Step 3: Calculate the $|E^*|$ using the sigmoid function:

$$|E^*| = 10^{\left(\frac{b_1 + \frac{b_2}{1 + \exp(-b_3 - b_4 \log(f_R))}} \right)} = 10^{\left(\frac{1.07 + \frac{3.42}{1 + \exp(-1.32 - 0.43 \log(21.6))}} \right)} = 11,031.4 \text{ MPa}$$

$$|E^*| = 11,031.4 \text{ MPa} = 1,601,069.9 \text{ psi}$$

Figure 6: Illustration of an example computation of $|E^*|$ at any T and f from given sigmoid and shift factor polynomial coefficients.

It should be noted that very soft mixes may not lead to better fatigue resistance. The fatigue resistance, in addition to the $|E^*|$, is also related to the tensile strain at the base of the pavement structure being analyzed. Therefore, excessively soft asphalt mixtures may lead to excessive tensile strain at the base of the asphalt layer, which can cancel out the beneficial effect of low $|E^*|$ (see MS-1 model in the MEPDG documentation).

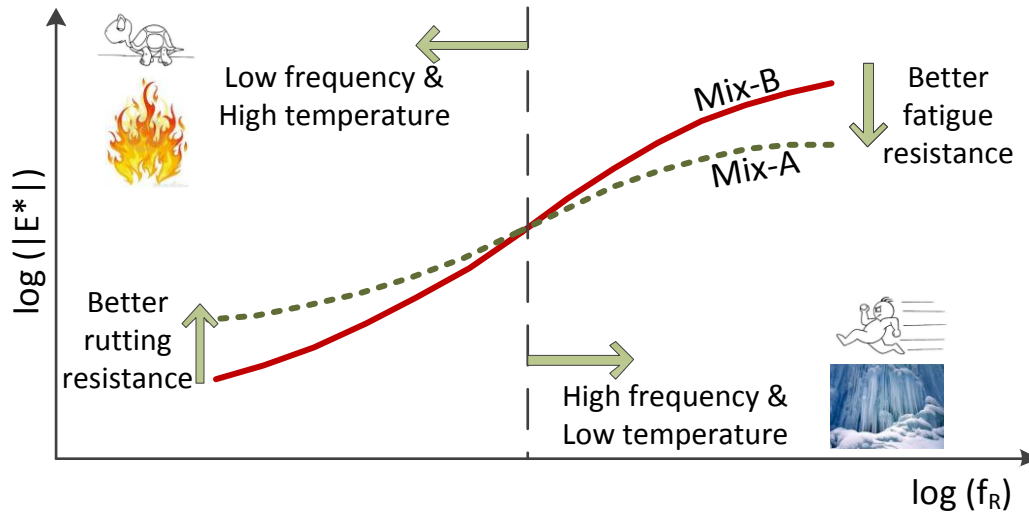


Figure 7: Illustration of two typical $|E^*|$ mastercurves and expected fatigue and rutting performance trends for these $|E^*|$ curves.

Details of Laboratory $|E^*|$ Tests

Figure 8 shows a picture of the Asphalt Mixture Performance Tester (AMPT) equipment used in this project while testing the asphalt mixtures for $|E^*|$. All samples were prepared in accordance with AASHTO PP60 “Preparation of Cylindrical Performance Test Specimens Using the Superpave Gyrotory Compactor (SGC)”. The air voids of all samples tested were within the range of $7\% \pm 0.5\%$, which is the recommended range of air voids for most performance tests in AASHTO specifications. This air void level is typically the median air void level expected in the field right after the construction. Running the $|E^*|$ experiments at different air void levels may lead to different $|E^*|$ values, but, such investigation was not within the scope of this study. It should be noted that the research team did run very limited $|E^*|$ tests at lower air void levels, which resulted in very similar $|E^*|$ values as compared to the $|E^*|$ values of the samples compacted to 7% air voids. A complete list of air voids of all mixtures tested in this study is given in Appendix C.

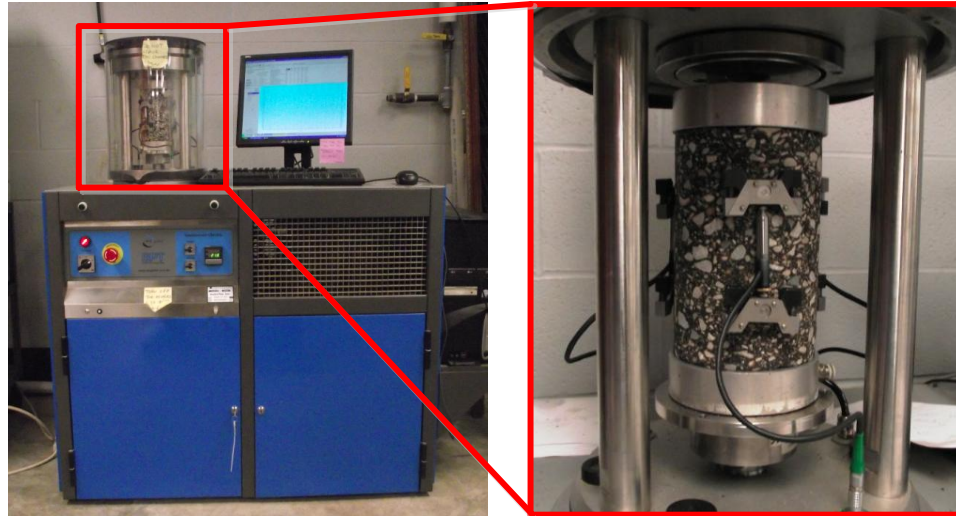


Figure 8: Asphalt Mixture Performance Tester (AMPT)

The $|E^*|$ tests were conducted in accordance with AASHTO T342 “Determining Dynamic Modulus Mastercurve of Hot Mix Asphalt (HMA)”. The tests were conducted at temperatures of -10, 10, 21, 37 and 54 degrees C. At each temperature, tests were run at frequencies of 25, 10, 5, 1, 0.5 and 0.1 Hz. The entire series of temperatures and frequencies were run on 3 different gyratory compacted samples. The average of the 3 replicates was used to develop the mastercurve. A detailed explanation of determination of $|E^*|$ master curves from the laboratory data can be found in AASHTO PP62-10 “Developing Dynamic Modulus Mastercurves for Hot Mix Asphalt (HMA)”.

Dynamic Shear Modulus ($|G^*|$) Master Curve of Asphalt Binders

The dynamic shear modulus ($|G^*|$) is a parameter that defines the stress-strain relationship of asphalt binders when they are subjected to cyclic shear load. The $|G^*|$ is measured using the Dynamic Shear Rheometer (DSR) shown in Figure 9. The $|G^*|$ is defined as:

$$|G^*| = \frac{\tau^{peak}}{\gamma^{peak}} \quad [5]$$

where τ^{peak} and γ^{peak} are peak shear stress and strain, respectively (see Figure 9). The $|G^*|$ is conducted at various loading frequencies and temperatures similar to the $|E^*|$, with the exception that the load is applied in shear mode (circular-torque load). The steps in generating the $|G^*|$ master curve is identical to the steps described in the previous section for $|E^*|$ master curve. Because of the strong relationship between the $|G^*|$ and $|E^*|$, Levels 2 and 3 in DARWin-ME utilize the $|G^*|$ mastercurve (along with other inputs) to predict the $|E^*|$ mastercurve. Level 1 analysis in DARWin-ME also requires $|G^*|$ as input, because $|G^*|$ is used to compute the viscosity-temperature relationship (a.k.a. A-VTS relationship) of the binder. The A-VTS relationship is needed in the global aging system model of DARWin-ME to predict the aging of the asphalt mixture over time.

Creep Compliance (D(t)) and Indirect Tensile Strength of Mixtures

The creep compliance (D(t)) and the Indirect Tensile (IDT) Strength of the asphalt mixtures are needed in DARWin-ME for prediction of thermal cracking in all 3 analysis levels. Typically AASHTO T 322 “Determining the Creep Compliance and Strength of Hot-Mix Asphalt (HMA) Using the Indirect Tensile Test Device” is used to measure both D(t) and IDT strength of the mixtures. Since D(t) is a linear viscoelastic property of the asphalt mixture, it can be mathematically computed from the $|E^*|$ master curve (Park and Shapery 1999). In this project, the D(t) values were computed using the interconversion procedure described by Park and Shapery (1999).

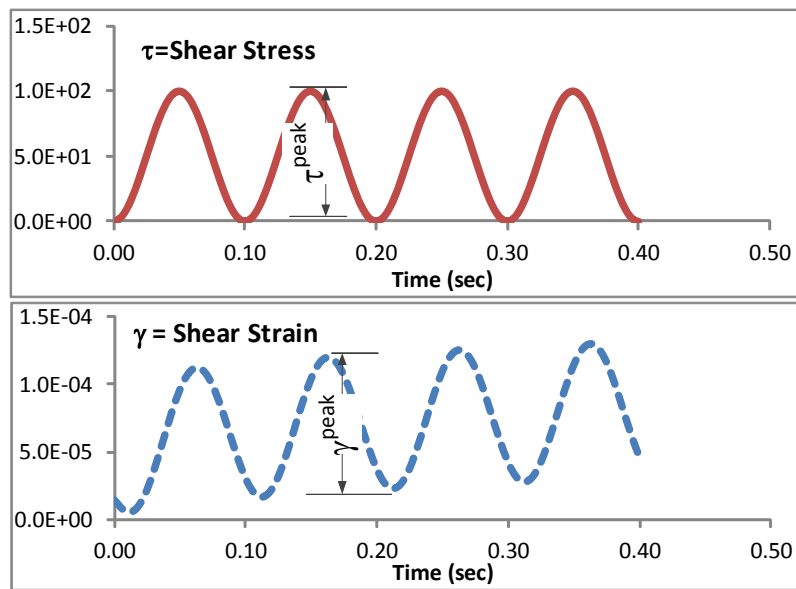
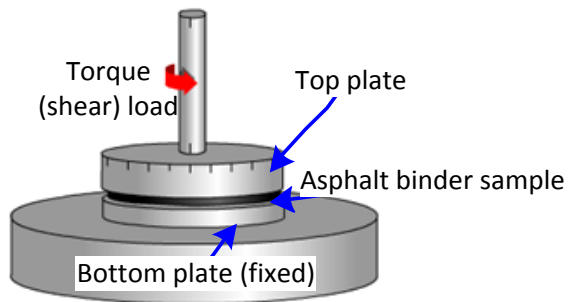


Figure 9: Illustration of dynamic shear rheometer (DSR)

The IDT strength tests were conducted at -10°C by applying a monotonic displacement controlled load along the diameter of a cylindrical sample (see Figure 10) at a rate of 12.5 mm per minute. Samples had a diameter of 150 mm and typically 37 mm thick. The maximum load before sample failure is used to calculate the IDT strength of the asphalt

mixture. The maximum tensile stress (i.e., IDT strength) is computed using the following formula:

$$\sigma_s = \frac{2P}{\pi D t_s} \quad [6]$$

where σ_s = IDT strength (kPa), P =applied load (kN), D =diameter of the sample (m), t_s =thickness of the sample (m). Figure 10 shows the indirect tensile (IDT) strength test loading scheme and a picture of an asphalt sample after the test.

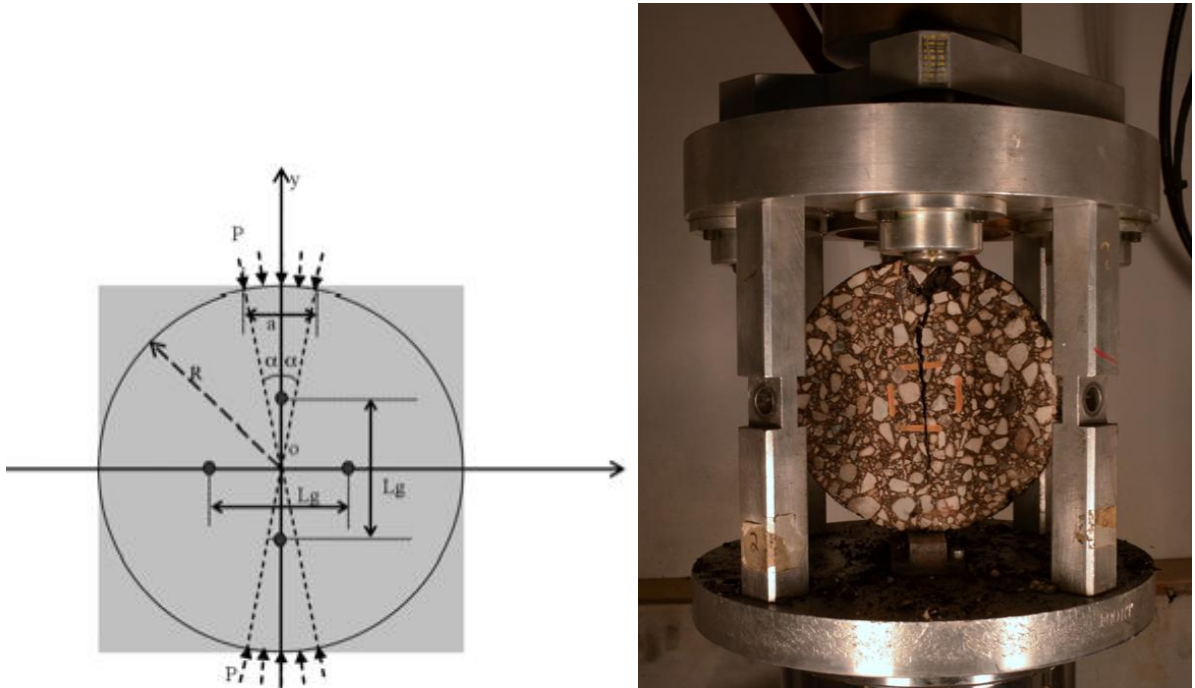


Figure 10: Indirect tensile (IDT) strength test loading scheme and a picture of an asphalt sample after the test.

DISCUSSION OF RESULTS

TASK 1-1: “Literature search to determine what existing or on-going research is being done on asphalt mixture characterization for M-E PDG”

After inception of M-E PDG, several States conducted asphalt mixture characterization studies in support of M-E PDG (Flintsch et al. 2008, Mohammad 2010, Clyne et al. 2003, Flintsch et al. 2005, Birgisson et al. 2005). The key objective of these studies was to obtain the fundamental material characteristics of asphalt mixtures that are required by the M-E PDG software. A summary of the literature on these efforts has been included in the subsections below. In addition, a literature review on $|E^*|$ predictive equations/models has also been conducted. It is important to evaluate existing $|E^*|$ predictive models using the data generated as part of this project for the Michigan mixtures and, if necessary, re-calibrate these models such that their accuracy is improved. An improved $|E^*|$ predictive equation may be needed to better predict the $|E^*|$ values of asphalt mixtures to be used by MDOT in the future, if $|E^*|$ of a similar mixture is not available in the database that is produced in this research.

Flintsch et al. 2008 (“Asphalt materials characterization in support of the mechanistic-empirical pavement design guide implementation efforts in Virginia”)

The testing program of this project included the dynamic modulus ($|E^*|$) as well as creep compliance and tensile strength parameters, which are needed to predict thermal cracking in M-E PDG. A total of 11 different asphalt mixture types were tested. All mixtures had the same binder, whose performance grade was PG 64-22. They concluded that $|E^*|$ of the mixtures in VA is sensitive to the constituent properties of asphalt mixture (aggregate type, asphalt content, percentage of recycled asphalt pavement, etc.). They also found that M-

E PDG's level 2 $|E^*|$ prediction equation reasonably estimated the measured dynamic modulus; however, it did not capture some of the differences between the mixes as found in the measured data. They used the Original Witzcak's (OW) equation (which is based on the viscosity of asphalt binder) to predict $|E^*|$ and compared it to their measurements (please see Appendix A for the OW equation). The authors did not measure viscosity values at different temperatures; instead, they used the following empirical equation to calculate the viscosity at different temperatures:

$$\log \log(\eta) = A + VTS \log(T_R) \quad [7]$$

where:

- η = Viscosity (cP).
- A = Intercept of temperature susceptibility relationship.
- VTS = Slope of temperature susceptibility relationship.
- T_R = Temperature in Rankine.

They used typical A and VTS constants from the M-E PDG table (please see Appendix B) for the PG 64-22 binder (M-E PDG 2007). Once A and VTS values are known, $|G^*|$ and phase angle can be computed using following empirical formula developed by Bari and Witzcak (2006):

$$|G^*|_b = 0.0051 f_s n_{f_s, T} (\sin \delta_b)^{7.1542 - 0.4929 f_s + 0.0211 f_s^2} \quad [8]$$

$$\delta_b = 90 + (-7.3146 - 2.6162 * VTS) * \log(f_s * \eta_{f_s, T}) + (0.1124 + 0.2029 * VTS) * \log(f_s * \eta_{f_s, T})^2 \quad [9]$$

$$\log \log \eta_{f_s, T} = 0.9699 f_s^{-0.0527} * A + 0.9668 f_s^{-0.0575} * VTS \log T_R \quad [10]$$

where:

f_s = Dynamic shear frequency.

δ_b = Binder phase angle (degrees).

$\eta_{f_s, T}$ = Viscosity of asphalt binder at a particular loading frequency (f_s) and temperature (T) (centipoise).

T_R = Temperature in Rankine scale.

Mohammad et al. (2007) (“Characterization of Louisiana Asphalt Mixtures Using Simple Performance Tests”)

In support of M-E PDG implementation in Louisiana, Mohammad et al. (2007) conducted $|E^*|$ tests on 13 different asphalt mixture types. They evaluated the Witczak and Hirsch models and found that predictions of the dynamic modulus $|E^*|$ values were reasonable. They indicated that the Witczak model reliability increases for higher Nominal Maximum Aggregate Size (NMAS), whereas the Hirsch model reliability increases for lower NMAS. They did not specify how they determined the viscosity or $|G^*|$ /phase angle values for binder for use in Witczak’s or Hirsch models.

Clyne et al. (2003) (“Dynamic and Resilient Modulus of MN DOT Asphalt Mixtures.”)

This project represented the results of laboratory testing to determine the complex modulus and phase angle of asphalt mixtures in Minnesota (MN). Laboratory tests were performed on four different asphalt mixtures from the MnROAD site. $|E^*|$ and phase angle vs. frequency mastercurves generated from the test data were compared to results obtained from Witczak’s predictive equations. The modulus values calculated using the Original Witczak’s (OW) predictive equation provided a reasonable prediction of the dynamic modulus for only two of the four mixtures evaluated. It was stated that the 2000 predictive

equation should be used with caution. However, smooth master curves for phase angle could not be obtained, and use of the same shift factors as for the complex modulus master curves did not result in smooth master curves for the phase angle. Authors also indicated that sample preparation techniques affect the results of dynamic modulus testing. The recommended procedure (NCHRP 9-29) of coring and cutting test specimens led to a lower modulus than that of specimens compacted directly to size for the mixture investigated. Authors indicated that the potential reason for this is that the cored specimens likely had rather uniform air voids throughout the specimen. The compacted specimens probably contained density gradients axially and radially throughout the specimens.

Birgisson et al. (2005) ("Evaluation of Predicted Dynamic Modulus for Florida Mixtures")

This project presented the results of a study by the Florida Department of Transportation and the University of Florida that focused on the evaluation of the dynamic modulus predictive equation used in the new AASHTO 2002 Guide (Witczak's predictive modulus equation) for mixtures typical to Florida. The resulting research program consisted of dynamic modulus testing of 28 mixtures common to Florida. The results showed that the predictive modulus equation used appeared (on the average) to work well for Florida mixtures, when used with a multiplier to account for the uniqueness of local mixtures. The results of the study also identified optimal viscosity-temperature relationships that result in the closest correspondence between measured and predicted dynamic modulus values. The authors developed regression relationships that can be used to correct the predicted modulus values on the average (Table 2). It was found that the dynamic modulus predictions using input viscosities obtained from dynamic shear rheometer test results were lower than the

measured values. Hence, consistent with the recommendations by Witzcak et al. (2002), if the user wants to underestimate the dynamic modulus slightly, it was recommended that viscosity-temperature regression coefficient (A and VTS) values used to generate input viscosities for the predictive equation be obtained from the DSR test. The study also indicated that the viscosity-temperature regression coefficients (A and VTS) should be obtained from the Brookfield rotational viscometer test or alternatively the mix/ laydown conditions proposed by Witzcak and Fonseca (1996). However, the latter two approaches may result in modulus predictions that are slightly higher modulus values than those obtained in the laboratory. The results also showed that dynamic modulus predictions at higher temperatures generally are closer to measured values than modulus predictions at lower temperatures. This is possibly the result of the database used to develop the predictive equation being biased toward mixtures tested at higher temperatures. Another possible explanation is that for the mixtures studied, the underlying sigmoidal function used in the Witzcak predictive equation may produce slightly biased dynamic modulus values at low temperatures ($<10^{\circ}\text{C}$). Overall, the results presented showed that the Witzcak predictive equation resulted in a slight bias for mixtures common to Florida. However, the results presented also allow for a correction of the bias between predicted and measured dynamic modulus.

Table 2: A and VTS values reported in Birgisson et al. (2005)

Regression Constants	From Brookfield Rotational Viscometer Test Results	From Dynamic Shear Rheometer Test Results	From Mix/Laydown Conditions Suggested by Witzcak and Fonseca (7)
A	-3.4655	-3.0165	-3.56455
VTS	10.407	9.0824	10.6768

Literature on $|E^*|$ Predictive Equations and Models

Several researchers developed relationships between the characteristics of asphalt mixture constituents (e.g., mix design parameters and binder characteristics) and $|E^*|$ master curve (Bonnaure et al. 1977, Andrei et al. 1999, Bari 2005, Christensen et al. 2003, Al-Khateeb et al. 2006). Table 3 shows some of these equations and input parameters used in each equation. Appendix A includes three of the most widely used equations. The most well-known relationship is the (original) Witczak’s (OW) equation (Andrei et al. 1999, see Appendix A), which, as mentioned previously, is implemented in M-E PDG (and DARWin-ME).

Table 3: Parameters used in different $|E^*|$ predictive models.

Parameters	Description	Used in $ E^* $ Predictive Model?						In MDOT Testing Program?
		OW	MW	H	A	K-1	K-2	
VMA	Voids in mineral aggregate (%)			Y	Y			Yes
VFA	Voids filled with asphalt (%)			Y				Yes
P ₂₀₀	Aggregate passing #200 sieve (%)	Y	Y			Y		Yes
P ₄	Aggregate passing #4 sieve (%)	Y	Y			Y		Yes
P _{3/8}	Aggregate passing 3/8-inch sieve (%)	Y	Y			Y		Yes
P _{3/4}	Aggregate passing 3/4-inch sieve (%)	Y	Y			Y		Yes
V _a	Air voids (by volume) (%)	Y	Y			Y		Yes
V _{beff}	Effective asphalt content (by volume) (%)	Y	Y			Y		Yes
A & VTS	Intercept & slope of viscosity-temperature relationship of binder	Y						No
f _s	Loading frequency (Hz)	Y						No
M _R	Resilient modulus of the asphalt mixture						Y	No
$ G^* _b$	Binder dynamic shear modulus		Y	Y	Y	Y		No
δ_b	Binder phase angle		Y			Y		No

Note: OW = Original Witczak (Andrei et al. 1999), MW = Modified Witczak (Bari 2005), H = Hirsch (Christensen et al. 2003), A = Al-Khateeb (Al-Khateeb et al. 2006), K-1 = Kim’s ANN model -1, K-2: Kim’s ANN Model -2 (Kim et al. 2010).

The empirical constants in Witczak’s equation was determined using 200 different asphalt mixture $|E^*|$ master curves obtained from various States (Andrei et al. 1999). The original Witczak’s model is based on the viscosity-temperature relationship of the binder and

mixture volumetrics. In order to be able to use the complex shear modulus ($|G^*|$) of the binder in $|E^*|$ equation, Bari (2005) developed a modified formulation (herein called Modified-Witczak (MW) model and shown in Appendix A). Christensen et al. (2003) investigated $|E^*|$ models and developed a more simplified formula (with less input parameters) to predict $|E^*|$ mastercurve (Hirsch (HM) model in Appendix A). Al-Khateeb et al. (2006) later simplified the Hirsch model and introduced a revised formulation.

A recent FHWA-funded research showed that the predictions of Witczak, Hirsch and Al-Khateeb equations were inaccurate at low frequencies/high temperatures (Sakhaeifar et al. 2009, Kim et al. 2010). Independent evaluations of these models were performed in various studies (e.g., Azari et al. 2007, Robbins and Timm 2011, Singh et al. 2010). These studies consistently showed inaccuracies of statistical models at certain frequencies and temperatures. This indicated the need for either local calibration of the constants in these equations, or if necessary, employ advanced computing tools such as the Artificial Neural Networks (ANNs) to develop models for better prediction of $|E^*|$ values and use them as Level 1 inputs in DARWin-ME. Such models were developed by Kim et al (2010) as part of a FHWA funded study. These models are shown in Table 3 as K-1 ($|G^*|$ -based) and K-2 (MR-based) models.

The research team evaluated the Original and Modified-Witczak (MW) models for use in $|E^*|$ prediction of asphalt mixtures commonly used in the State of Michigan. The models did not perform very well for MDOT mixtures. Regression parameters used in the MW model were calibrated using the MATLAB software and statistical analysis were performed on the calibrated model so that it produced better predictions of $|E^*|$ for typical

MDOT mixtures. It is recommended that the revised model should be used to predict $|E^*|$ values as Level 1 inputs in DARWin-ME software. The calibrated model performed very well and the details of the study are shown later in the report.

TASK 1-2: “Review MDOT's HMA testing program”

The research team reviewed the current asphalt mixture and binder test data available in MDOT’s routine testing program and compared it with the test data required by the DARWin-ME. Tables 4 through 6 show the material inputs required by the DARWin-ME (or M-E PDG), where the material parameters that don’t exist in the MDOT’s testing program have been shaded. In Level 1 analysis, MDOT does not test for $|E^*|$, IDT strength and $D(t)$ for asphalt mixtures. MDOT’s testing program includes testing of $|G^*|$ and phase angle at a certain temperatures for verification of PG of binders used in pavement projects. With slight modifications in the testing procedure, MDOT can obtain the $|G^*|$ and phase angle required by the DARWin-ME. Currently softening point of asphalt binders is also not routinely measured. Other binder parameters shown under “Option 2” in Table 4 are only available in some cutback asphalt projects. Under the category of “asphalt general”, air voids, effective binder content and total unit weight are available as part of the Job Mix Formulas (JMFs) submitted by the contractors. During design of a new pavement, engineers may use typical values based on the JMFs submitted in the earlier construction seasons. Thermal conductivity, heat capacity and Poisson’s ratio values typically do not vary significantly from one asphalt mixture to another, therefore, default values in DARWin-ME or values from the literature may be used. In Levels 2 and 3, $|E^*|$ is predicted using Witczak’s formulation,

therefore, aggregate gradation parameters are needed as shown in Table 4 and Table 5, which are available in JMFs. In Level 3 analysis, one of the 3 options, PG, is available in JMFs.

Table 4: Level 1 analysis material inputs.

Asphalt Mixture	Asphalt Binder		Asphalt General
	Option 1	Option 2	
E* master curve	G* master curve	Softening point	Effective binder content
Creep compliance (D(t)) master curve	Phase angle master curve	Absolute viscosity (@140F)	Air Voids (%)
		Kinematic viscosity (@275F)	Total unit weight
		Specific gravity (@77F)	Thermal conductivity of asphalt
IDT strength		Penetration	Heat capacity asphalt
		Brookfield Viscosity	Poisson's ratio

Table 5: Level 2 analysis material inputs.

Asphalt Mixture	Asphalt Binder		Asphalt General
	Option 1	Option 2	
Cumulative % retained ¾" sieve	G* master curve	Softening point	Effective binder content
Cumulative % retained 3/8" sieve	Phase angle master curve	Absolute viscosity (@140F)	Air Voids (%)
Cumulative % retained #4 sieve		Kinematic viscosity (@275F)	Total unit weight
Creep compliance (D(t)) master curve		Specific gravity (@77F)	Thermal conductivity of asphalt
IDT strength		Penetration	Heat capacity asphalt
		Brookfield Viscosity	Poisson's ratio

Table 6: Level 3 analysis material inputs.

Asphalt Mixture	Asphalt Binder			Asphalt General
	Option 1	Option 2	Option 3	
Cumulative % retained ¾" sieve	Superpave performance grade (e.g., PG64-22)	Conventional viscosity grade (e.g., AC 20)	Conventional penetration grade (e.g., Pen 60-70)	Effective binder content
Cumulative % retained 3/8" sieve				Air Voids (%)
Cumulative % retained #4 sieve				Total unit weight
% Passing #200 sieve				Thermal conductivity of asphalt
Creep compliance (D(t)) master curve				Heat capacity asphalt
IDT strength				Poisson's ratio

TASK 1-3: “In consultation with the Research Advisory Panel (RAP), choose construction projects that will allow sampling of mixtures in the matrix developed by the principle investigator”

The projects have been selected and samples were collected by MDOT during summer 2011 and 2012. A total of 64 different types of asphalt mixtures were sampled and a wide range of $|E^*|$ master curves that are representative of typical MDOT mixtures were obtained.

TASK 1-4: “Laboratory testing of samples collected”

Table C.1 in Appendix C shows a list of asphalt mixture samples prepared and tested since October 1, 2011. As shown, a total of 213 different specimens were prepared from 64 unique asphalt mixture types. These 64 unique asphalt mixture types are shown in Tables C.2 through C.5 in Appendix C. In addition, RTFO aging and $|G^*|$ testing of binders received since mid-December 2011 has been completed. A total of 44 unique binders have been characterized. Sample testing for IDT strength has also been completed. Due to the lack of sampled material; 2 asphalt mixtures were not tested for IDT strength. A total of 62 different types of asphalt mixtures have been tested at the target air void level of 7% (+/-0.5%) (see Appendix C). IDT strength tests are conducted on 38mm thick, 150mm diameter samples at -10°C in accordance with AASHTO T322 "Determining the Creep Compliance and Strength of Hot-Mix Asphalt (HMA) Using the Indirect Tensile Test Device". In order to illustrate the overall range of $|E^*|$ values for all mixtures tested, the $|E^*|$ mastercurves were plotted in Figure 11. As shown, the difference between the lowest and highest $|E^*|$ values is approximately 2 orders of magnitude.

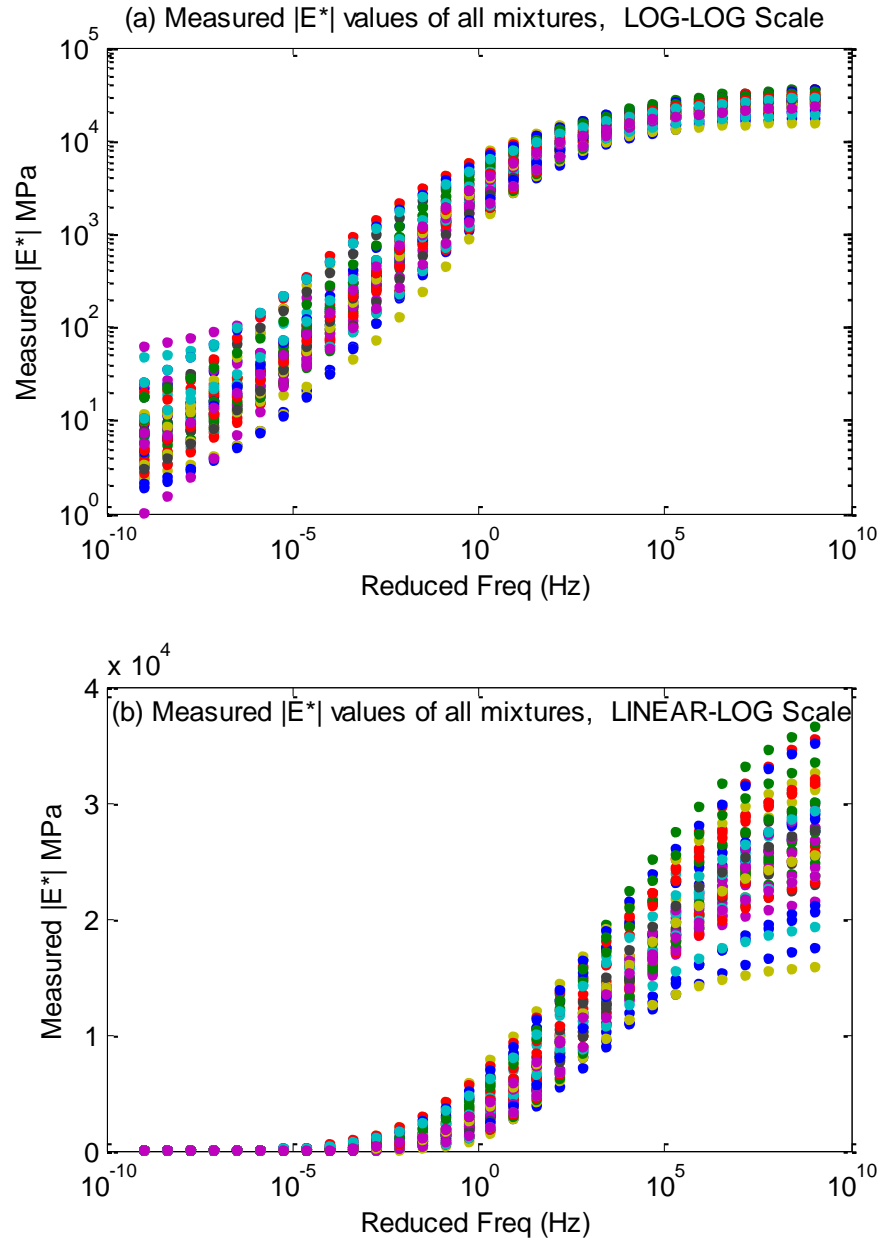


Figure 11: Dynamic Modulus mastercurves of all tested asphalt mixture specimens. The plot in log-log scale is to show the differences in low frequency/high temperature, and the linear-log scale is to show the differences in high frequency/low temperature).

Table 7 shows the $|E^*|$ sigmoid coefficients, along with the $a(T)$ shift factor coefficients obtained after generation of the mastercurve. These coefficients produce $|E^*|$ in MPa. The input temperature should be in Celsius and the frequency should be in Hz. The reference temperature in all of the coefficients is 21°C . In order to determine the $|E^*|$ and

mixture phase angle values at any temperature and (load) frequency, the following basic steps are followed:

- Step 1: Calculate the shift factor coefficient $a(T)$ using the following equation described earlier: $\log(a(T)) = a_1(T^2 - T_{ref}^2) + a_2(T - T_{ref})$. Note $T_{ref} = 21^\circ\text{C}$ for the mixtures in Table 7.
- Step 2: Calculate the reduced frequency: $f_R = f a(T)$
- Step 3: Calculate the $|E^*|$: $\log(|E^*|) = b_1 + \frac{b_2}{1 + \exp(-b_3 - b_4 \log(f_R))}$

These steps can be followed to compute $|E^*|$ at different temperatures and frequencies in order to input to DARWin-ME. This may be necessary only if the DYNAMOD software is somehow not available to the designer. An example calculation of $|E^*|$ from the coefficients shown in Table 7 was provided in Figure 6.

Table 7: $|E^*|$ master curve coefficients obtained from laboratory measurements

Sample ID	MDOT mix type	Binder PG	a_1	a_2	b_1	b_2	b_3	b_4
2	3E30	64-22	4.61E-04	-0.135	1.07	3.42	1.32	0.43
2-WMA	3E30	64-28	7.82E-05	-0.104	1.00	3.39	1.01	0.50
4	4E30	70-28P	6.58E-04	-0.154	0.64	3.84	1.07	0.38
18A	3E10	70-28P	3.85E-04	-0.134	0.00	4.61	1.37	0.36
18B	3E10	58-22	5.41E-04	-0.140	0.29	4.16	1.19	0.42
20A	4E10	64-28	6.60E-04	-0.155	0.23	4.32	1.30	0.36
20B	5E10	64-28	6.92E-04	-0.157	0.12	4.38	1.24	0.35
20C	4E10	64-28	6.43E-04	-0.152	0.62	3.79	1.05	0.41
21	5E10	64-28	6.71E-04	-0.155	0.33	4.13	1.12	0.37
23	4E10	70-28P	6.79E-04	-0.150	0.78	3.72	0.92	0.40
24A	5E10	70-28	6.91E-04	-0.160	1.15	3.13	0.90	0.40
24B	5E10	70-28	7.26E-04	-0.153	0.32	4.16	1.04	0.37
26A	3E3	58-22	4.20E-04	-0.142	0.60	3.93	1.21	0.38
26B	3E3	58-28	4.61E-04	-0.143	-0.52	5.09	1.24	0.31
26C	3E3	58-28	1.23E-03	-0.194	0.91	3.44	0.94	0.47
28B	4E3	64-28	3.37E-04	-0.148	0.62	3.93	0.96	0.35
29A	5E3	64-28	1.34E-05	-0.126	0.50	3.90	1.26	0.39
29B	5E3	64-28	3.37E-04	-0.148	-0.09	4.48	0.97	0.38

31A	4E3	70-28P	5.77E-04	-0.156	0.56	3.90	1.06	0.35
31B	4E3	70-28P	5.52E-04	-0.141	0.81	3.80	0.83	0.39
32A	5E3	70-28P	5.86E-04	-0.151	0.45	4.07	0.99	0.36
32B	5E3	70-28P	3.37E-04	-0.148	1.21	3.23	0.63	0.39
37	5E03	58-28	9.62E-04	-0.153	0.19	4.22	1.01	0.44
44	4E1	58-28	8.06E-04	-0.161	-0.07	4.58	1.16	0.34
45	5E1	58-28	5.29E-04	-0.148	0.35	4.03	1.14	0.34
47	4E1	64-28	6.40E-04	-0.155	0.42	4.06	1.17	0.36
48	5E1	64-28	7.10E-04	-0.155	-0.04	4.46	1.24	0.37
49A	GGSP	70-28P	6.12E-04	-0.145	1.56	2.92	0.58	0.42
49B	GGSP	70-28P	3.37E-04	-0.148	1.59	2.92	0.49	0.34
49C	GGSP	70-28P	4.97E-04	-0.132	1.51	2.85	0.44	0.48
51A	LVSP	58-28	1.32E-03	-0.173	1.04	3.17	0.60	0.59
51B	LVSP	58-28	5.23E-04	-0.143	0.51	3.94	0.92	0.40
51C-WMA	LVSP	58-28	5.92E-04	-0.143	1.10	3.24	0.73	0.50
62	3E3	58-28	3.52E-04	-0.128	0.08	4.42	0.95	0.42
64	4E3	58-34	2.41E-05	-0.118	1.14	3.34	0.65	0.46
65	5E3	58-34	5.05E-04	-0.138	0.62	3.88	0.67	0.39
67	4E3	64-34P	7.05E-04	-0.149	1.22	3.22	0.45	0.46
68	5E3	64-34P	6.13E-04	-0.140	1.20	3.11	0.61	0.51
80	4E1	58-34	5.37E-04	-0.142	0.65	3.86	0.71	0.39
81	5E1	58-34	1.31E-03	-0.188	0.83	3.63	0.70	0.40
85	4E1	64-34P	5.23E-04	-0.146	1.31	3.04	0.67	0.42
86	5E1	64-34P	7.99E-04	-0.147	1.05	3.37	0.52	0.47
90	4E30	70-22P	3.74E-04	-0.134	0.62	3.88	1.30	0.37
97	5E50	70-22P	7.11E-04	-0.164	0.35	4.16	1.34	0.34
102	4E10	64-22P	4.98E-04	-0.151	-1.02	5.59	1.89	0.30
103	5E10	64-22P	3.04E-04	-0.149	0.65	3.88	1.38	0.34
105	4E10	70-22P	1.17E-04	-0.128	0.29	4.21	1.40	0.35
106	5E10	70-22P	2.77E-04	-0.140	-0.09	4.61	1.38	0.34
108	4E3	64-22	5.14E-04	-0.145	0.00	4.49	1.59	0.37
109	5E3	64-22	3.62E-04	-0.142	-0.19	4.71	1.50	0.36
111	4E3	70-22P	2.97E-04	-0.151	-0.55	5.12	1.75	0.29
112	5E3	70-22P	9.21E-04	-0.168	0.61	3.80	1.29	0.38
127	LVSP	58-22	2.90E-04	-0.143	-0.93	5.46	1.45	0.33
200	3E10	58-28	6.96E-04	-0.157	0.06	4.39	1.31	0.38
201	ASCRL	64-28	7.23E-04	-0.151	0.16	4.35	1.33	0.32
202	5E10	64-22	6.23E-04	-0.158	-0.09	4.58	1.37	0.37
203	4E30	70-22P	3.37E-04	-0.148	0.70	3.92	1.32	0.31
204	5E30	70-22	4.62E-04	-0.144	0.81	3.76	1.21	0.36
205	2E3	58-28	5.31E-04	-0.145	0.20	4.35	1.22	0.36
206	5E1	64-22	1.29E-04	-0.141	0.66	3.87	1.37	0.31
207	5E1	64-22	6.45E-04	-0.158	0.27	4.14	1.35	0.38
208-WMA	LVSP	64-22	3.39E-04	-0.123	0.98	3.49	1.00	0.45
209-HMA	5E10	64-22	4.50E-04	-0.137	0.75	3.73	1.07	0.43
209-WMA	5E10	64-22	7.95E-04	-0.158	0.86	3.53	1.06	0.44
210-WMA	5E10	64-28	7.58E-04	-0.150	0.07	4.37	1.20	0.42

Summary of $|E^*|$ values based on MDOT mix designation for each region

Table 8, Table 9 and Table 10 show a summary of the $|E^*|$ values at temperatures of -10, 21 and 54°C, at a loading frequency of 10Hz. These tables are provided to illustrate the relative differences in $|E^*|$ values of various asphalt mixture types used in MI. As shown in Table 8, 3E mixtures are generally stiffer than 4E and 5E mixtures (e.g., compare HMA# 18 versus 20 versus 21). However the trend is not always consistent in all temperatures (e.g., HMA# 31 versus 32 at -10°C). A clear trend should not be expected since there are many variables (e.g., aggregate gradation, binder $|G^*|$ mastercurve, VMA, VFA...etc.) that play a role in the magnitude of $|E^*|$ at different temperatures and frequencies.

Comparison of variation in $|E^*|$ mastercurves based on MDOT mix designation

Figure 12 shows $|E^*|$ master curves of the 3E3 mixtures, where a single master curve is not visible. Appendix D shows the $|E^*|$ mastercurves of all other mixtures grouped based on the MDOT mix designation (e.g., 4E10, 3E03 etc.). The objective of plotting these graphs was to investigate if MDOT mix types for a given region (e.g., 5E10 for Metro Region) exhibit same or similar $|E^*|$ mastercurve values. After carefully analyzing the $|E^*|$ mastercurves, it was concluded that it is not appropriate to come up with a single $|E^*|$ mastercurve for a given MDOT mix, for a given region. The main reason is that aggregate gradation play a key role in $|E^*|$ mastercurve and it is not unique for an MDOT mix type in a region (e.g., 3E3 in Metro). For example, two 3E3 projects in Metro region may (and most probably will) have different gradations (and mix designs).

Table 8: Summary of |E*| values for different asphalt mixture types in North, Grand, Bay, Southwest and University Regions

North, Grand, Bay, Southwest and University Regions (NGBSU)													
	Mix No:	3			4			5					
Mainline / High Stress	Layer:	Base			Leveling/Top			Top					
	Traffic	HMA #	E* (MPa)			HMA #	E* (MPa)			HMA #	E* (MPa)		
			10Hz, -10°C	10Hz, 21°C	10Hz, 54C		10Hz, -10°C	10Hz, 21°C	10Hz, 54C		10Hz, -10°C	10Hz, 21°C	10Hz, 54C
M	E30	2	24183	9108	1175	4	21668	5683	498	5			
HS	E30	2	24183	9108	1175	7				8			
M	E50	10				12				13			
HS	E50	10				15				16			
M	E10	18	26710	7668	668	20	24989	7175	698	21	19780	4893	398
HS	E10	18	26710	7668	668	23	22232	5300	475	24	15287	4133	444
M	E3	26	21470	5649	453	28	22301	5618	449	29	17958	6068	605
HS	E3	26	21470	5649	453	31	17363	4834	437	32	21282	4796	399
M	E03	34				36				37	18761	4017	214
HS	E03	34				39				40			
M	E1	42				44	20696	4833	440	45	15280	4207	429
HS	E1	42				47	20879	5707	536	48	18204	4659	369

Table 9: Summary of |E*| values for different asphalt mixture types in Metro Region

Metro Region													
Mainline / High Stress	Mix No:	3				4				5			
	Layer:	Base				Leveling/Top				Top			
	Traffic	HMA #	E* (MPa)			HMA #	E* (MPa)			HMA #	E* (MPa)		
			10Hz, -10C	10Hz, 21C	10Hz, 54C		10Hz, -10C	10Hz, 21C	10Hz, 54C		10Hz, -10C	10Hz, 21C	10Hz, 54C
M	E30	2	24183	9108	1175	90	22256	7408	913	91			
HS	E30	2	24183	9108	1175	93				94			
M	E50	10				96				97	23603	7405	813
HS	E50	10				99				100			
M	E10	18	26710	7668	668	102	26014	10224	1443	103	24044	8588	849
HS	E10	18	26710	7668	668	105	21314	7375	852	106	21293	6425	656
M	E3	26	21470	5649	453	108	23374	8419	948	109	23442	7706	549
HS	E3	26	21470	5649	453	111	25192	9402	1434	112	20122	6323	705
M	E03	34				114				115			
HS	E03	34				117				118			
M	E1	42				120				121			
HS	E1	42				123				124			

Table 10: Summary of |E*| values for different asphalt mixture types in Superior Region

Mix No:		3				4				5			
Layer:		Base				Leveling/Top				Top			
Mainline / High Stress	ESAL	HMA #	E* (MPa)			HMA #	E* (MPa)			HMA #	E* (MPa)		
			10Hz, -10C	10Hz, 21C	10Hz, 54C		10Hz, -10C	10Hz, 21C	10Hz, 54C		10Hz, -10C	10Hz, 21C	10Hz, 54C
M	E10	54				56				57			
HS	E10	54				59				60			
M	E3	62	19556	4142	241	64	19103	4519	527	*65	17663	3193	260
HS	E3	62	19556	4142	241	67	19403	3339	261	68	16849	3456	264
M	E03	70				72				73			
HS	E03	70				75				76			
M	E1	78				80	18831	3483	297	81	17265	3570	
HS	E1	83				85				86			

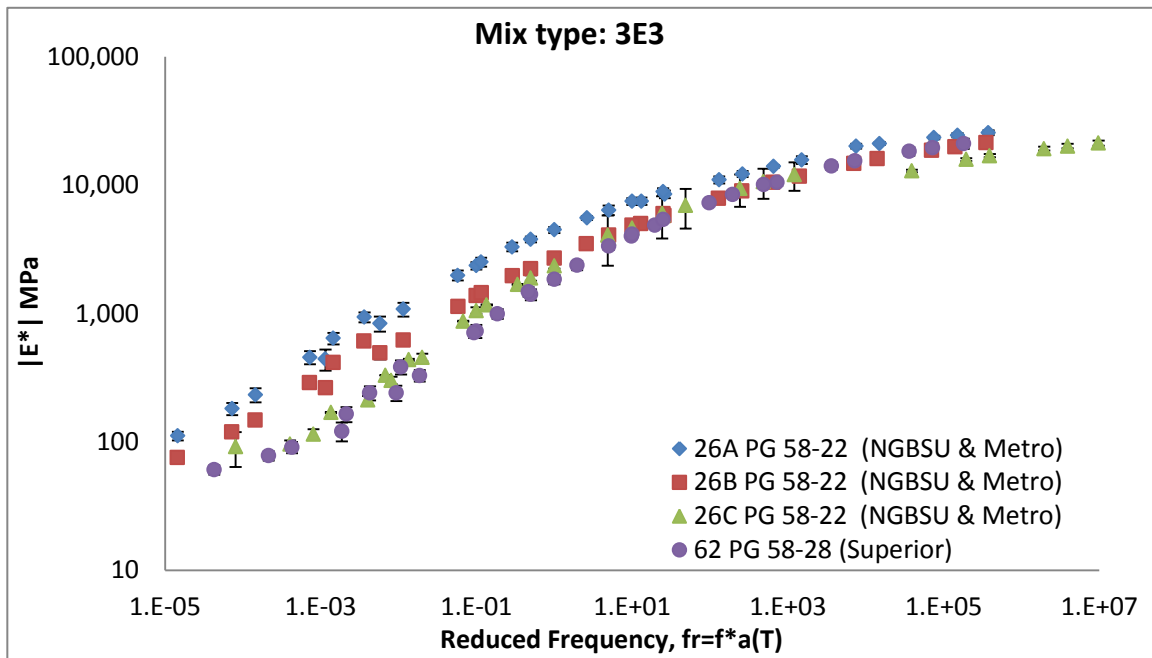


Figure 12: $|E^*|$ mastercurves of four 3E3 mixtures, 3 of which (26* mixes) are from same region. NGBSU = North, Grand, Bay, Southwest and University Regions.

As a result, $|E^*|$ can be very different. An evidence of this phenomenon is the three 3E3 mixtures (26A, 26B and 26C) we tested as part of this project. As shown in Figure 12, mixtures 26A, 26B and 26C exhibited different $|E^*|$ values. In fact, 26C had a very similar $|E^*|$ mastercurve as 64, which has a different binder PG and was in a different region (Superior).

If there are more than one mixture tested in this project for a given MDOT mix designation (e.g., 3E3) and region, it is recommended that the designer will choose the $|E^*|$ that will result in the least conservative predictions of fatigue cracking and rutting. The designer can refer to Figure 7 to compare different $|E^*|$ curves in terms of expected rutting and fatigue performance and make an appropriate decision.

Summary of $|G^*|$ and phase angle of the binders

Figure 13 shows the $|G^*|$ master curves of four different binders with same performance grade of PG 64-28. As shown, a single PG did not necessarily produce the same $|G^*|$ master curve. The rest of the $|G^*|$ master curves grouped based on the PG are given in Appendix E.

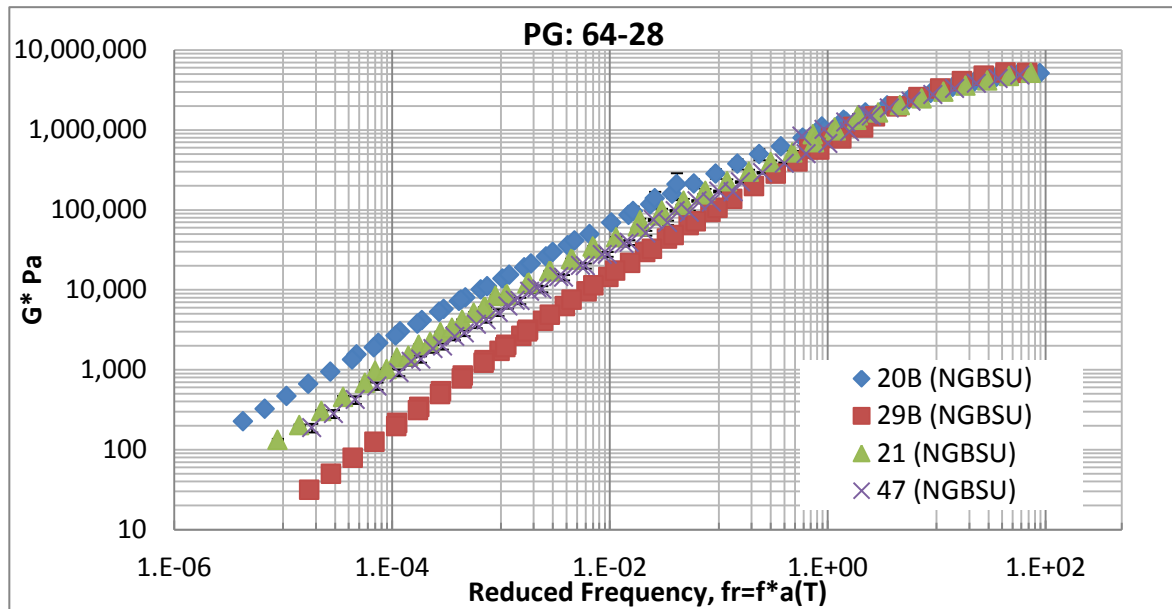


Figure 13: $|G^*|$ Master curves of four different PG64-28 binders. NGBSU = North, Grand, Bay, Southwest and University Regions.

Table 11 shows the $|G^*|$ master curve coefficients obtained from laboratory measurements. In order to determine the $|G^*|$ and binder phase angle values at any temperature and frequency, the following basic steps are followed:

- Step 1: Calculate the shift factor coefficient $a(T)$ using the following equation described earlier: $\log(a(T)) = a_1(T^2 - T_{ref}^2) + a_2(T - T_{ref})$. Note $T_{ref} = 21^\circ\text{C}$ for the mixtures in Table 7.
- Step 2: Calculate the reduced frequency: $f_R = f a(T)$

- Step 3: Calculate the $|G^*|$: $\log(|G^*|) = b_1 + \frac{b_2}{1 + \exp(-b_3 - b_4 \log(f_R))}$
- Step 4: The phase angle (ϕ) of the binder can be calculated the following formula:

$$\phi = d_1 e^{-\frac{(d_2 - \log(f_R))^2}{2d_3^2}}$$

Table 11: $|G^*|$ master curve coefficients obtained from laboratory measurements

Binder PG_ Corresponding mix	a1	a2	b1	b2	b3	b4	d1	d2	d3
PG58-22_127	9.08E-04	-1.77E-01	-3.568	11.232	1.930	0.358	99.77	-24.17	22.95
PG58-22_18B	7.06E-04	-1.54E-01	-3.041	10.794	1.828	0.365	100.44	-21.42	26.01
PG58-22_26A	4.95E-04	-1.26E-01	-2.295	10.706	1.287	0.354	99.43	-24.44	23.65
PG58-28_200	6.39E-04	-1.41E-01	-2.925	10.826	1.534	0.325	99.61	-23.98	23.95
PG58-28_205	3.72E-04	-1.08E-01	-3.175	10.792	1.511	0.364	100.49	-21.28	26.12
PG58-28_26C	3.71E-04	-1.08E-01	-3.175	10.792	1.511	0.364	100.49	-21.28	26.12
PG58-28_37	5.61E-04	-1.29E-01	-4.206	12.509	1.434	0.316	111.35	-11.98	11.56
PG58-28_44	8.36E-04	-1.59E-01	-0.268	7.726	1.469	0.448	110.13	-13.42	12.69
PG58-28_45	5.35E-04	-1.27E-01	-3.177	10.773	1.610	0.363	99.78	-23.68	23.97
PG58-28_51A	6.03E-04	-1.34E-01	-2.602	10.347	1.527	0.388	99.43	-24.46	23.62
PG58-34_65	5.96E-04	-1.34E-01	-2.602	10.347	1.527	0.388	99.43	-24.46	23.62
PG58-34_80	7.59E-04	-1.49E-01	-2.422	10.382	1.278	0.304	99.43	-24.46	23.61
PG64-22_102	2.97E-04	-1.08E-01	-2.320	10.908	1.296	0.329	99.59	-24.27	23.41
PG64-22_103	5.12E-04	-1.28E-01	-3.078	11.544	1.451	0.340	99.81	-24.02	23.06
PG64-22_108	3.72E-04	-1.08E-01	-3.175	10.792	1.511	0.364	100.49	-21.28	26.12
PG64-22_109	4.78E-04	-1.25E-01	-2.733	10.831	1.550	0.354	100.22	-22.17	25.36
PG64-22_202	8.91E-04	-1.77E-01	-3.088	11.169	1.723	0.326	99.75	-24.25	22.90
PG64-22_206	5.83E-04	-1.53E-01	-3.031	11.044	1.658	0.297	99.75	-24.27	22.89
PG64-22_208	5.51E-04	-1.35E-01	-3.260	11.001	1.778	0.357	99.87	-23.89	23.12
PG64-28_20B	6.79E-04	-1.49E-01	-2.591	10.965	1.295	0.277	99.37	-24.72	23.40
PG64-28_21	5.49E-04	-1.31E-01	-2.901	10.954	1.428	0.314	99.56	-24.17	23.79
PG64-28_28B	8.19E-04	-1.60E-01	-2.281	10.610	1.383	0.344	99.42	-24.47	23.62
PG64-28_29B	5.50E-04	-1.25E-01	-3.538	12.040	1.243	0.330	100.98	-20.51	26.23
PG64-28_47	3.72E-04	-1.08E-01	-3.175	10.792	1.511	0.364	100.49	-21.28	26.12
PG64-28_48	6.36E-04	-1.43E-01	-2.348	10.499	1.426	0.328	99.42	-24.47	23.61
PG64-34P_67	4.95E-04	-1.19E-01	-6.224	16.771	0.879	0.174	88.75	-35.89	40.82
PG64-34P_68	2.40E-04	-9.85E-02	-2.335	11.115	0.946	0.284	99.40	-24.64	23.50
PG70-22_204	9.40E-04	-1.85E-01	-0.301	7.813	1.632	0.355	88.44	-36.93	41.48

PG70-22P_112	8.88E-04	-1.78E-01	-2.940	11.242	1.513	0.262	99.76	-24.25	22.83
PG70-22P_203	8.20E-04	-1.71E-01	-3.033	11.041	1.654	0.276	99.75	-24.27	22.89
PG70-28P_24A	6.61E-04	-1.48E-01	-3.174	11.298	1.397	0.250	94.48	-32.59	30.64
PG70-28P_31A	7.60E-04	-1.58E-01	-1.369	9.929	1.074	0.279	98.98	-25.31	23.73
PG70-28P_4	7.00E-04	-1.47E-01	0.076	8.174	0.961	0.341	66.50	-48.99	104.04
PG70-28P_49A	6.66E-04	-1.45E-01	-1.787	10.885	0.899	0.249	99.24	-25.01	23.26

Summary of IDT Strength and D(t) values

Table 12 shows the IDT strength values (at -10°C) of all the mixtures tested as part of this study. Typically, the values range from 304 psi to 668 psi.

Table 12: IDT Strength values of all mixtures

Sample ID	Average IDT Strength (psi)	Standard Deviation (psi)	MDOT mix type	Binder PG
2	562.0	28.4	3E30	PG64-22
2-WMA	414.4	27.2	3E30	PG64-28
4	570.0	23.2	4E30	PG70-28P
18A	391.0	62.5	3E10	PG70-28P
18B	544.0	38.7	3E10	PG58-22
20A	530.0	41.3	4E10	PG64-28
20B	524.0	24.5	5E10	PG64-28
20C	457.0	28.9	4E10	PG64-28
21	533.0	24.6	5E10	PG64-28
23	542.0	18.6	4E10 High Stress	PG70-28P
24A	428.0	34.4	5E10	PG70-28
24B	589.0	21.0	5E10	PG70-28
26A	463.0	24.4	3E3	PG58-22
26B	384.0	37.8	3E3	PG58-28
26C	394.0	15.1	3E3	PG58-28
28B	484.0	25.8	4E3	PG64-28
29A	462.0	14.9	5E3	PG64-28
29B	496.0	28.1	5E3	PG64-28
31A	518.0	45.7	4E3	PG70-28P
31B	553.0	14.4	4E3	PG70-28P
32A	540.0	23.8	5E3	PG70-28P
32B	531.0	10.4	5E3 High Stress	PG70-28P
37	533.0	25.3	5E03	PG58-28
44	470.0	34.0	4E1	PG58-28
45	395.0	43.2	5E1	PG58-28
47	506.0	5.7	4E1 High Stress	PG64-28

48	491.0	27.0	5E1 High Stress	PG64-28
49A	447.0	17.9	GGSP	PG70-28P
49B	382.0	20.4	GGSP	PG70-28P
49C	382.0	20.4	GGSP	PG70-28P
51A	396.0	51.2	LVSP	PG58-28
51B	470.0	18.3	LVSP	PG58-28
51C-WMA	437.2	15.2	LVSP	PG58-28
62	480.0	24.7	3E3	PG58-28
64	448.0	58.1	4E3	PG58-34
65	415.0	12.9	5E3	PG58-34
67	466.0	25.7	4E3 High Stress	PG64-34P
68	476.0	30.3	5E3 High Stress	PG64-34P
80	474.0	18.6	4E1	PG58-34
81	409.0		5E1	PG58-34
85	467.4	13.7	4E1 High Stress	PG64-34P
86	485.7	20.6	5E1 High Stress	PG64-34P
90	534.0		4E30	PG70-22P
97	601.0	5.8	5E50	PG70-22P
102	575.0	22.3	4E10	PG64-22P
103	498.0	89.8	5E10	PG64-22P
105	526.0	41.1	4E10 High Stress	PG70-22P
108	549.0	19.6	4E3	PG64-22
109	566.0	36.0	5E3	PG64-22
111	607.0	13.3	4E3 High Stress	PG70-22P
112	634.0	11.6	5E3 High Stress	PG70-22P
127	450.0	50.9	LVSP	PG58-22
200	570.0	26.2	3E10	PG58-28
201	304.0	9.3	ASCRL	PG64-28
202	606.0	10.8	5E10	PG64-22
203	529.0	17.0	4E30 High Stress	PG70-22P
204	668.0	15.0	5E30 High Stress	PG70-22
205	363.0	48.0	2E3	PG58-28
206	551.0	27.6	5E1	PG64-22
208-WMA	496.0	23.2	LVSP	PG64-22
209-HMA	532.0	11.8	5E10	PG64-22
209-WMA	487.0	39.8	5E10	PG64-22

A typical D(t) table is shown in Table 13. These values were computed using the $|E^*|$ master curve using the prony-series based interconversion procedure explained in Park and Schapery (1999). Creep compliances of all the mixtures are provided in the DYNAMOD software that is submitted as part of this report.

Table 13: A typical D(t) data for an asphalt mixture (49B)

D(t) (1/psi)			
Time (sec)	Temperature (°F)		
	-4	14	32
1	3.56E-07	4.89E-07	7.62E-07
2	3.75E-07	5.28E-07	8.49E-07
5	4.03E-07	5.89E-07	9.86E-07
10	4.29E-07	6.45E-07	1.12E-06
20	4.58E-07	7.10E-07	1.27E-06
50	5.04E-07	8.14E-07	1.52E-06
100	5.45E-07	9.10E-07	1.75E-06

Evaluation and Calibration of the Witczak’s equation for Michigan Mixtures

As seen in Appendix C, Tables C-2 and C-3, there are numerous Michigan mixtures where $|E^*|$ characterization could not be done as part of this project because they were not used in a field project during the period of this research. For these mixtures, $|E^*|$ predictive models, such as the Witczak’s model or the ANN model, may be utilized to estimate the mastercurves. For this, first, the research team evaluated the modified Witczak (Bari 2005) model, which is implemented in the M-E PDG (and in DARWin-ME). The performance of Witczak’s model is evaluated using two different approaches; goodness-of-fit statistics, and comparison of measured and predicted values with line of equality (LOE) (visual inspection). The goodness-of-fit statistics include S_e/S_y (standard error of estimate /standard deviation), and the correlation coefficient (R^2). The ratio of S_e/S_y is a measure of improvement in the accuracy of prediction due to the empirical model. Smaller ratio of S_e/S_y indicates better prediction by the model. On the other hand, R^2 measures model accuracy, values closer to one indicate better estimation by the model (Singh et. al, 2010). It is noted that R^2 is a better parameter for linear models with a large sample size. However, for non-linear models, such as the empirical models, ratio of S_e/S_y is a more rational measure of prediction reliability

(Kim et. al, 2005). The goodness-of-fit statistics (S_e/S_y , R^2) were calculated using the following equations:

$$S_e = \sqrt{\frac{\sum (y - \hat{y})^2}{(n - k)}} \quad [11]$$

$$S_y = \sqrt{\frac{\sum (y - \bar{y})^2}{(n - 1)}} \quad [12]$$

$$R^2 = 1 - \frac{(n - k)}{(n - 1)} \left(\frac{S_e}{S_y} \right)^2 \quad [13]$$

where:

S_e : Standard error of estimate,

S_y : Standard deviation,

R^2 : Correlation coefficient,

y : Measured dynamic modulus,

\hat{y} : Predicted dynamic modulus,

\bar{y} : Mean value of measured dynamic modulus,

n : Sample size,

k : Number of independent variables in the model. In this report, this is equal to the number of coefficients in Equation 13 (i.e. $k=21$).

Figure 14 shows the predicted versus measured values based on the modified Witczak's equation developed as part of the NCHRP 1-40D, which is based on the nationally calibrated coefficients. As shown, the goodness-of-fit statistics for the linear-linear plot are $S_e/S_y = 0.5084$, $R^2 = 0.7881$, and for the log-log plot $S_e/S_y = 0.446$, $R^2 = 0.8369$. It should be recalled that the smaller the S_e/S_y and the larger the R^2 , the better the goodness-of-fit is. There are significant differences in $|E^*|$ values at high temperature/low frequencies (lower left side of the graph in Figure 14).

Using the laboratory $|E^*|$ data collected in this study, the research team used the MATLAB software to calibrate the coefficients of Witczak's equation. Figure 15 shows the predicted versus measured $|E^*|$ values using the calibrated coefficients.

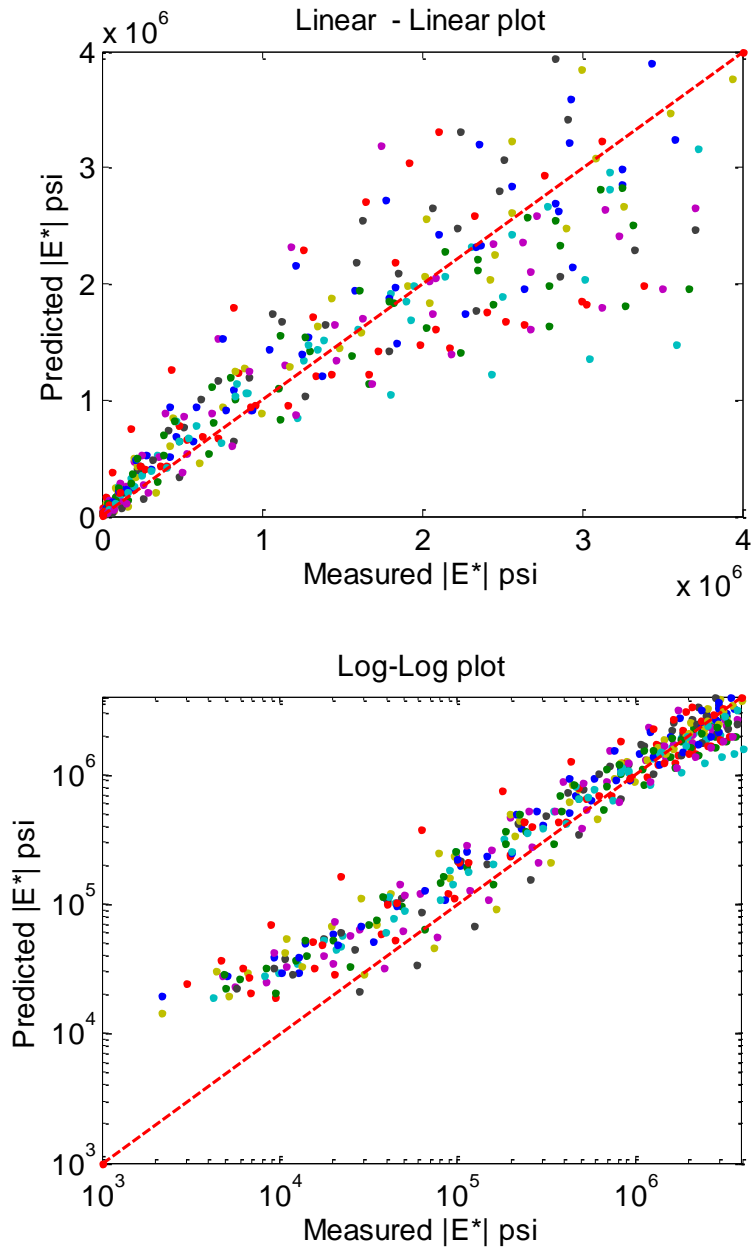


Figure 14: The modified Witzak’s equation developed as part of the NCHRP 1-40D. The plot shows the predicted versus measured values before calibration for MDOT mixtures. $S_e/S_y = 0.5084$, $R^2 = 0.7881$ (linear-linear plot), and $S_e/S_y = 0.446$, $R^2 = 0.8369$ (log-log plot).

As shown, the predicted values are much closer to the line of equality as compared to results shown in Figure 14. As shown in Figure 15, the goodness-of-fit statistics for the linear-linear plot are $S_e/S_y = 0.3029$, $R^2 = 0.9248$, and for the log-log plot $S_e/S_y = 0.2053$, $R^2 = 0.965$, which are much better than the statistics shown in Figure 14.

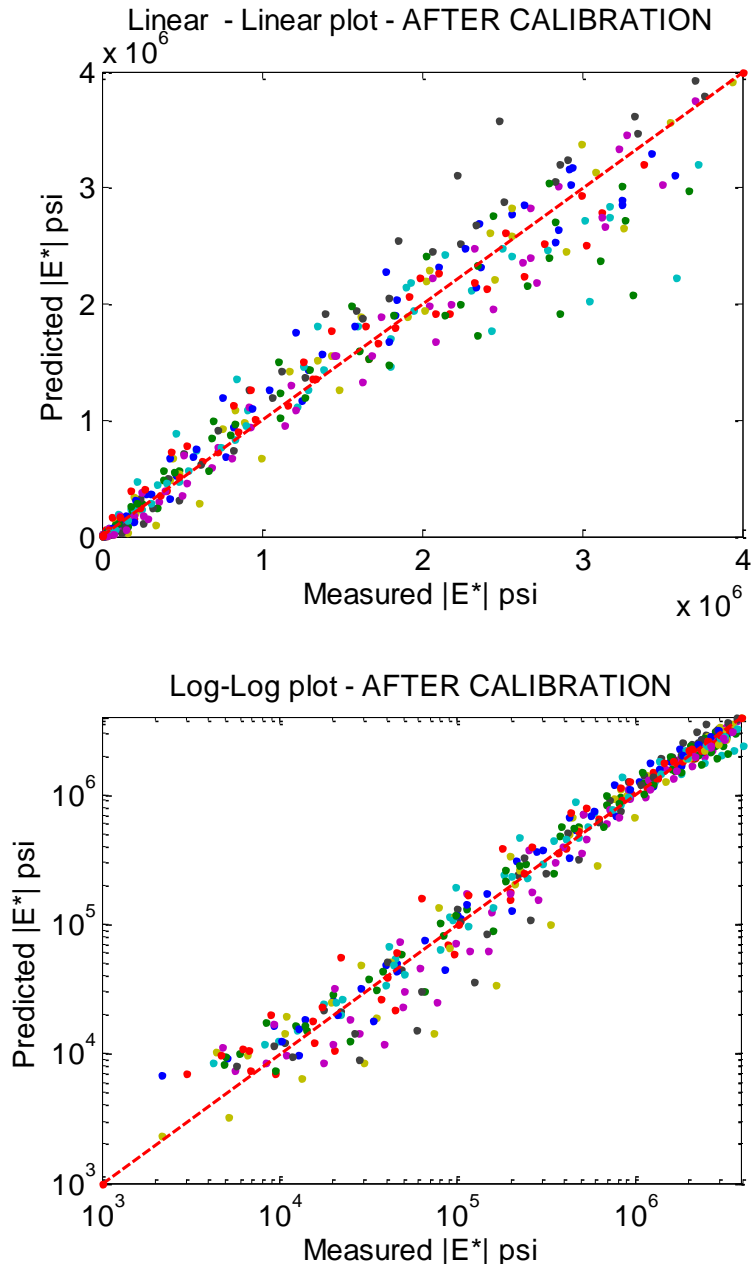


Figure 15: The modified Witzak’s equation developed as part of the NCHRP 1-40D. The plot shows the predicted versus measured values after calibration for MDOT mixtures. $Se/Sy = 0.3029$, $R^2 = 0.9248$ (linear-linear plot), and $Se/Sy = 0.2053$, $R^2 = 0.965$ (log-log plot).

Table 14 shows a comparison between coefficients used in the original and optimized models. Each coefficient in Table 14 is shown in the following equation (which is the modified Witzak equation):

$$\log_{10} |E^*| = a1 + a2(|G^*|_b^{a3}) * \left(a4 + a5p_{200} + a6(p_{200})^2 + a7p_4 + a8(p_4)^2 + a9p_{3/8} + a10(p_{3/8})^2 + a11V_a + a12 \left(\frac{V_{beff}}{V_{beff} + V_a} \right) \right) \quad [14]$$

$$+ \frac{a13 + a14V_a + a15 \left(\frac{V_{beff}}{V_{beff} + V_a} \right) + a16p_{3/8} + a17(p_{3/8})^2 + a18p_{3/4}}{1 + \exp(a19 + a20 \log |G^*|_b + a21 \log \delta_b)}$$

Validation of the Calibrated Modified Witczak |E*| Predictive Model for MDOT Mixtures

About 15% (9 out of 65) of the asphalt mixtures characterized were tested for |E*| and then used in the validation of the calibrated Modified Witczak predictive model. These 9 mixtures were not used during the calibration of the model shown in Figure 15. Figure 16 shows a comparison between laboratory measured |E*| values and predicted |E*| values using the model calibrated for MDOT mixtures. The calibrated model showed very good results as compared to the measured laboratory data. The goodness-of-fit statistics for the log-log plot $Se/Sy = 0.3749$, $R^2 = 0.885$, are better than the statistics shown in Figure 14.

Table 14: Comparison between coefficients used in the original and optimized models.

Coefficients	E* Predictive model	
	Original model	Optimized model
a1	-0.349	-0.97535
a2	0.754	1.212316
a3	-0.0052	0.009132
a4	6.65	8.153804
a5	-0.032	-0.00188
a6	0.0027	0.001256
a7	0.011	0.006975
a8	-0.0001	-1.90E-05
a9	0.006	0.011852
a10	-0.00014	-0.00017
a11	-0.08	-0.22348
a12	-1.06	-4.84772
a13	2.558	1.092204
a14	0.032	0.074729
a15	0.713	2.350258
a16	0.0124	-0.03973
a17	-0.0001	0.000576
a18	-0.0098	0.014317
a19	-0.7814	0.112725
a20	-0.5785	-0.64427
a21	0.8834	0.38239

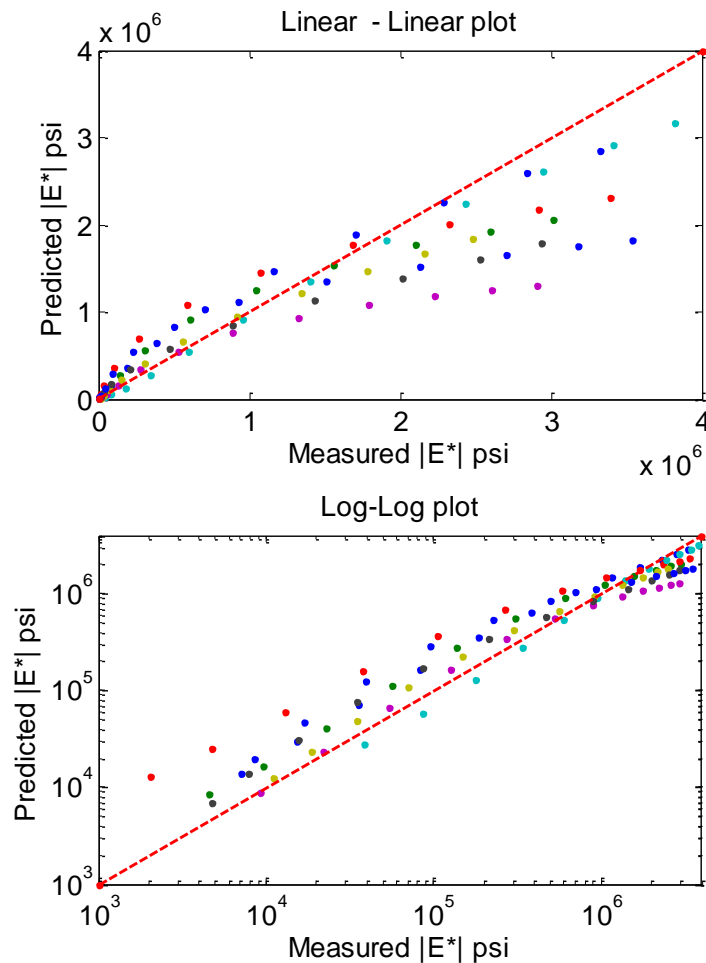


Figure 16: The modified Witczak’s equation developed as part of the NCHRP 1-40D. The plot shows the predicted versus measured values for MDOT mixtures using the calibrated coefficients. $Se/Sy = 0.3749$, $R^2 = 0.885$ (log-log plot).

Evaluation of the ANNACAP software for predicting $|E^*|$ of MDOT mixtures

The research team evaluated the ANNACAP software, which is an artificial neural network (ANN)-based $|E^*|$ prediction model developed by FHWA’s Long Term Pavement Performance (LTPP) program (FHWA 2011 (web link), Kim 2010). The research team used the ANNACAP software to predict the $|E^*|$ values using the volumetric properties of the MDOT mixtures tested, then compared with the laboratory-measured $|E^*|$ values. Figure 17 shows the measured versus ANNACAP-predicted $|E^*|$ values, where the correlation

coefficient (R^2) was 0.775. As shown, the software, which was trained (i.e., calibrated) nationally, did not perform very well in predicting $|E^*|$ values of MDOT mixtures tested in this project.

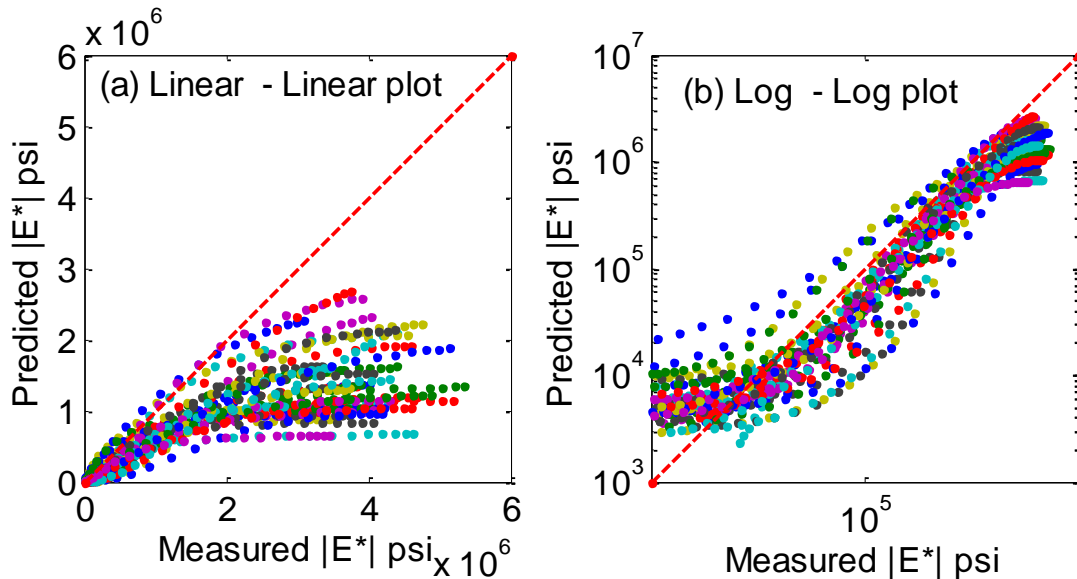


Figure 17: Predicted versus measured values for MDOT mixtures using the ANNACAP software: (a) Linear-Linear plot, (b) Log-Log plot.

Development and Validation of a New ANN-based $|E^*|$ Predictive Model Trained for Michigan Mixtures

In the field of Computer Science, Artificial Neural Networks (ANNs) have been extensively utilized for pattern recognition in images, with special emphasis to the application of face detection (Propp and Samal 1992, Rowley et al. 1998, Sung and Poggio 1998). For road materials, ANNs have been employed to classify aggregates size (Kim et al. 2004), predict pavement layer moduli (Ceylan et al. 2007; Kim and Kim 1998), simulate rutting and fatigue performance of asphalt mixtures (Huang et al., 2007; Tarefder et al. 2005a), estimate the thickness of the pavement layers (Gucunski and Krstic 1996), approximate the resilient modulus of base materials (Tutumluer and Seyhan 1998), and relate

mixture variables to permeability and roughness (Choi et al. 2004; Tarefder et al. 2005b). ANN models are very useful in predicting certain engineering outputs (e.g., $|E^*|$) from a number of input variables (e.g., asphalt volumetrics).

In an effort to develop an improved $|E^*|$ predictive model for the future MDOT mixtures that are not similar to the ones tested in this study, an ANN model was developed using the data generated as part of this project. In this study, an ANN was developed to predict $|E^*|$ at different temperatures and frequencies using the following inputs:

- (i) p_{200} = Percentage of aggregate passing #200 sieve
- (ii) p_4 = Cumulative percentage of aggregate retained in #4 sieve
- (iii) $p_{3/8}$ = Cumulative percentage of aggregate retained in 3/8-inch sieve
- (iv) $p_{3/4}$ = Cumulative percentage of aggregate retained in 3/4-inch sieve
- (v) V_a = Percentage of air voids (by volume of mix)
- (vi) V_{beff} = Percentage of effective asphalt content (by volume of mix)
- (vii) $|G^*|_b$ = Dynamic shear modulus of asphalt binder (psi)
- (viii) δ_b = Binder phase angle associated with $|G^*|_b$ (degrees)
- (ix) f = reduced frequency (Hz) corresponding to each $|G^*|$ and δ_b .

These are the same inputs used in FHWA's ANNACAP model, except the reduced frequency (see Table 3, ANNACAP = K-1 model). It is noted that the ANN-algorithm developed in this study automatically generates the $|G^*|$ master curve and determines the shift factor polynomial coefficients (i.e., a_1 and a_2 of $a_T(T)$ – see Equation [4]) and uses them to calculate the reduced frequency (i.e., the input (ix) above). Therefore, the user does not need to find reduced frequency. The user inputs the $|G^*|$ and phase angle values at certain frequencies and

temperatures, then the software generates the $|G^*|$ master curve and computes the reduced frequency, which is subsequently used in ANN to compute $|E^*|$.

Structure of the ANN

A feed-forward (back-propagation) network of one hidden layer and one output layer was determined to be the optimum network for the ANN model (

Figure 18). This ANN structure was obtained by a trial and error process that involves trial of many ANN structures (Demuth and Beale 2004).

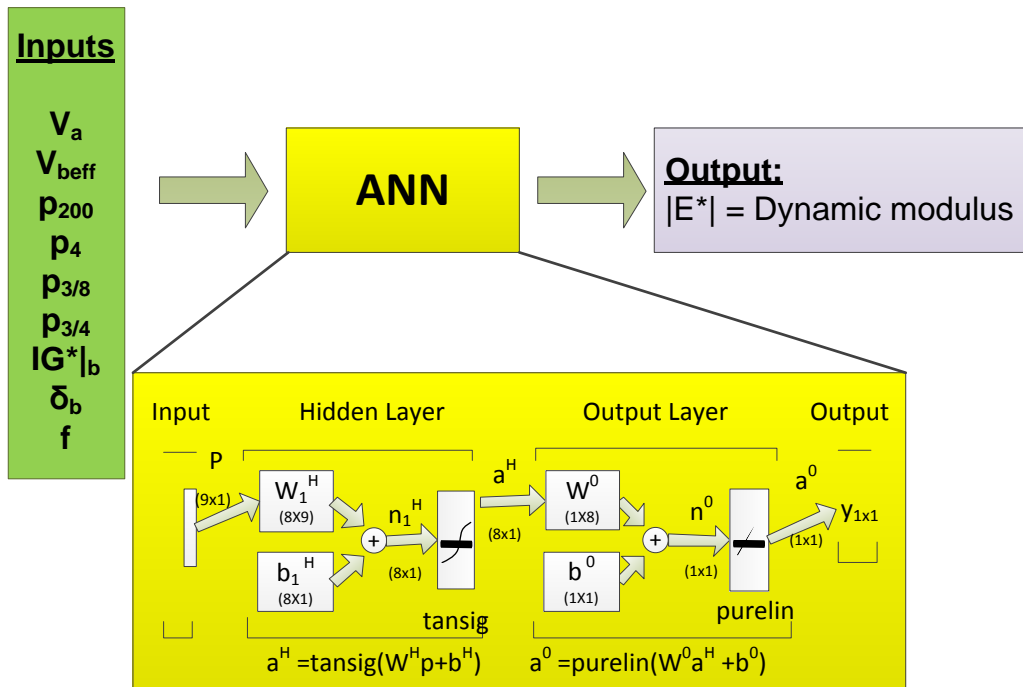


Figure 18: Structure of the ANN model.

The steps below describe how the ANN shown in

Figure 18 calculates output y (which is the $|E^*|$ in this case) from a set of 9 inputs (which are p_{200} , p_4 , $|G^*|$, etc. shown in the previous page). These steps are herein called “forward computation”.

Step 1: Compute the output of the Hidden Layer (\mathbf{a}^H) using Equations [15] and [16]. The variables in bold letters in these equations indicate that they are matrices (or vectors) and the multiplication and summation in the equation are matrix operations. The *tansig* function in Equation [16], however, is applied to each element of the vector.

$$\mathbf{n}^H = \mathbf{W}^H \mathbf{p} + \mathbf{b}^H \quad [15]$$

$$\mathbf{a}^H = \text{tansig}(\mathbf{n}^H) \quad [16]$$

where \mathbf{p} is the input vector (9×1), \mathbf{W}^H is the weight matrix (8×9) and \mathbf{b}^H is the bias vector (8×1) of the Hidden Layer, and the *tansig* is the transfer function given as:

$$\text{tansig}(x) = \frac{2}{1 + \exp(-2x)} - 1 \quad [17]$$

Step 2: Compute the output of the Output Layer by using the output of the Hidden Layer (\mathbf{a}^H) as follows:

$$n^o = \mathbf{W}^o \mathbf{a}^H + b^o \quad [18]$$

$$y = \text{purelin}(n^o) = n^o \quad [19]$$

where y is the positive or negative scalar output of the entire network, \mathbf{a}^H is the output of the Hidden Layer (8×1), \mathbf{W}^o is the weight matrix (1×8) and b^o is the bias constant of the Output Layer.

Training the ANN

The training initiates with random weights (i.e., \mathbf{W}^H and \mathbf{W}^0) and biases (i.e., \mathbf{b}^H and b^0). The forward computation described in the previous section is repeated many times while adjusting these weights and biases. Each repetition is called an *epoch*, which continues until the error between the predicted output from the ANN (i.e., $y = |E^*|_{\text{predicted}}$) and actual target output (i.e., $y_{\text{target}} = |E^*|_{\text{measured}}$) is minimized. The ANN model was trained by using 41 different Job Mix Formulas (JMFs). It is noted that a JMF is the mix design the contractor uses when paving a particular mix. Twelve individual $|G^*|$ values and 12 phase angle values were picked from the $|G^*|$ and phase angle master curves of for each HMA type to cover a wide range of frequencies and temperatures. This resulted in a total of 492 data points. MATLAB's ANN toolbox was used for this purpose. In this toolbox, the mean square error between the measured and predicted $|E^*|$ decreases as the number of epochs increases. It is noted that the training dataset is divided into three subsets: *Training* (80% of the dataset), *Validation* (10% of the dataset), and *Test* (10% of the dataset). The ANN primarily uses the information from the *Training* dataset and adjusts the weights and biases accordingly. While doing so, it also looks at the prediction accuracy of *Validation* dataset and makes sure that error in *Validation* data set is close to the error from the *Training* dataset. If the error in *Validation* dataset is significantly larger than the error in *Training* dataset, it means that the ANN is over trained to the *Training* dataset and memorized the *Training* dataset rather than learning the overall interrelation between the input and output. Lastly, the *Testing* dataset, which is not used during adjusting weights and biases, is used as an independent validation of the model. Figure 19 shows the change in the mean squared error as the epochs increase. As shown, all curves (Training, Validation and Test) are close to each other, which means that

the ANN developed in this study learned from the training data, it did not memorize.

Performance of the ANN model was evaluated from the plot of the predicted versus measured values of $|E^*|$ for the training, validation and testing datasets as shown in Figure 20. Coefficient of determination (R^2) with respect to the line of equality was computed, which is used to measure the goodness-of-fit of the trend. As shown in Figure 20, ANN predictions lay around the line-of-equality with R^2 's ranging from 0.951 to 0.963. Considering the sample-to-sample variability and other factors, this is a good result and better than the Modified Witczak model (see Figure 14) and the ANNACAP (see Figure 17).

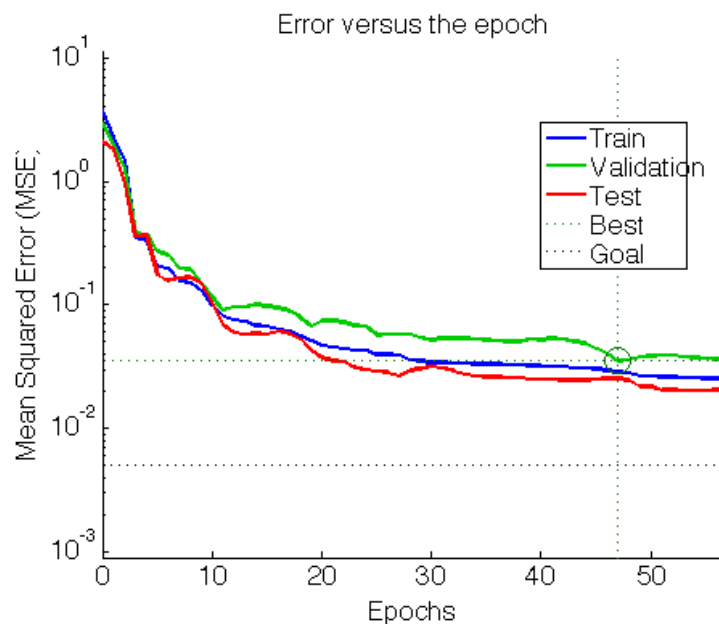


Figure 19: Errors versus the epochs in the ANN model developed in this project

Even though during the training, 10% of the data is set aside by the ANN algorithm for testing of the ANN model, an additional (independent) validation was performed by setting aside 9 different asphalt mixture $|E^*|$ data, which were not used in the ANN development process. Then, these 9 mixtures were used in forward computation of $|E^*|$ values using the ANN developed. Figure 21 presents the predicted versus measured values using this independent data set. As shown, independent validation of the ANN model

exceeds the accuracy of the calibrated Modified Witczak model (see Figure 16). Both of the calibrated Modified Witczak and the ANN models are incorporated into the DYNAMOD software developed as part of this project.

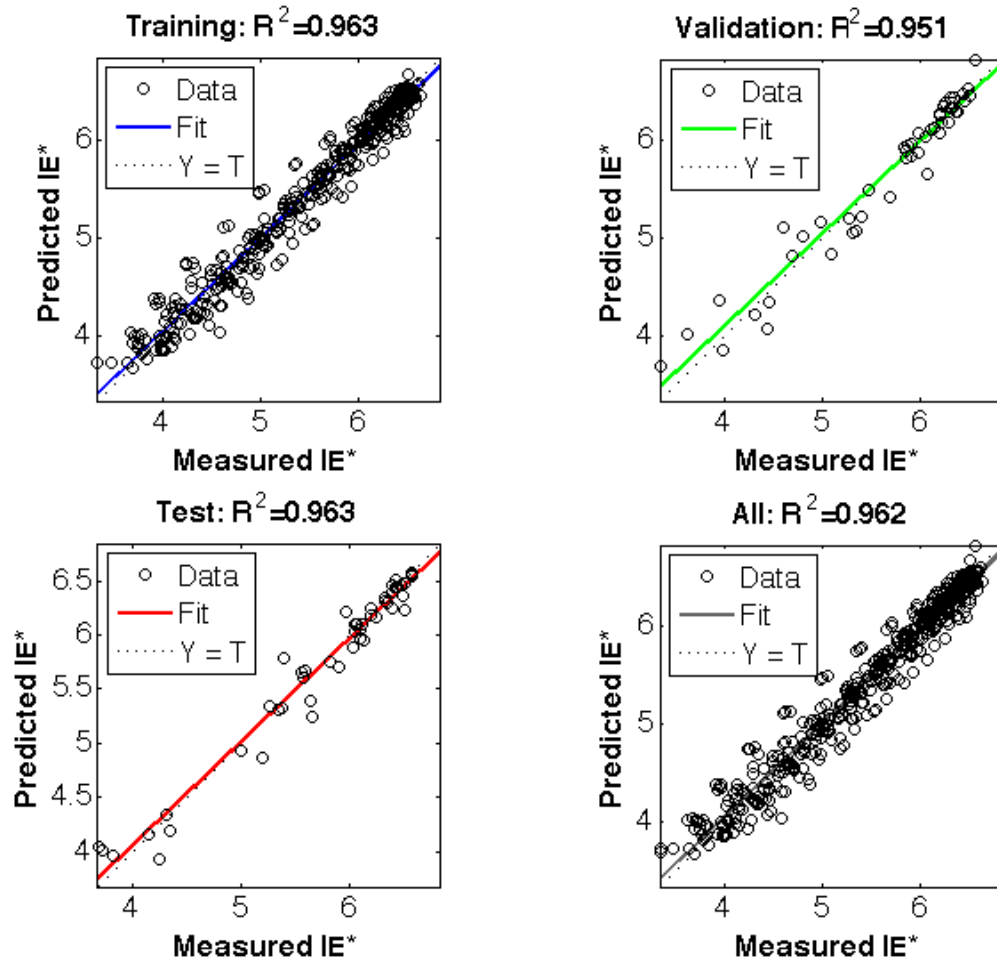


Figure 20: Predicted versus measured $|E^*|$ values for Training, Validation and Testing datasets as well as all the data (for mixtures used during development of the model).

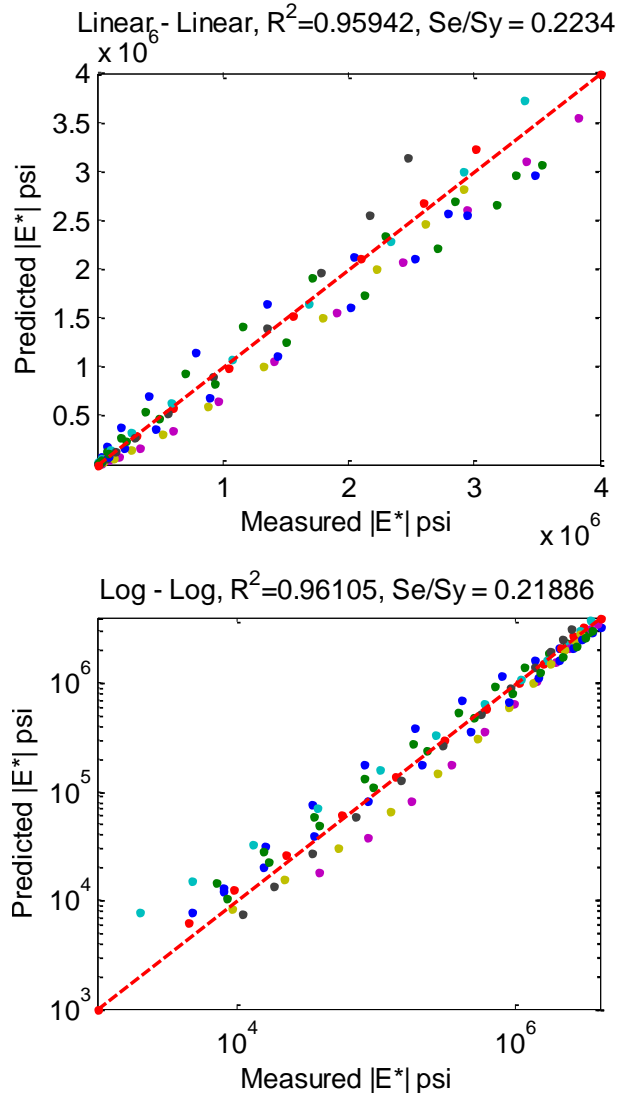


Figure 21: Predicted versus measured values for MDOT mixtures using the MSU-ANN model for mixtures not used during development of the model

Development of the DYNAMOD Software

In order to facilitate the use of all the laboratory data, a user-friendly standalone software called DYNAMOD was developed for MDOT engineers/designers to use for the following:

1. The designer will have ability to view the $|E^*|$ mastercurve and generate an input file directly readable by M-E PDG/DARWin-ME software of any mixture tested as

part of the project. In addition, the $|E^*|$ mastercurve of any other mixture can be predicted using the calibrated empirical Modified Witczak model and the ANN model implemented in the software. Figure 22 shows a snapshot of the $|E^*|$ database tab.

2. The designer will have the ability to view the $|G^*|$ master curve and generate an input file directly readable by M-E PDG/DARWin-ME software of any binder tested as part of the project. Figure 23 shows a snapshot of the $|G^*|$ database tab.
3. The designer will have ability to view the Indirect Tensile Strength (IDT) and Creep compliance (D(t)) excel file for any asphalt mixture tested as part of the project. Figure 24 shows a snapshot of the IDT database.

A tutorial is included in Appendix F, which includes a detailed description of the software.

	2 (BASE)	3 (BASE)	3 (LEVELING)	4 (LEVELING/TOP)	5 (TOP)
Mainline - E50	2E50 (PG64-22) [9]	3E50 (PG64-22) [10]	3E50 (PG70-22p) [95]	4E50 (PG70-22p) [96]	5E50 (PG70-22p) [97]
High stress - E50	2E50 (PG64-22) [9]	3E50 (PG64-22) [10]	3E50 (PG76-22p) [98]	4E50 (PG76-22p) [99]	5E50 (PG76-22p) [100]
Mainline - E30	2E30 (PG64-22) [1]	3E30 (PG64-22) [2]	3E30 (PG70-22p) [89]	4E30 (PG70-22p) [90]	5E30 (PG70-22p) [91]
High stress - E30	2E30 (PG64-22) [1]	3E30 (PG64-22) [2]	3E30 (PG76-22p) [92]	4E30 (PG76-22p) [93]	5E30 (PG76-22p) [94]
Mainline - E10	2E10 (PG58-22) [17]	3E10 (PG58-22) [18]	3E10 (PG64-22) [101]	4E10 (PG64-22) [102]	5E10 (PG64-22) [103]
High stress - E10	2E10 (PG58-22) [17]	3E10 (PG58-22) [18]	3E10 (PG70-22p) [104]	4E10 (PG70-22p) [105]	5E10 (PG70-22p) [106]
Mainline - E3	2E3 (PG58-28) [25]	3E3 (PG58-22) [26]	3E3 (PG64-22) [107]	4E3 (PG64-22) [108]	5E3 (PG64-22) [109]
High stress - E3	2E3 (PG58-22) [25]	3E3 (PG58-22) [26]	3E3 (PG70-22p) [110]	4E3 (PG70-22p) [111]	5E3 (PG70-22p) [112]
Mainline - E1	2E1 (PG58-22) [41]	3E1 (PG58-22) [42]	3E1 (PG58-22) [119]	4E1 (PG58-22) [120]	5E1 (PG58-22) [121]
High stress - E1	2E1 (PG58-22) [41]	3E1 (PG58-22) [42]	3E1 (PG64-22) [122]	4E1 (PG64-22) [123]	5E1 (PG64-22) [124]
Mainline - E03	2E03 (PG58-22) [33]	3E03 (PG58-22) [34]	3E03 (PG58-22) [113]	4E03 (PG58-22) [114]	5E03 (PG58-22) [115]
High stress - E03	2E03 (PG58-22) [33]	3E03 (PG58-22) [34]	3E03 (PG64-22) [116]	4E03 (PG64-22) [117]	5E03 (PG64-22) [118]
Mainline - GGSP	NA	NA	NA	NA	GGSP (PG70-22P) [125]
High stress - GGSP	NA	NA	NA	NA	GGSP (PG76-22P) [126]
Mainline - LVSP	NA	NA	NA	LVSP (PG58-22) [127]	LVSP (PG58-22) [127]
High stress - LVSP	NA	NA	NA	LVSP (PG64-28) [128]	LVSP (PG64-28) [128]

Figure 22: Snapshot of the $|E^*|$ database in the DYNAMOD software developed by the research team

MDOT |E*|, |G*| and IDT Strength Database

|E*| Database |G*| Database |IDT| Database

View |G*| XLS File Export |G*| as DARWin-ME Input

	PG 58	PG 64	PG 70	PG 76
-22	PG 58-22	PG 64-22	PG 70-22	PG 76-22
-22P	PG 58-22P	PG 64-22P	PG 70-22P	PG 76-22P
-28	PG 58-28	PG 64-28	PG 70-28	PG 76-28
-28P	PG 58-28P	PG 64-28P	PG 70-28P	PG 76-28P
-34	PG 58-34	PG 64-34	PG 70-34	PG 76-34
-34P	PG 58-34P	PG 64-34P	PG 70-34P	PG 76-34P

Figure 23: Snapshot of the |G*| database in the DYNAMOD software developed by the research team

MDOT |E*|, |G*| and IDT Strength Database

|E*| Database |G*| Database |IDT| Database

Metro View |IDT| Excel File

	2 (BASE)	3 (BASE)	3 (LEVELING)	4 (LEVELING/TOP)	5 (TOP)
Mainline - E50	2E50 (PG64-22) [9]	3E50 (PG64-22) [10]	3E50 (PG70-22p) [95]	4E50 (PG70-22p) [96]	5E50 (PG70-22p) [97]
High stress - E50	2E50 (PG64-22) [9]	3E50 (PG64-22) [10]	3E50 (PG76-22p) [98]	4E50 (PG76-22p) [99]	5E50 (PG76-22p) [100]
Mainline - E30	2E30 (PG64-22) [1]	3E30 (PG64-22) [2]	3E30 (PG70-22p) [89]	4E30 (PG70-22p) [90]	5E30 (PG70-22p) [91]
High stress - E30	2E30 (PG64-22) [1]	3E30 (PG64-22) [2]	3E30 (PG76-22p) [92]	4E30 (PG76-22p) [93]	5E30 (PG76-22p) [94]
Mainline - E10	2E10 (PG58-22) [17]	3E10 (PG58-22) [18]	3E10 (PG64-22) [101]	4E10 (PG64-22) [102]	5E10 (PG64-22) [103]
High stress - E10	2E10 (PG58-22) [17]	3E10 (PG58-22) [18]	3E10 (PG70-22p) [104]	4E10 (PG70-22p) [105]	5E10 (PG70-22p) [106]
Mainline - E3	2E3 (PG58-28) [25]	3E3 (PG58-22) [26]	3E3 (PG64-22) [107]	4E3 (PG64-22) [108]	5E3 (PG64-22) [109]
High stress - E3	2E3 (PG58-22) [25]	3E3 (PG58-22) [26]	3E3 (PG70-22p) [110]	4E3 (PG70-22p) [111]	5E3 (PG70-22p) [112]
Mainline - E1	2E1 (PG58-22) [41]	3E1 (PG58-22) [42]	3E1 (PG58-22) [119]	4E1 (PG58-22) [120]	5E1 (PG58-22) [121]
High stress - E1	2E1 (PG58-22) [41]	3E1 (PG58-22) [42]	3E1 (PG64-22) [122]	4E1 (PG64-22) [123]	5E1 (PG64-22) [124]
Mainline - E03	2E03 (PG58-22) [33]	3E03 (PG58-22) [34]	3E03 (PG58-22) [113]	4E03 (PG58-22) [114]	5E03 (PG58-22) [115]
High stress - E03	2E03 (PG58-22) [33]	3E03 (PG58-22) [34]	3E03 (PG64-22) [116]	4E03 (PG64-22) [117]	5E03 (PG64-22) [118]
Mainline - GGSP	NA	NA	NA	NA	GGSP (PG70-22P) [125]
High stress - GGSP	NA	NA	NA	NA	GGSP (PG76-22P) [126]
Mainline - LVSP	NA	NA	NA	LVSP (PG58-22) [127]	LVSP (PG58-22) [127]
High stress - LVSP	NA	NA	NA	LVSP (PG64-28) [128]	LVSP (PG64-28) [128]

Figure 24: Snapshot of the IDT database in the DYNAMOD software developed by the research team

CONCLUSIONS

This project partially addressed the need for generating a catalog of DARWin-ME (or ME-PDG) software input variables for typical asphalt mixtures used in Michigan. The testing program included (i) complex (dynamic) modulus ($|E^*|$) tests using AMPT (Asphalt Mixture Performance Tester), (ii) complex (dynamic) shear modulus ($|G^*|$) tests (frequency sweep) using DSR (Dynamic Shear Rheometer) and (iii) Indirect Tensile (IDT) Strength tests. Creep compliance ($D(t)$) values at low temperatures (as required by DARWin-ME) were computed using the $|E^*|$ master curve via linear viscoelastic interconversion procedures. The work plan also included evaluation of the Modified Witzczak's $|E^*|$ predictive equation and re-calibration of this equation for MDOT mixtures. The research team also evaluated the ANNACAP software (a recent product of FHWA-sponsored research) for prediction of $|E^*|$. Based on the tests and analyses presented in this report, the following conclusions were drawn:

1. The Modified-Witzczak (MW) model was calibrated for use in $|E^*|$ prediction of asphalt mixtures commonly used in the State of Michigan to be used in the Level 1 analysis of the DARWin-ME software. The calibrated model performed well in comparison with the laboratory measured data.
2. The ANNACAP software, which was developed by the FHWA's LTPP program, was evaluated for use in the $|E^*|$ prediction of asphalt mixtures commonly used in the State of Michigan. The software did not perform well for MDOT mixtures in predicting $|E^*|$.

3. A new ANN-based model was developed as part of this research. The new ANN-based model did very well in predicting $|E^*|$ values of Michigan mixtures.
4. A user friendly software called DYNAMOD was developed for MDOT engineers/designers to be utilized in viewing $|E^*|$ and $|G^*|$ mastercurves of tested mixtures and binders and to predict $|E^*|$ values for mixtures that have not been tested for use in the Level 1 analysis in the DARWin-ME software.
5. The research team provided a summary of $|E^*|$ values based on MDOT mix designation. As expected; 3E mixtures were generally stiffer than 4E and 5E mixtures. However the trend was not always consistent in all temperatures. A clear trend should not be expected since there are many variables that play a role in the magnitude of $|E^*|$ at different temperatures and frequencies.
6. The research team provided a comparison of variation in $|E^*|$ mastercurves based on MDOT mix designations (e.g., 3E10). The research team does not recommend grouping mixtures based on MDOT mix designation and use average of $|E^*|$ values for the given designation. Instead, the $|E^*|$ master curves of different mixtures tested in this project could be viewed in the DYNAMOD software, and depending on whether rutting or fatigue cracking is a concern, an unconservative curve should be chosen based on expected behavior illustrated in Figure 7.

RECOMMENDATIONS FOR FURTHER RESEARCH

Even though various asphalt mixtures and binders were characterized in this project; it is recommended that a wider range of materials be characterized in the future. Only 44 unique asphalt binders were characterized in this study. The tested binders did not cover all asphalt performance grades used by MDOT. In addition, more asphalt mixtures should be characterized for $|E^*|$ and low temperature cracking.

Warm Mix Asphalt (WMA) is becoming more popular than HMA in pavement design throughout the US. Only a limited number of WMAs were characterized in this study. Two graphs comparing WMA and HMA $|E^*|$ master curves are shown in Figure 25 and Figure 26. Figure 25 clearly shows that the WMA is softer than the HMA. In Figure 26, WMA is shown as in-between HMAs 51A and 51B, however, it should be noted that when the JMFs were compared, the gradation of 51A was much coarser than the 51B and 51C, which were almost identical. Therefore, it is more appropriate to compare 51B-HMA and 51C-WMA. As shown, 51C-WMA is slightly softer than the 51B-HMA. It is recommended that more WMAs used in the State of Michigan be characterized and added to the database to be utilized in future pavement designs.

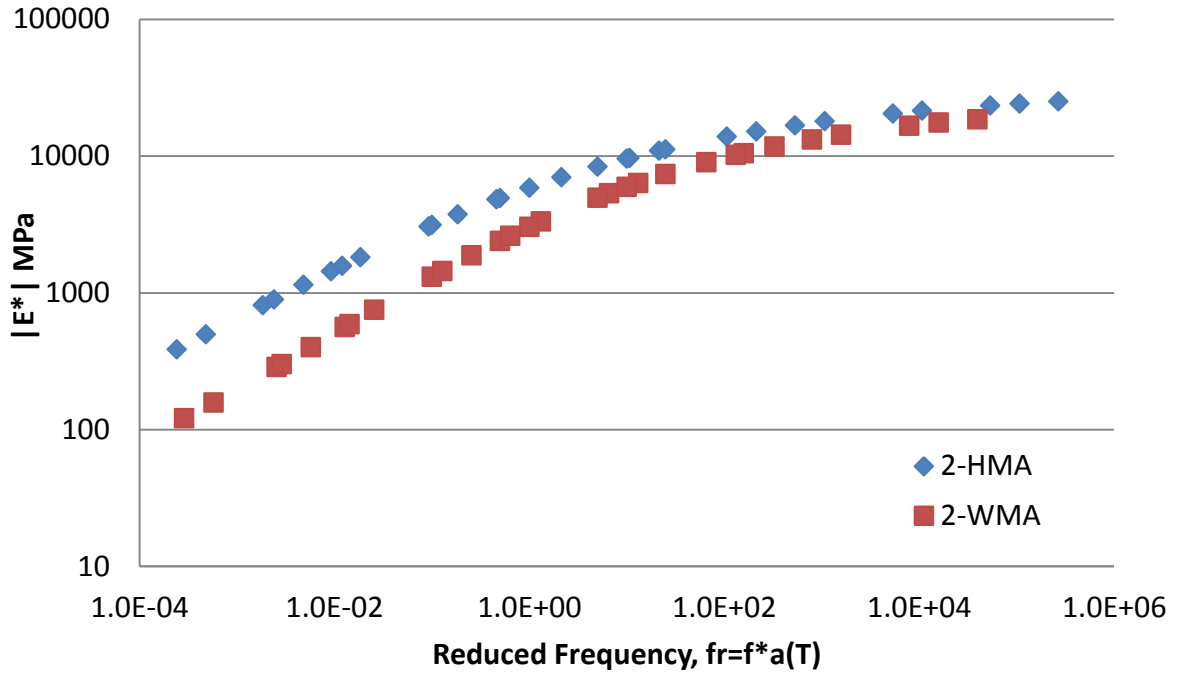


Figure 25: WMA versus HMA for the same type of MDOT mixture (3E30)

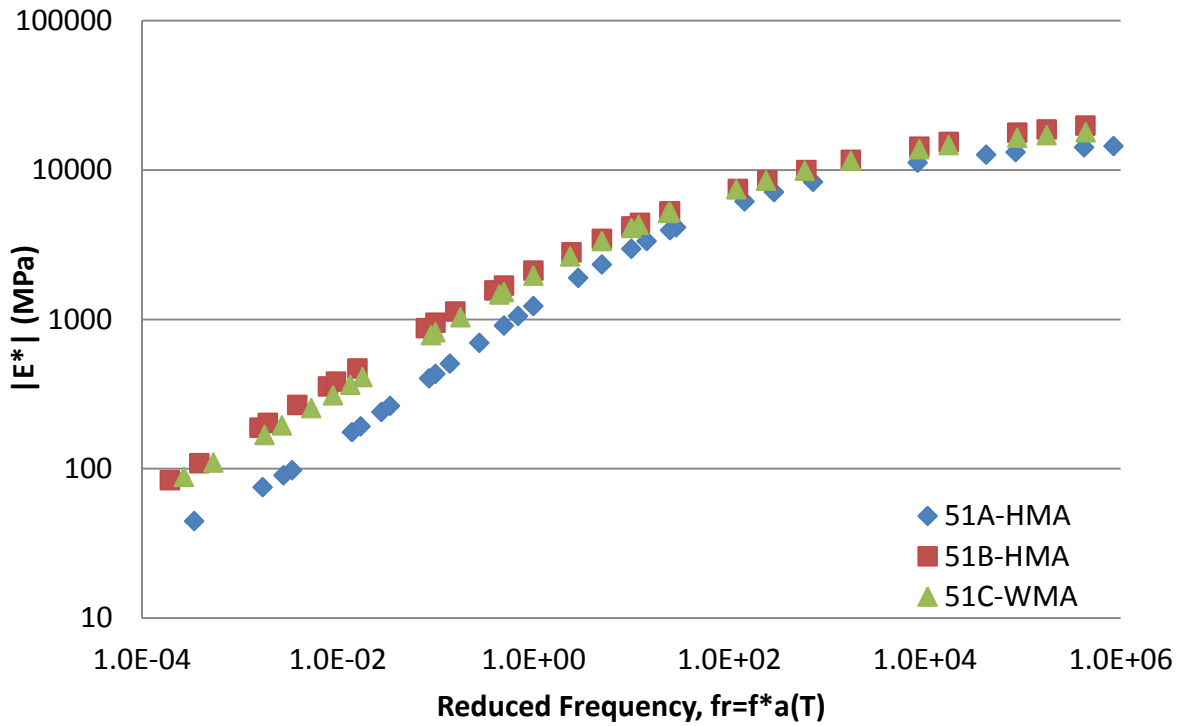


Figure 26: WMA versus HMA for the same type of MDOT mixture (LVSP)

One important factor that was not taken into consideration for pavement material characterization in this project is oxidation/aging of asphalt mixtures. The provided database is very helpful in terms of newly constructed pavements. On the other hand, if MDOT engineers were to design an overlay for rehabilitation, the moduli of existing layers are not available. It is indeed recommended that an aging study be carried out on asphalt materials used in the State of Michigan. Asphalt mixtures characterized in this study can be used for that purpose. Since the $|E^*|$ test is considered a non-destructive test, available samples can be further used in an investigation of the effect of oxidation/aging on asphalt pavement material properties. Along with the available mixtures; field cores should be obtained and tested as well.

RECOMMENDATIONS FOR IMPLEMENTATION

This research produced the DYNAMOD software, which can serve as a database for $|E^*|$, $|G^*|$, IDT strength and $D(t)$ parameters for many Michigan asphalt mixtures and binders tested during this project. The DYNAMOD also includes calibrated Modified Witczak model as well as the ANN model developed in this research for prediction of $|E^*|$ from the volumetric properties of the mixtures. The following is recommended when using the DYNAMOD software during future DARWin-ME analyses and designs:

1. Typically asphalt mixtures are selected based on the MDOT mix designation (e.g., 4E1, 3E03 etc.) and binder PG (e.g., PG70-22). If the selected MDOT mix designation and the binder PG have been tested as part of this research and shown in the DYNAMOD as shaded green, the laboratory data in the DYNAMOD software should be exported and used in DARWin-ME analysis as Level 1 input. It should be acknowledged that there will be many uncertainties at the design stage about the mix to be placed during actual construction. These include (i) the job mix formula (JMF) of actual mix that will be placed, which will most certainly have different gradation, type of aggregate, binder content and volumetric properties than the mixture(s) tested in this research, and (ii) the source of the asphalt binder, even though the PG might be the same. If there are more than one mixture tested for a given MDOT mix designation (e.g., 4E1) it is recommended that the designer will choose the $|E^*|$ that will result in least conservative predictions of fatigue cracking and rutting. The designer can refer to Figure 7 to compare different $|E^*|$ curves in terms of expected rutting and fatigue performance and make an appropriate decision. Similarly, if there

- is more than one binder tested for the same PG, the Figure 7 can also be used as a guide to select the least conservative $|G^*|$ in terms of rutting and fatigue cracking.
2. If $|E^*|$ of a specific type of MDOT mix has not been tested and shown as shaded yellow in DYNAMOD software, it is recommended that the designer should use either the calibrated Modified Witczak or the ANN model to predict the $|E^*|$ and use as a Level 1 input in DARWin-ME. Both of these models are available in the DYNAMOD software. The ANN model is, in general, more accurate than the Modified Witczak model. However, it should be noted that the ANNs are usually not very good at extrapolating. Therefore, if a mixture that is expected to be used in the field will have vastly different JMF than the JMFs of the asphalt mixtures used in this research, it is recommended that the Modified Witczak be used for prediction of the $|E^*|$.
 3. It is recommended that MDOT should run $|G^*|$ tests on binders that were not tested as part of this research and complete the database as much as possible. MDOT laboratory has capability to measure $|G^*|$ and phase angle required by DARWin-ME. If $|G^*|$ data is not available in the DYNAMOD and not tested later, the designer either can choose Level 3 analysis in DARWin-ME or choose a $|G^*|$ of a PG close to the PG of the binder that is expected to be used and use as Level 1 or 2 input in DARWin-ME.
 4. For IDT and $D(t)$, there is no predictive model from volumetrics. Therefore, if a specific type of MDOT mix has not been tested for IDT strength, the closest green shaded mixture in the DYNAMOD may be selected and used in DARWin-ME.

REFERENCES

- AASHTO PP 60-09 Preparation of Cylindrical Performance Test Specimens Using the Superpave Gyratory Compactor (SGC), in AASHTO PP 60-09. 2011, American Association of State Highway and Transportation Officials, Washington, D.C.
- AASHTO PP 61-10 Developing Dynamic Modulus Master Curves for Hot Mix Asphalt (HMA) Using the Asphalt Mixture Performance Tester (AMPT), in AASHTO PP 61-10. 2011, American Association of State Highway and Transportation Officials, Washington, D.C.
- AASHTO PP 62-10 Developing Dynamic Modulus Master Curves for Hot Mix Asphalt (HMA), in AASHTO PP 62-10. 2011, American Association of State Highway and Transportation Officials, Washington, D.C.
- AASHTO T 322-07 Determining the Creep Compliance and Strength of Hot-Mix Asphalt (HMA) Using the Indirect Tensile Test Device, in AASHTO T 322-07. 2007, American Association of State Highway and Transportation Officials, Washington, D.C.
- AASHTO T 342-11 Determining Dynamic Modulus of Hot Mix Asphalt (HMA), in AASHTO T 342-11. 2011, American Association of State Highway and Transportation Officials, Washington, D.C.
- AASHTO, "Mechanistic-Empirical Pavement Design Guide: A Manual of Practice: Interim Edition," American Association of State Highway and Transportation Officials 2008.
- Advanced Research Associates. (2004). 2002 Design Guide: Design of New and Rehabilitated Pavement Structures, NCHRP 1-37A Project, National Cooperative Highway Research Program, National Research Council, Washington, DC.
- Al-Khateeb, G., A. Shenoy, N. Gibson, T. Harman. (2006). A New Simplistic Model for Dynamic Modulus Predictions of Asphalt Paving Mixtures. Association of Asphalt Paving Technologists Annual Meeting. Paper Preprint CD.
- Al-Khateeb, G., Shenoy, A., Gibson, N., and Harman, T. "A New Simplistic Model for Dynamic Modulus Predictions of Asphalt Paving Mixtures", Journal of the AAPT, Vol. 75E, 2006.
- Andrei, D., Witczak, M.W., and W. Mirza. (1999) "Development of Revised Predictive Model for the Dynamic (Complex) Modulus of Asphalt Mixtures," Interteam Technical Report, NCHRP Project 1-37A, University of Maryland.
- ASTM D 2493-09. (2009). Viscosity-Temperature Chart for Asphalts, ASTM International, West Conshohocken, PA.
- Azari, H., Al-Khateeb, G. Shenoy, A. and Gibson, N. H. (2007) "Comparison of Simple Performance Test $|E^*|$ of Accelerated Loading Facility Mixtures and Prediction $|E^*|$:

- Use of NCHRP 1-37A and Witczak's New Equations", *Transportation Research Record: Journal of the Transportation Research Board*, Vol. 1998, pp 1-9.
- Bari, J. (2005). Development of a New Revised Version of the Witczak E* Predictive Models for Hot Mix Asphalt Mixtures. PhD Dissertation. Arizona State University.
- Bari, J. and Witczak, M.W. (2007) "New Predictive Models for the Viscosity and Complex Shear Modulus of Asphalt Binders for Use with the Mechanistic-Empirical Pavement Design Guide", *Transportation Research Record: Journal of the Transportation Research Board*, No 2001, pp 9-19.
- Bari, J., and Witczak, M.W. "Development of a New Revised Version of the Witczak E* Predictive Model for Hot Mix Asphalt Mixtures", 2005.
- Birgisson, B., G. Sholar, and R. Roque (2005) Evaluation of Predicted Dynamic Modulus for Florida Mixtures, *Journal of the Transportation Research Board*, TRR 1929, Washington, D.C.
- Bonnaure, F., G. Gest, A. Garvois, and P. Uge. (1977) "A New Method of Predicting the Stiffness of Asphalt Paving Mixes," *Journal of the Association of Asphalt Paving Technologists*, Vol. 46
- Ceylan, H., Gopalakrishnan, K. and Guclu A. (2007). "Advanced Approaches to Characterizing Nonlinear Pavement System Responses." *Transportation Research Record: Journal of the Transportation Research Board*, No. 2005: 86-94.
- Choi, J.-H., Adams, T.M. and Bahia, H.U. (2004). "Pavement roughness modeling using back-propagation neural networks." *Computer-Aided Civil and Infrastructure Engineering*, Vol. 19 (4): 295-303.
- Christensen Jr., D. W., T. K. Pellinen, and R. F. Bonaquist. (2003). Hirsch Model for Estimating the Modulus of Asphalt Concrete. *Journal of the Association of Asphalt Paving Technologists (AAPT)*, Vol. 72.
- Clyne, T.R., Li, X., Marasteanu, M.O., and Skok, E.L. Dynamic and Resilient Modulus of MN DOT Asphalt Mixtures. MN/RC-2003-09. Minnesota Department of Transportation, Minneapolis, 2003.
- Demuth, H. and Beale, M., 2004. *Neural Network Toolbox for use with Matlab (User's guide)*. Version 4, The Mathworks, Inc., Natick, MA.
- FHWA (2011): Web site:
<http://www.fhwa.dot.gov/publications/research/infrastructure/pavements/ltp/10035/012.cfm>
- Flintsch, G., Loulizi, A., Diefenderfer, S. D., Diefenderfer, B. K., and Galal, K. (2008) "Asphalt Materials Characterization In Support Of The Mechanistic-Empirical

- Pavement Design Guide Implementation Efforts In Virginia” Transportation Research Record: Journal of the Transportation Research Board, Issue 2057, pp 114-125.
- Flintsch, G., Loulizi, A., Diefenderfer, S. D., Diefenderfer, B. K., and Galal, K. (2008) “Asphalt Materials Characterization In Support Of The Mechanistic-Empirical Pavement Design Guide Implementation Efforts In Virginia” Transportation Research Record: Journal of the Transportation Research Board, Issue 2057, pp 114-125.
- Flintsch, G.W., Al-Qadi, I.L., Loulizi, A., and Mokarem, D. Laboratory Tests for Hot-Mix Asphalt Characterization in Virginia. VTRC 05-CR22. Virginia Transportation Research Council, Charlottesville, 2005.
- Gucunski, N. and Krstic, V. (1996). “Backcalculation of pavement profiles from spectral-analysis-of-surface-waves test by neural networks using individual receiver spacing approach.” *Transportation Research Record: Journal of the Transportation Research Board*, No. 1526: 6-13.
- Huang, C., Najjar, Y.M. and Romanoschi, S.A. (2007). “Predicting asphalt concrete fatigue life using artificial neural network approach.” Transportation Research Board Annual Meeting, Washington, DC.
- Kim, H., Rauch, A.F. and Haas, C.T. (2004). “Automated quality assessment of stone aggregates based on laser imaging and a neural network.” *Journal of Computing In Civil Engineering*, Vol. 18 (1): 58-64.
- Kim, Y. and Kim, R. (1998). “Prediction of layer moduli from falling weight deflectometer and surface wave measurements using artificial neural network.” *Transportation Research Record: Journal of the Transportation Research Board*, No. 1639: 53-61.
- Kim, Y. R., B.Underwood, M.Sakhaei Far, N.Jackson, and J.Puccinelli (2010), LTPP Computer Parameter: Dynamic Modulus, Federal Highway Administration Technical Report No FHWA-HRT-10-035, 260p.
- Kim, Y. R., Modeling of Asphalt Concrete, 1st ed., McGraw Hill, ASCE press, 2009.
- Kim, Y.R., King, M., and Momen, M. "Typical Dynamic Moduli Values of Hot Mix Asphalt in North Carolina and Their Prediction", CD-ROM. 84th Annual Meeting, TRB, 2005.
- M-E PDG Version 1.0, NCHRP 1-40 D (2007) Guide for Mechanistic-Empirical Design of New and Rehabilitated Pavement Structures, Final Report. NCHRP, National Research Council, Washington, D. C., March 2004, updated 2007.
- Mirza, M.W. and Witzak, M.W. (1995). “Development of a Global Aging System for Short and Long Term Aging of Asphalt Cements,” *Journal of the Association of Asphalt Paving Technologists*, 64, 393–418.

- Mohammad, L. (2010) Characterization of Louisiana Asphalt Mixtures for using Simple Performance Tests and M-E PDG, Recent research from Louisiana Department of Transportation and Development, URL: <http://rip.trb.org/browse/dproject.asp?n=12267>
- Mohammad, L., Saadeh, S., Obularedd, S., and Cooper, S. (2007) Characterization Of Louisiana Asphalt Mixtures Using Simple Performance Tests. Transportation Research Board 86th Annual Meeting, CD-ROM.
- Park, S. W. and R. A. Schapery. Methods of Interconversion between Linear Viscoelastic Material Functions. Part I – a Numerical Method Based on Prony Series. International Journal of Solids and Structures, Vol. 36, 1999, pp. 1653-1675.
- Propp, M. and Samal, A. (1992) “Artificial neural network architecture for human face detection”. *Intell. Eng. Systems Artificial Neural Networks 2*, pages 535–540.
- Robbins, M. M. and Timm, D. (2011) “Evaluation of Dynamic Modulus Predictive Equations for NCAT Test Track Asphalt Mixtures”, Proceedings of the Transportation Research Board 90th Annual Conference, January 23-27, 2011.
- Rowley, H., Baluja, S. and Kanade, T.(1998). “Neural network-based face detection” In *IEEE Patt. Anal. Mach. Intell.*, volume 20, pages 22–38.
- Sakhaeifar, M.S., Underwood, S., Ranjithan, R., and Kim, Y.R. (2009) “The Application Of Artificial Neural Networks For Estimating The Dynamic Modulus Of Asphalt Concrete”, Transportation Research Record: Journal of the Transportation Research Board, Vol. 2127, pp 173-186.
- Singh, D., Zaman, M., and Commuri, S. "Evaluation of Predictive Models for Estimating Dynamic Modulus of HMA Mixtures Used in Oklahoma", 2010.
- Sung, K. and Poggio, T. (1998) “Example-based learning for view-based face detection”, In *IEEE Patt. Anal. Mach. Intell.*, volume 20, pages 39–51.
- Tarefder, R.A, White, L. and Zaman, M. (2005b). “Neural network model for asphalt concrete permeability.” *Journal of Materials in Civil Engineering*, Vol. 17 (1) 19-27.
- Tarefder, R.A, White, L. and Zaman, M. (2005b). “Neural network model for asphalt concrete permeability.” *Journal of Materials in Civil Engineering*, Vol. 17 (1) 19-27.
- Tutumluer, E. and Seyhan, U. (1998). “Neural network modeling of anisotropic aggregate behavior from repeated load triaxial tests.” *Transportation Research Record: Journal of the Transportation Research Board*, No. 1615: 86-93.
- Witczak, M.W. and Fonseca, O.A., (1996). “Revised predicted model for dynamic (complex) modulus of asphalt mixtures”, Transportation Research Record, 1540. Washington DC: Transportation Research Board-National Research Council, 15–23.

Witczak, M.W., T.K. Pellinen, and M.M. El-Basyouny. (2002), "Pursuit of the simple performance test for asphalt concrete fracture/cracking", Journal of the Association of Asphalt Paving Technologists. Vol. 71, pp.767-778.

APPENDIX A: DYNAMIC MODULUS ($|E^*|$) PREDICTIVE EQUATIONS

Original Witczak Model (Andrei et al. 1999) - OW

Andrei et al. (1999) developed a revised version of the original Witczak $|E^*|$ predictive equation based on data from 205 mixtures with 2,750 data points

$$\log_{10} |E^*| = -1.249937 + 0.02923p_{200} - 0.001767(p_{200})^2 - 0.002841p_4 - 0.05809V_a - 0.082208 \frac{V_{beff}}{V_{beff} + V_a} + \frac{3.871977 - 0.0021p_4 + 0.003958p_{3/8} - 0.000017(p_{3/8})^2 + 0.00547p_{3/4}}{1 + \exp(-0.603313 - 0.313351 \log f - 0.393532 \log \eta)} \quad [A.1]$$

where:

- $|E^*|$ = Asphalt mix modulus, psi ($\times 10^5$).
- p_{200} = Percentage of aggregate passing #200 sieve.
- p_4 = Cumulative percentage of aggregate retained in #4 sieve.
- $p_{3/8}$ = Cumulative percentage of aggregate retained in 3/8-inch (9.56-mm) sieve.
- $p_{3/4}$ = Cumulative percentage of aggregate retained in 3/4-inch (19.01-mm) sieve.
- V_a = Percentage of air voids (by volume of mix).
- V_{beff} = Percentage of effective asphalt content (by volume of mix).
- f = Loading frequency (hertz).
- η = Binder viscosity at temperature of interest ($\times 10^6$ poise).

Modified Witczak Model (Bari 2005) - MW

In order to include binder $|G^*|$ in the predictive model, Witczak reformulated the model to include the binder variable directly. The revised model is as follows:

$$\log_{10} |E^*| = -0.349 + 0.754 \left(|G^*|_b^{-0.0052} \right) \left(\begin{aligned} &6.65 - 0.032P_{200} + 0.0027(P_{200})^2 + 0.011P_4 - 0.0001(P_4)^2 \\ &+ 0.006P_{3/8} - 0.00014(P_{3/8})^2 - 0.08V_a - 1.06 \left(\frac{V_{beff}}{V_{beff} + V_a} \right) \end{aligned} \right) \\ + \frac{2.558 + 0.032V_a + 0.713 \left(\frac{V_{beff}}{V_{beff} + V_a} \right) + 0.0124P_{3/8} - 0.0001(P_{3/8})^2 - 0.0098P_{3/4}}{1 + \exp(-0.7814 - 0.5785 \log |G^*|_b + 0.8834 \log \delta_b)} \quad [\text{A. 2}]$$

where:

$|G^*|_b$ = Dynamic shear modulus of asphalt binder (pounds per square inch).

δ_b = Binder phase angle associated with $|G^*|_b$ (degrees).

Because some of the mixtures in their database did not contain $|G^*|_b$ data, Bari and Witczak (2007) used the Cox-Mertz rule, using correction factors for the non-Newtonian behaviors (see equations 3–5), was used to calculate $|G^*|_b$ from A-VTS values:

$$|G^*|_b = 0.0051 f_s \eta_{f_s, T} (\sin \delta_b)^{7.1542 - 0.4929 f_s + 0.0211 f_s^2} \quad [\text{A. 3}]$$

$$\delta_b = 90 + (-7.3146 - 2.6162 * VTS') * \log(f_s * \eta_{f_s, T}) \\ + (0.1124 + 0.2029 * VTS') * \log(f_s * \eta_{f_s, T})^2 \quad [\text{A. 4}]$$

$$\log \log \eta_{f_s, T} = 0.9699 f_s^{-0.0527} * A + 0.9668 f_s^{-0.0575} * VTS \log T_R \quad [\text{A. 5}]$$

where:

f_s = Dynamic shear frequency.

δ_b = Binder phase angle predicted from equation 4 (degrees).

$\eta_{f_s, T}$ = Viscosity of asphalt binder at a particular loading frequency (f_s) and temperature (T) determined from equation 5 (centipoise).

T_R = Temperature in Rankine scale

Hirsch Model (Christensen et al. 2003) - HM

$$|E^*|_m = P_c \left[4,200,000 \left(1 - \frac{VMA}{100} \right) + 3 |G^*|_b \left(\frac{VFA * VMA}{10,000} \right) \right] + \frac{(1 - P_c)}{\frac{(1 - VMA/100)}{4,200,000} + \frac{VMA}{3 |G^*|_b (VFA)}} \quad [\text{A. 6}]$$

$$\phi = -21(\log Pc)^2 - 55 \log Pc \quad [\text{A. 7}]$$

$$P_c = \frac{(20 + 3 |G^*|_b (VFA)/(VMA))^{0.58}}{650 + (3 |G^*|_b (VFA)/(VMA))^{0.58}} \quad [\text{A. 8}]$$

where:

$|E^*|_m$ = Dynamic modulus of asphalt mixture (psi).

Pc = Aggregate contact volume.

ϕ = Phase angle of asphalt mixture.

APPENDIX B: RELATIONSHIP BETWEEN ASPHALT BINDER GRADE AND VISCOSITY PARAMETERS.

The ASTM D 2493 (2009) shows an approximate linear relationship (a.k.a. A-VTS relationship) between the temperature and the dynamic viscosity of asphalt binders.

$$\log \log(\eta) = \begin{cases} A + VTS \log(T_R) & T_R > T_{critical} \\ 2.7 \times 10^{12} & T_R \leq T_{critical} \end{cases} \quad [B. 1]$$

where η = Dynamic Viscosity (cP), A = Intercept, VTS = Slope, T_R = Temperature in Rankine, $T_{critical}$ = Temperature in Rankine at which the viscosity is equal to 2.7×10^{12} cP. Table B.1 shows the A and VTS parameters for different binder grades reported in the M-E PDG documentation. These typical values are shown for Superpave binders, AC viscosity-graded binders, and penetration-graded (PEN) binders.

Table B.1. Relationship between asphalt binder grade and viscosity parameters.

Asphalt Binder Grade	A	VTS	Asphalt Binder Grade	A	VTS
46-34	11.5040	-3.9010	70-28	9.7150	-3.2170
46-40	10.1010	-3.3930	70-34	8.9650	-2.9480
46-46	8.7550	-2.9050	70-40	8.1290	-2.6480
52-10	13.3860	-4.5700	76-10	10.0590	-3.3310
52-16	13.3050	-4.5410	76-16	10.0150	-3.3150
52-22	12.7550	-4.3420	76-22	9.7150	-3.2080
52-28	11.8400	-4.0120	76-28	9.2000	-3.0240
52-34	10.7070	-3.6020	76-34	8.5320	-2.7850
52-40	9.4960	-3.1640	82-10	9.5140	-3.1280
52-46	8.3100	-2.7360	82-16	9.4750	-3.1140
58-10	12.3160	-4.1720	82-22	9.2090	-3.0190
58-16	12.2480	-4.1470	82-28	8.7500	-2.8560
58-22	11.7870	-3.9810	82-34	8.1510	-2.6420
58-28	11.0100	-3.7010	AC-2.5	11.5167	-3.8900
58-34	10.0350	-3.3500	AC-5	11.2614	-3.7914
58-40	8.9760	-2.9680	AC-10	11.0134	-3.6954
64-10	11.4320	-3.8420	AC-20	10.7709	-3.6017
64-16	11.3750	-3.8220	AC-3	10.6316	-3.5480
64-22	10.9800	-3.6800	AC-40	10.5338	-3.5104
64-28	10.3120	-3.4400	PEN 40-50	10.5254	-3.5047
64-34	9.4610	-3.1340	PEN 60-70	10.6508	-3.5537
64-40	8.5240	-2.7980	PEN 85-100	11.8232	-3.6210
70-10	10.6900	-3.5660	PEN 120-150	11.0897	-3.7252
70-16	10.6410	-3.5480	PEN 200-300	11.8107	-4.0068
70-22	10.2990	-3.4260			

**APPENDIX C: A LIST OF ASPHALT MIXTURE SAMPLES
PREPARED AND TESTED BETWEEN 10/ 1/11 & 12/31/12**

Table C.1: List of HMAs prepared/tested and their air voids

Unique HMA No	Sample No	HMA ID	Sample ID	AV%	Core Avg. AV%	STDEV AV	COV (%)	Compaction method
1	1	18-S1	18-1	5.7	5.7	0.3	5.9	Slab-Shearbox
	2		18-2	6.1				
	3		18-3	5.4				
	4	18-S2	18-4	7.9	7.37	0.005	6.4	Gyratory
	5		18-5	7.1				Gyratory
	6		18-6	7.1				Gyratory
2	7	28(B)-S1	28-1	6.6	6.7	0.2	2.7	Slab-Shearbox
	8		28-2	6.9				
	9		28-3	6.5				
3	10	29(A)-S1	29-1	8.9	9.1	0.4	4	Slab-Shearbox
	11		29-3	9.4				
	12	29(A)-S2	29-1	7.5	7.57	0.001	1.3	Gyratory
	13		29-2	7.6				Gyratory
	14		29-3	7.6				Gyratory
4	15	44-S1	44-1	8.0	8.3	0.4	4.3	Slab-Shearbox
	16		44-2	8.2				
	17		44-3	8.7				
	18	44-S2	44-4	7.0	7	0	0.6	Slab-Shearbox
	19		44-5	7.0				
	20		44-6	6.9				
5	21	49A-S1	49A-1	4.2	4.4	0.3	7.5	Slab-Shearbox
	22		49A-2	4.6				
	23	49A-S2	49A-1	6.4	7.03	0.7	9.8	Gyratory
	24		49A-2	6.9				Gyratory
	25		49A-3	7.8				Gyratory
6	26	203-S1	203-1	3.8	4.1	0.3	8	Slab-Shearbox
	27		203-2	4.4				
	28		203-3	4.2				
	29	203-GYRO	203-GYRO	4.7	4.7	-	-	Gyratory
	30	203-S2	203-4	6.5	6.4	0.2	2.9	Slab-Shearbox
	31		203-5	6.2				

	32		203-6	6.6				
7	33	204-S1	204-1	6.4	6.3	0.1	1.9	Slab-Shearbox
	34		204-2	6.2				
	35		204-3	6.2				
	36	204-S2	204-1	6.9	6.86	0.07	1	Gyratory
	37		204-2	6.8				Gyratory
8	38	205-S1	205-1	9.0	8.8	0.2	2.7	Slab-Shearbox
	39		205-2	8.8				
	40		205-3	8.6				
	41	205-GYRO	205-GYRO	8.9	8.9	-	-	Gyratory
	42	205	205-1	7.0	6.74	0.27	4	Gyratory
	43		205-2	6.7				Gyratory
44	205-3		6.5	Gyratory				
9	45	24A	24A-1	6.7	6.9	0.2	2.8	Gyratory
	46		24A-2	7.1				Gyratory
	47		24A-3	6.7				Gyratory
	48		24A-4	7.0				Gyratory
10	49	32B	32-1	8.2	7.1	0.7	10.2	Gyratory
	50		32B-2	7.2				Gyratory
	51		32B-3	6.6				Gyratory
	52		32B-4	6.6				Gyratory
11	53	37	37-1	7.3	7.3	0.29	3.9	Gyratory
	54		37-2	7.6				Gyratory
	55		37-3	7.0				Gyratory
12	56	67	67-1	6.7	7.2	0.5	6.9	Gyratory
	57		67-2	7.7				Gyratory
	58		67-3	7.2				Gyratory
13	59	81	81-1	8.3	8	0.4	5.2	Gyratory
	60		81-2	7.6				Gyratory
	61		81-3	8.2				Gyratory
14	62	51A	51A-1	7.7	7.3	0.4	5.6	Gyratory
	63		51A-2	6.9				Gyratory
	64		51A-3	7.2				Gyratory
15	65	64	64-1	6.1	7	0.8	11.4	Gyratory
	66		64-2	7.7				Gyratory
	67		64-3	7.2				Gyratory
16	68	102	102-1	7.2	7.8	0.6	7.6	Gyratory
	69		102-2	7.9				Gyratory

	70		102-3	8.4				Gyratory
17	71	103	103-1	7.0	7.2	0.2	3.1	Gyratory
	72		103-2	7.3				Gyratory
	73		103-3	7.4				Gyratory
18	74	109	109-1	7.8	7.6	0.2	2.2	Gyratory
	75		109-2	7.5				Gyratory
	76		109-3	7.6				Gyratory
19	77	105	105-1	6.4	6.8	0.4	6.2	Gyratory
	78		105-2	7.1				Gyratory
	79		105-3	7.1				Gyratory
20	80	111	111-1	7.5	7.2	0.8	10.6	Gyratory
	81		111-2	7.7				Gyratory
	82		111-3	6.3				Gyratory
21	83	48	48-1	7.3	7.2	0.2	2.3	Gyratory
	84		48-2	7.3				Gyratory
	85		48-3	7.0				Gyratory
22	86	31B	31B-1	7.2	7.5	0.3	3.5	Gyratory
	87		31B-2	7.5				Gyratory
	88		31B-3	7.7				Gyratory
23	89	45	45-1	7.2	7.2	0.1	0.8	Gyratory
	90		45-2	7.2				Gyratory
	91		45-3	7.1				Gyratory
24	92	21	21-1	7.4	7.4	0.16	2.2	Gyratory
	93		21-2	7.2				Gyratory
	94		21-3	7.6				Gyratory
25	95	62	62-1	6.4	6.7	0.3	3.8	Gyratory
	96		62-2	6.7				Gyratory
	97		62-3	6.9				Gyratory
26	98	112	112-1	7.6	7.5	0.2	2.2	Gyratory
	99		112-2	7.3				Gyratory
	100		112-3	7.4				Gyratory
27	101	206	206-1	7.4	7.7	0.3	3.6	Gyratory
	102		206-2	8.0				Gyratory
	103		206-3	7.8				Gyratory
28	104	108	108-1	7.4	7.5	0.1	1.4	Gyratory
	105		108-2	7.6				Gyratory
	106		108-3	7.5				Gyratory
29	107	68	68-1	7.3	7.6	0.4	4.8	Gyratory

	108		68-2	8.0				Gyratory
	109		68-3	7.3				Gyratory
30	110	207	207-1	7.6	7.6	0.1	1.7	Gyratory
	111		207-2	7.5				Gyratory
	112		207-3	7.7				Gyratory
31	113	47	47-1	6.2	6.83	0.68	10	Gyratory
	114		47-2	6.8				Gyratory
	115		47-3	7.5				Gyratory
32	116	127	127-1	7.5	7.5	0.05	0.6	Gyratory
	117		127-2	7.5				Gyratory
	118		127-3	7.6				Gyratory
33	119	106	106-1	6.8	7.52	0.64	8.5	Gyratory
	120		106-2	7.9				Gyratory
	121		106-3	7.9				Gyratory
34	122	4	4--1	6.8	6.95	0.19	2.7	Gyratory
	123		4--2	7.0				Gyratory
	124		4--3	7.1				Gyratory
35	125	20A	20A-1	7.6	7.33	0.35	4.8	Gyratory
	126		20A-2	7.5				Gyratory
	127		20A-3	6.9				Gyratory
36	128	2	2-1	7.7	7.38	0.26	3.5	Gyratory
	129		2-2	7.3				Gyratory
	130		2-3	7.2				Gyratory
37	131	20B	20B-1	6.2	6.4	0.28	4.4	Gyratory
	132		20B-2	6.7				Gyratory
	133		20B-3	6.4				Gyratory
38	134	23	23-1	7.2	7.01	0.2	2.8	Gyratory
	135		23-2	6.9				Gyratory
	136		23-3	7.0				Gyratory
39	137	24B	24B-1	6.8	6.84	0.2	3.1	Gyratory
	138		24B-2	6.7				Gyratory
	139		24B-3	7.1				Gyratory
40	140	26A	26A-1	6.8	7.06	0.3	3.8	Gyratory
	141		26A-2	7.0				Gyratory
	142		26A-3	7.3				Gyratory
41	143	26B	26B-1	6.4	7.04	0.9	12.3	Gyratory
	144		26B-2	7.7				Gyratory
42	145	26C	26C-1	7.6	7.53	0.4	5	Gyratory

	146		26C-2	7.1				Gyratory
	147		26C-3	7.9				Gyratory
43	148	31A	31A-1	7.2	7.49	0.3	3.5	Gyratory
	149		31A-2	7.6				Gyratory
	150		31A-3	7.7				Gyratory
44	151	32A	32A-1	7.4	6.92	0.4	6	Gyratory
	152		32A-2	6.7				Gyratory
	153		32A-3	6.7				Gyratory
45	154	51B	51B-1	7.1	7.44	0.28	3.8	Gyratory
	155		51B-2	7.7				Gyratory
	156		51B-3	7.5				Gyratory
46	157	65	65-1	6.8	7.2	0.46	6.4	Gyratory
	158		65-2	7.7				Gyratory
	159		65-3	7.1				Gyratory
47	160	80	80-1	7.4	7.15	0.28	4	Gyratory
	161		80-2	6.8				Gyratory
	162		80-3	7.2				Gyratory
48	163	97	97-1	7.0	6.82	0.12	1.8	Gyratory
	164		97-2	6.8				Gyratory
	165		97-3	6.7				Gyratory
49	166	200	200-1	8.0	7.25	0.63	8.7	Gyratory
	167		200-2	6.8				Gyratory
	168		200-3	7.0				Gyratory
50	169	201	201-1	11.4	11.4	0.12	1.1	Gyratory
	170		201-2	11.5				Gyratory
	171		201-3	11.2				Gyratory
51	172	202	202-1	7.4	7.57	0.3	4	Gyratory
	173		202-2	7.4				Gyratory
	174		202-3	7.9				Gyratory
52	175	WMA	WMA-1	6.8	7.27	0.45	6.2	Gyratory
	176		WMA-2	7.3				Gyratory
	177		WMA-3	7.7				Gyratory
53	178	90	90-1	7.48	7.25	0.66	9.1	Gyratory
	179		90-2	6.50				Gyratory
	180		90-3	7.77				Gyratory
54	181	208	208-1	7.29	6.86	0.003	5.5	Gyratory
	182		208-2	6.70				Gyratory
	183		208-3	6.59				Gyratory

55	184	49C	49C-1	7.23	6.97	0.003	4.9	Gyratory
	185		49C-2	6.58				Gyratory
	186		49C-3	7.11				Gyratory
56	187	85	85-1	7.53	7.47	0.0006	0.9	Gyratory
	188		85-2	7.41				Gyratory
	189		85-3	7.46				Gyratory
57	190	86	86-1	7.73	6.70	0.009	13.3	Gyratory
	191		86-2	6.22				Gyratory
	192		86-3	6.15				Gyratory
58	193	51C	51C-1	7.36	7.21	0.0024	3.4	Gyratory
	194		51C-2	7.33				Gyratory
	195		51C-3	6.93				Gyratory
59	196	2B	2B-1	7.33	7.25	0.0007	1.04	Gyratory
	197		2B-2	7.24				Gyratory
	198		2B-3	7.18				Gyratory
60	199	209A	209A-1	6.88	7.07	0.17	2.4	Gyratory
	200		209A-2	7.21				Gyratory
	201		209A-3	7.11				Gyratory
61	202	209B	209B-1	7.19	7.153	0.119	1.7	Gyratory
	203		209B-2	7.25				Gyratory
	204		209B-3	7.02				Gyratory
62	205	49B	49B-1	6.15	6.35	0.24	4.0	Gyratory
	206		49B-2	6.61				Gyratory
	207		49B-3	6.28				Gyratory
63	208	29B	29B-1	8.86	9.12	0.4	4.0	Gyratory
	209		29B-2	9.38				Gyratory
64	211	20C	20C-1	7.42	7.53	0.1	1.0	Gyratory
	212		20C-2	7.57				Gyratory
	213		20C-3	7.61				Gyratory

Table C.2: HMAs received and tested for |E*| mastercurve.

	Mix No:	2		3		3		4		5	
	Layer:	Base		Base		Leveling		Leveling/Top		Top	
	Mix Type	Binder PG	HMA #	Binder PG	No	Binder PG	HMA #	Binder PG	HMA #	Binder PG	HMA #
North, Grand, Bay, Southwest and University Regions											
M	E30	64-22	1	64-22	*2	70-28P	3	70-28P	4	70-28P	5
HS	E30	64-22	1	64-22	*2	76-28P	6	76-28P	7	76-28P	8
M	E50	64-22	9	64-22	10	70-28P	11	70-28P	12	70-28P	13
HS	E50	64-22	9	64-22	10	76-28P	14	76-28P	15	76-28P	16
M	E10	58-22	17	* 58-22	*18	64-28	19	64-28	20	64-28	21
HS	E10	58-22	17	* 58-22	*18	70-28P	22	70-28P	23	70-28P	24
M	E3	58-22	25	58-22	26	64-28	27	* 64-28	*28	64-28	29
HS	E3	58-22	25	58-22	26	70-28P	30	70-28P	31	70-28P	32
M	E03	58-22	33	58-22	34	58-28	35	58-28	36	58-28	37
HS	E03	58-22	33	58-22	34	64-28	38	64-28	39	64-28	40
M	E1	58-22	41	58-22	42	58-28	43	58-28	44	58-28	45
HS	E1	58-22	41	58-22	42	64-28	46	64-28	47	64-28	48
Metro Region											
M	E30	64-22	1	* 64-22	*2	70-22P	89	* 70-22P	*90	70-22P	91
HS	E30	64-22	1	* 64-22	*2	76-22P	92	76-22P	93	76-22P	94
M	E50	64-22	9	64-22	10	70-22P	95	70-22P	96	70-22P	97
HS	E50	64-22	9	64-22	10	76-22P	98	76-22P	99	76-22P	100
M	E10	58-22	17	* 58-22	*18	64-22	101	64-22	102	* 64-22	*103
HS	E10	58-22	17	* 58-22	*18	70-22P	104	* 70-22P	*105	70-22P	106
M	E3	58-22	25	58-22	26	64-22	107	64-22	108	64-22	109
HS	E3	58-22	25	58-22	26	70-22P	110	70-22P	111	70-22P	112
M	E03	58-22	33	58-22	34	58-22	113	58-22	114	58-22	115
HS	E03	58-22	33	58-22	34	64-22	116	64-22	117	64-22	118
M	E1	58-22	41	58-22	42	58-22	119	58-22	120	58-22	121
HS	E1	58-22	41	58-22	42	64-22	122	64-22	123	64-22	124
Superior Region											
M	E10	58-28	53	58-28	54	58-34	55	58-34	56	58-34	57
HS	E10	58-28	53	58-28	54	64-34P	58	64-34P	59	64-34P	60
M	E3	58-28	61	58-28	62	58-34	63	58-34	64	* 58-34	*65
HS	E3	58-28	61	58-28	62	64-34P	66	64-34P	67	64-34P	68
M	E03	58-28	69	58-28	70	58-34	71	58-34	72	58-34	73
HS	E03	58-28	69	58-28	70	64-34P	74	64-34P	75	64-34P	76
M	E1	58-28	77	58-28	78	58-34	79	58-34	80	* 58-34	*81
HS	E1	58-28	82	58-28	83	64-34P	84	64-34P	85	64-34P	86

Note: M=Mainline, HS=High Stress

Legend:	Received	Tested	*Tested by MTU
---------	----------	--------	----------------

Table C.3: HMAs received and tested for |E*| mastercurve: GGSP and LVSP Mixtures

HMA Type	Layer:	Leveling/Top					
	Region:	(1)		(2)		(3)	
	Mix Type	Binder	HMA#	Binder	HMA#	Binder	HMA#
M	GGSP	70-28P	49	70-22P	125	-	-
HS	GGSP	76-28P	50	76-22P	126		
M	LVSP	58-28	51	58-22	127	58-34	87
HS	LVSP	64-28	52	64-22	128	64-34P	88
Note: (1) North, Grand, Bay, Southwest and University, (2) Metro, (3) Superior							

Table C.4: HMAs received and tested for |E*| mastercurve: Superpave (NOT IN LIST)

HMA Type	Mix No:	2		3		4		5	
	Layer:	Base		Base		Leveling/Top		Top	
	Mix Type	Binder	HMA#	Binder	HMA#	Binder	HMA#	Binder	HMA#
M	E10			58-28	200				
HS	E10							64-22	202
HS	E30					70-22P	203	70-22P	204
M	E3	58-28	205						
M	E1							64-22	206
M	E1							64-22	207

Table C.5: HMAs received and tested for |E*| mastercurve: GGSP and LVSP (NOT IN LIST)

HMA Type	Layer:	Leveling/Top					
	Region:	1		2		3	
	Mix Type	Binder	HMA#	Binder	HMA#	Binder	HMA#
M	ASCRL	64-28	201				

APPENDIX D: $|E^*|$ MASTERCURVES OF THE MIXTURES GROUPED BASED ON THE MDOT MIX DESIGNATION

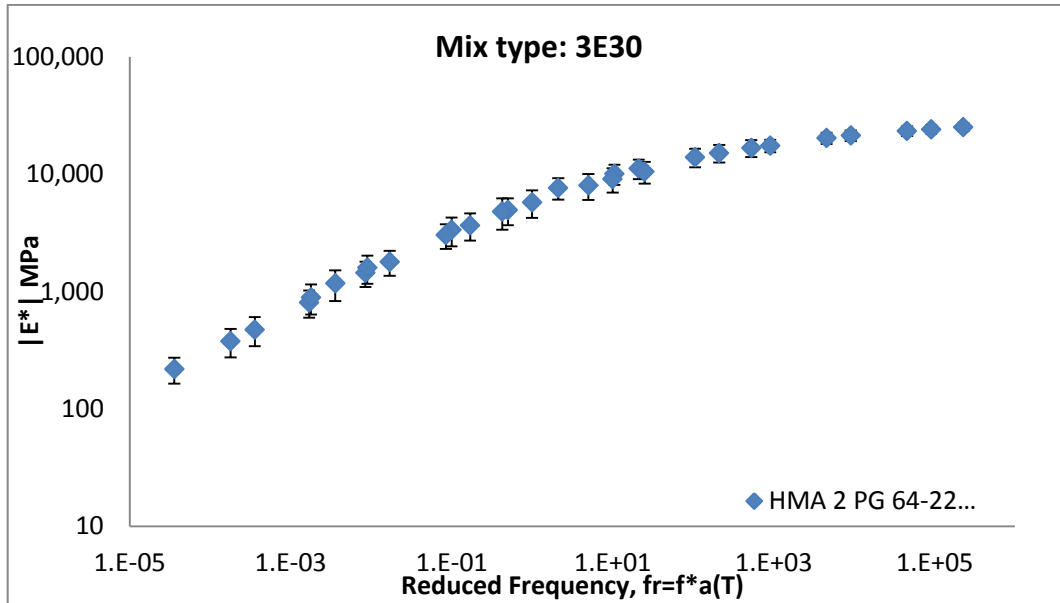


Figure D.1: Dynamic modulus $|E^*|$ master curves for 3E30 mixes

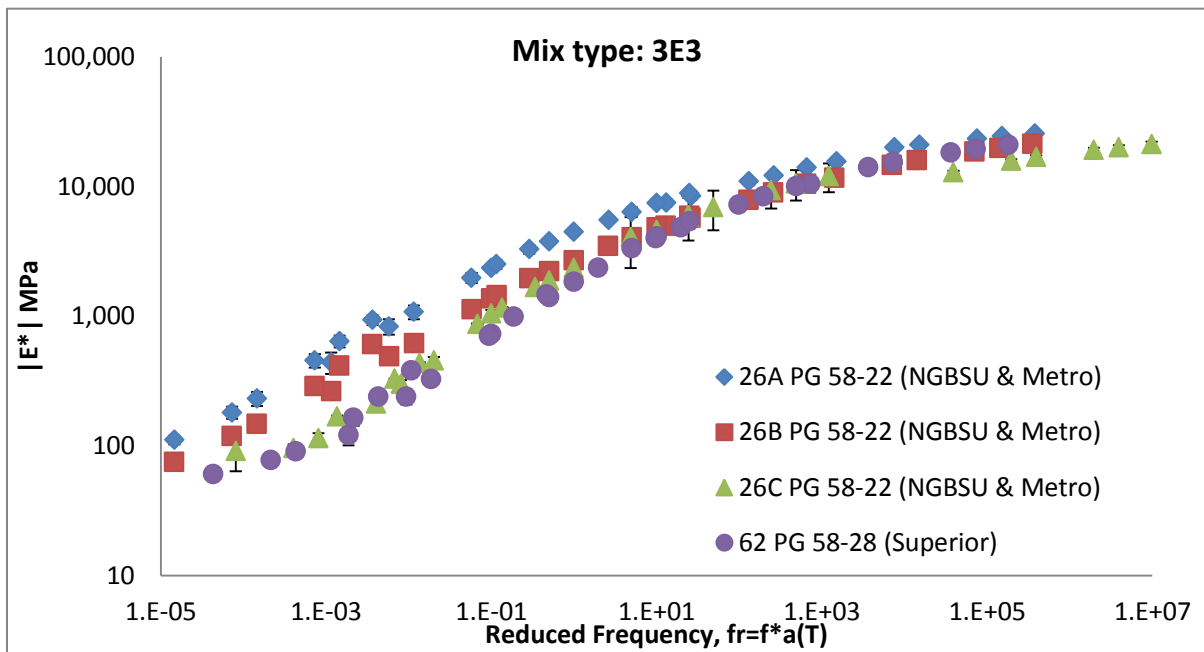


Figure D.2: Dynamic modulus $|E^*|$ master curves for 3E3 mixes

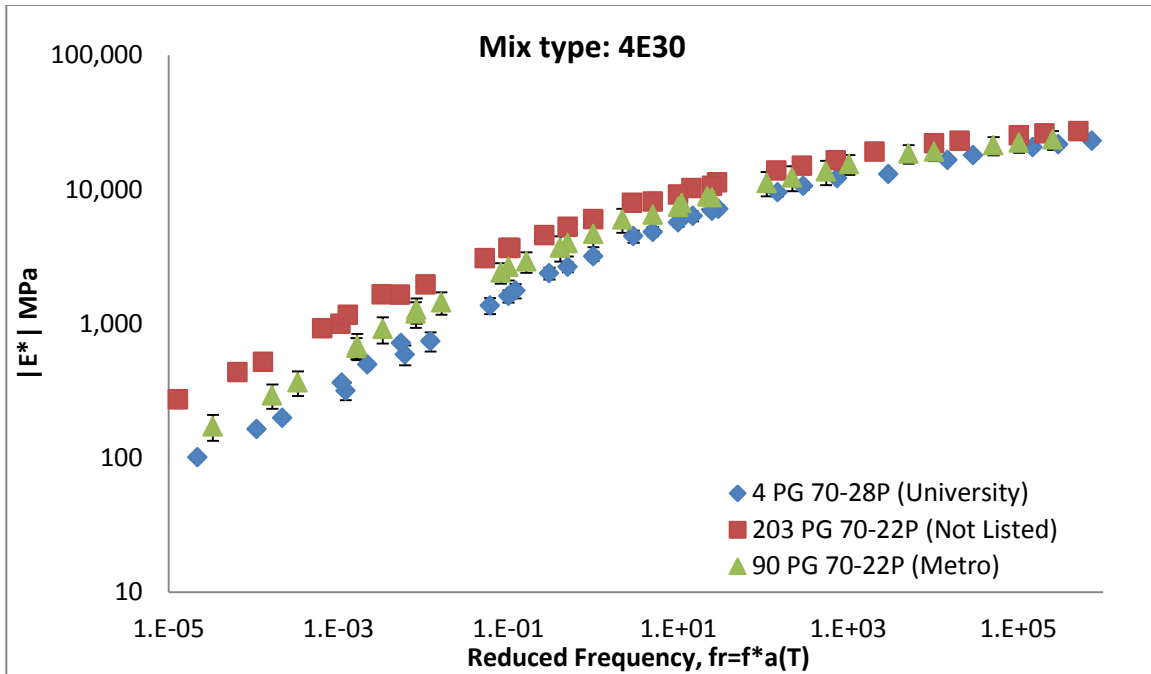


Figure D.3: Dynamic modulus $|E^*|$ master curves for 3E10 mixes

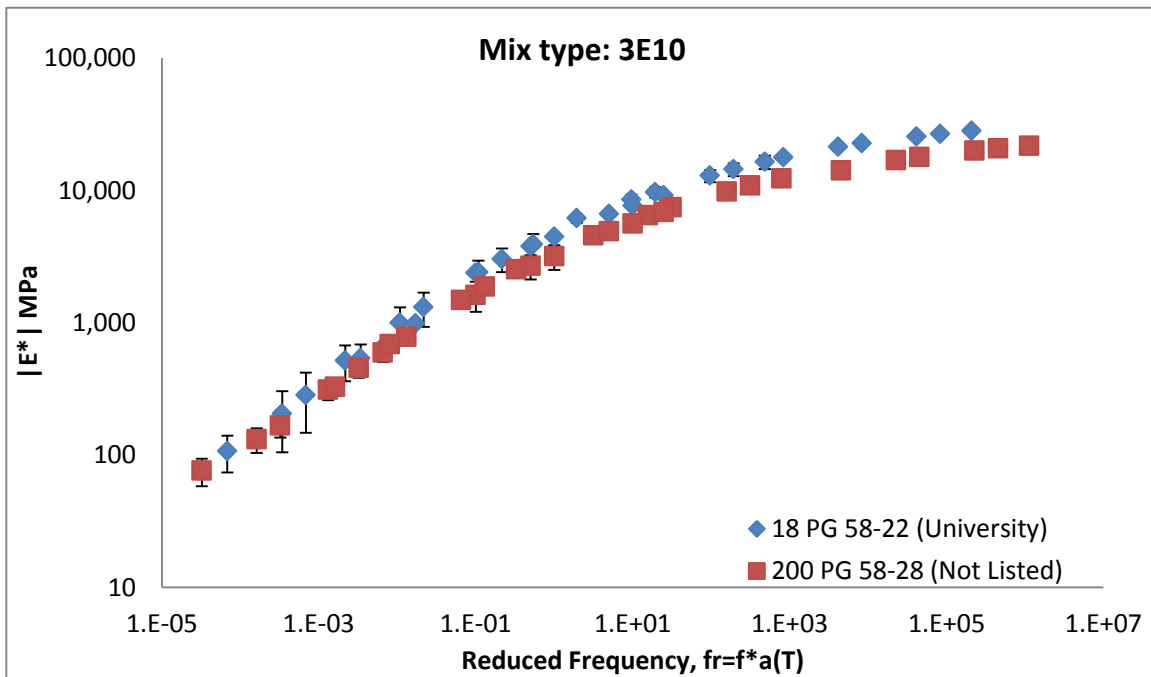


Figure D.4: Dynamic modulus $|E^*|$ master curves for 4E30 mixes

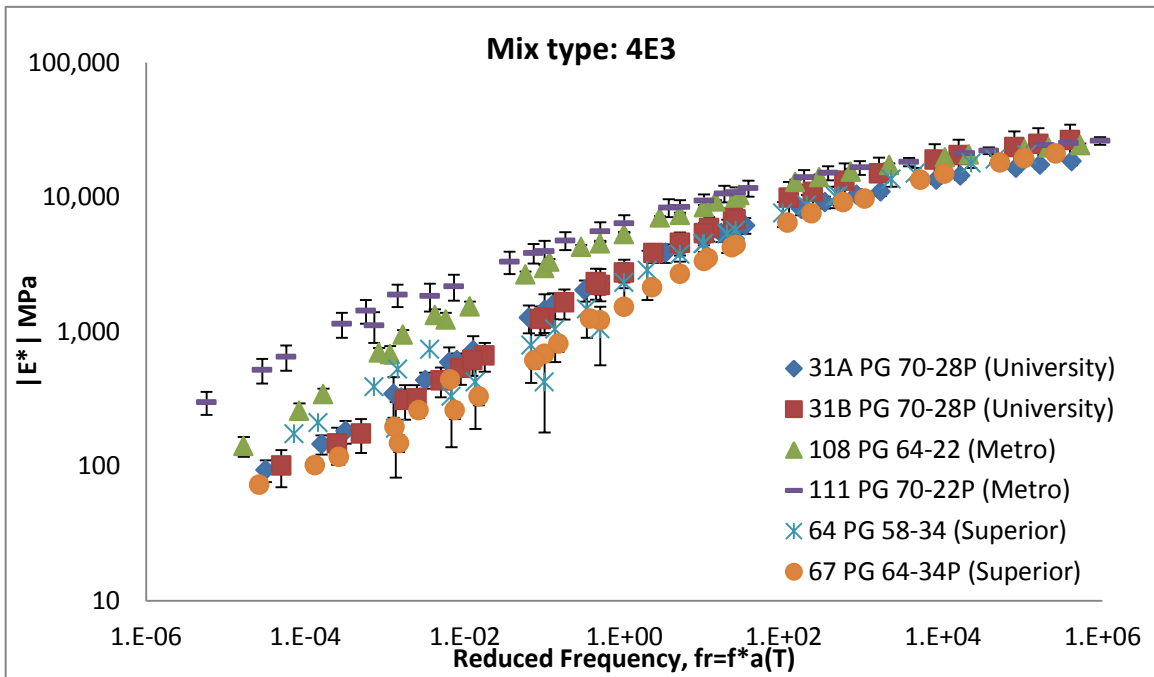


Figure D.5: Dynamic modulus $|E^*|$ master curves for 4E3 mixes

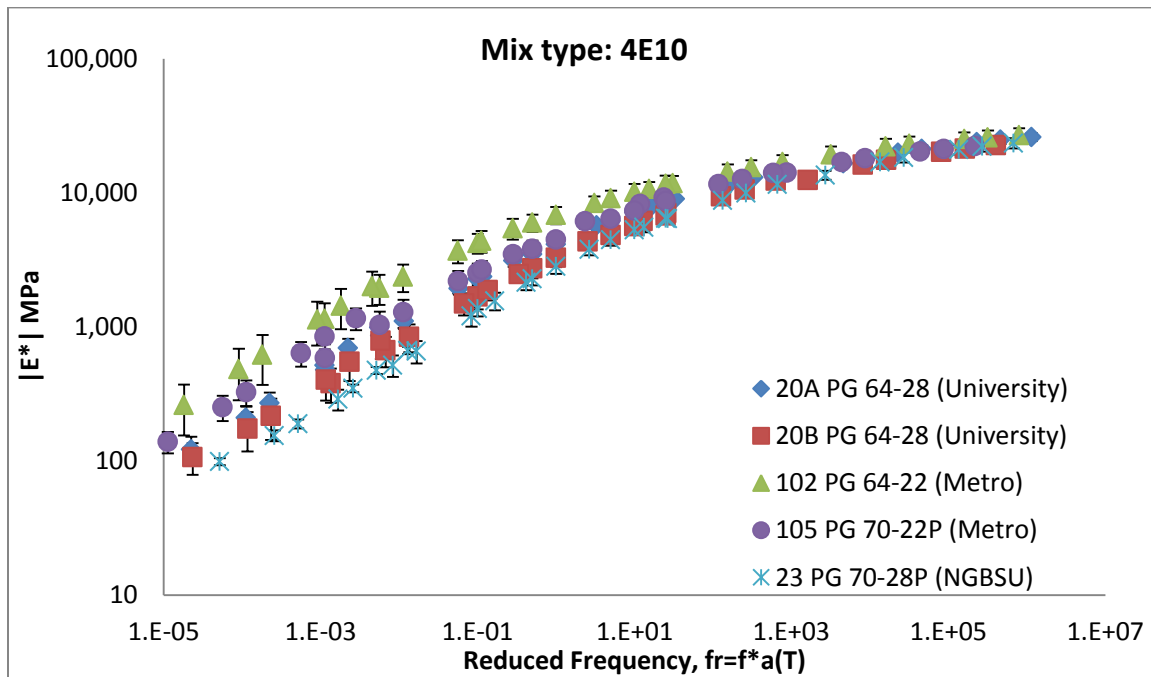


Figure D.6: Dynamic modulus $|E^*|$ master curves for 4E10 mixes

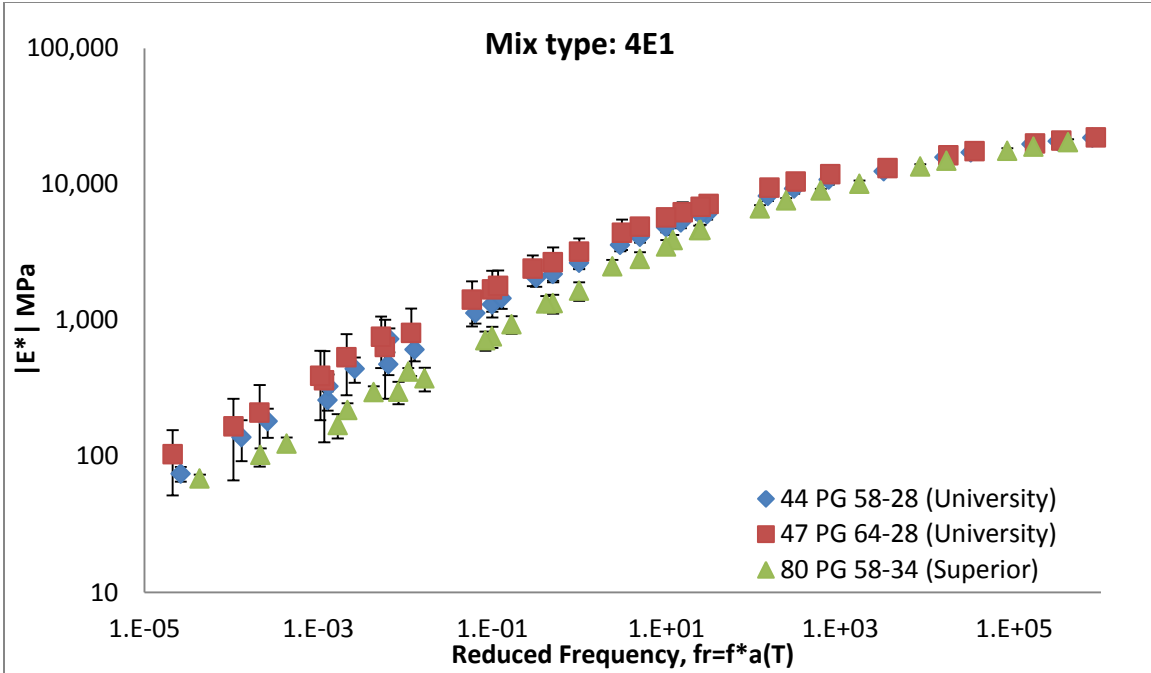


Figure D.7: Dynamic modulus $|E^*|$ master curves for 4E1 mixes

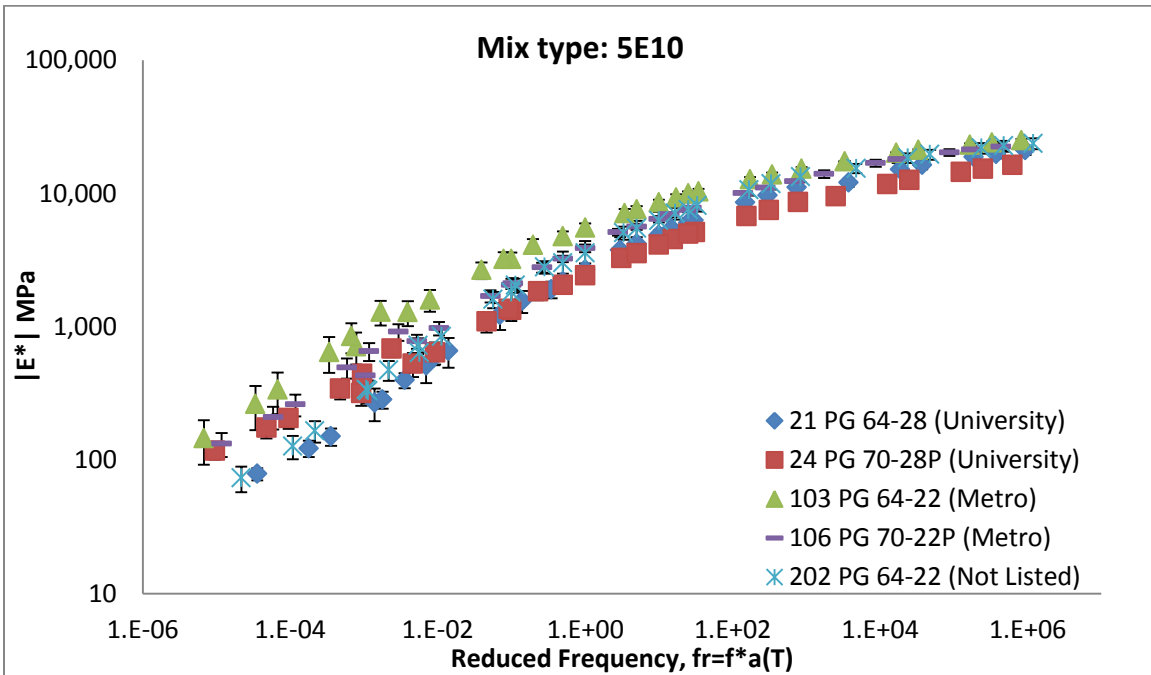


Figure D.8: Dynamic modulus $|E^*|$ master curves for 5E10 mixes

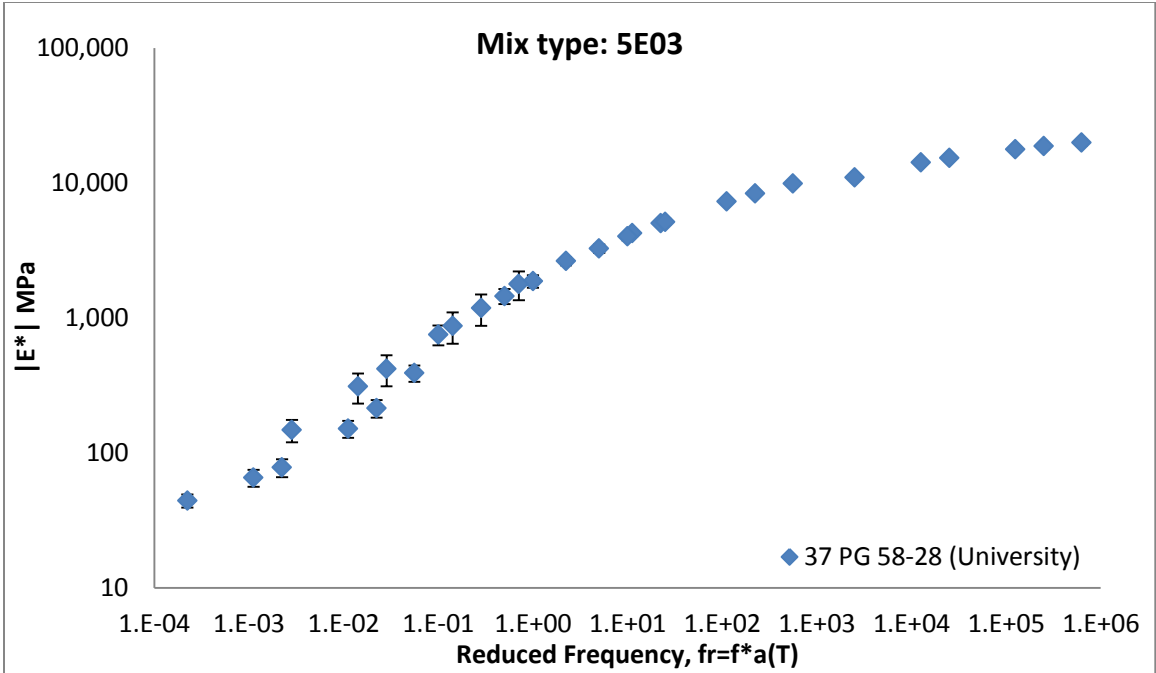


Figure D.9: Dynamic modulus $|E^*|$ master curves for 5E03 mixes

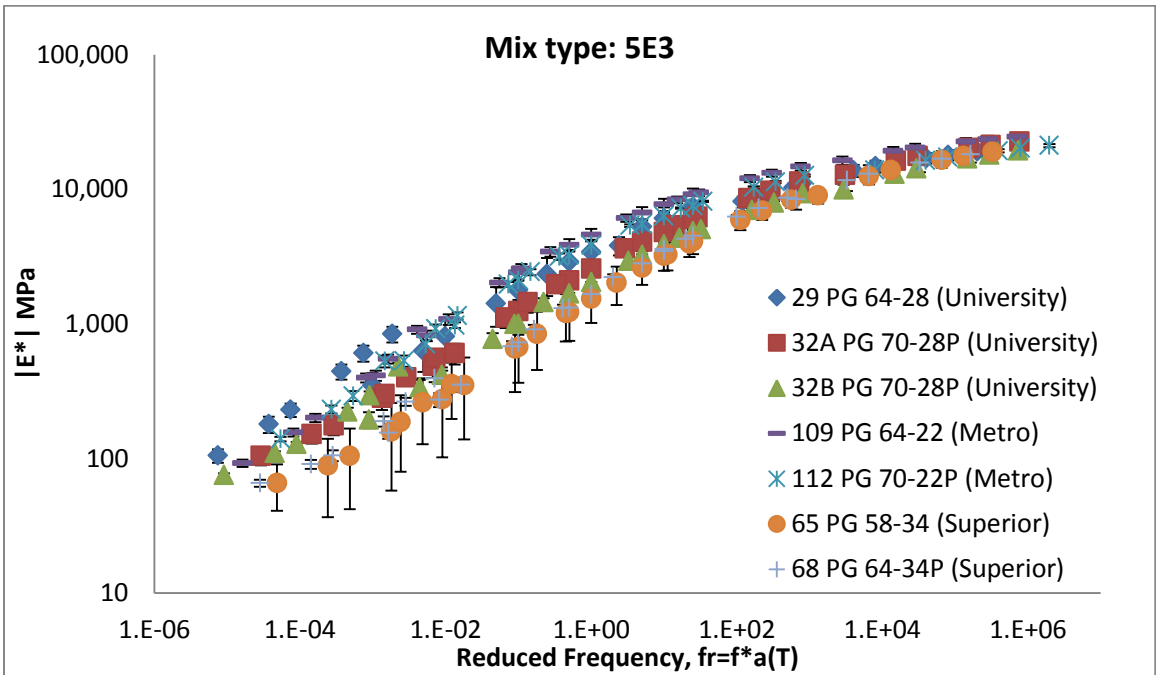


Figure D.10: Dynamic modulus $|E^*|$ master curves for 5E3 mixes

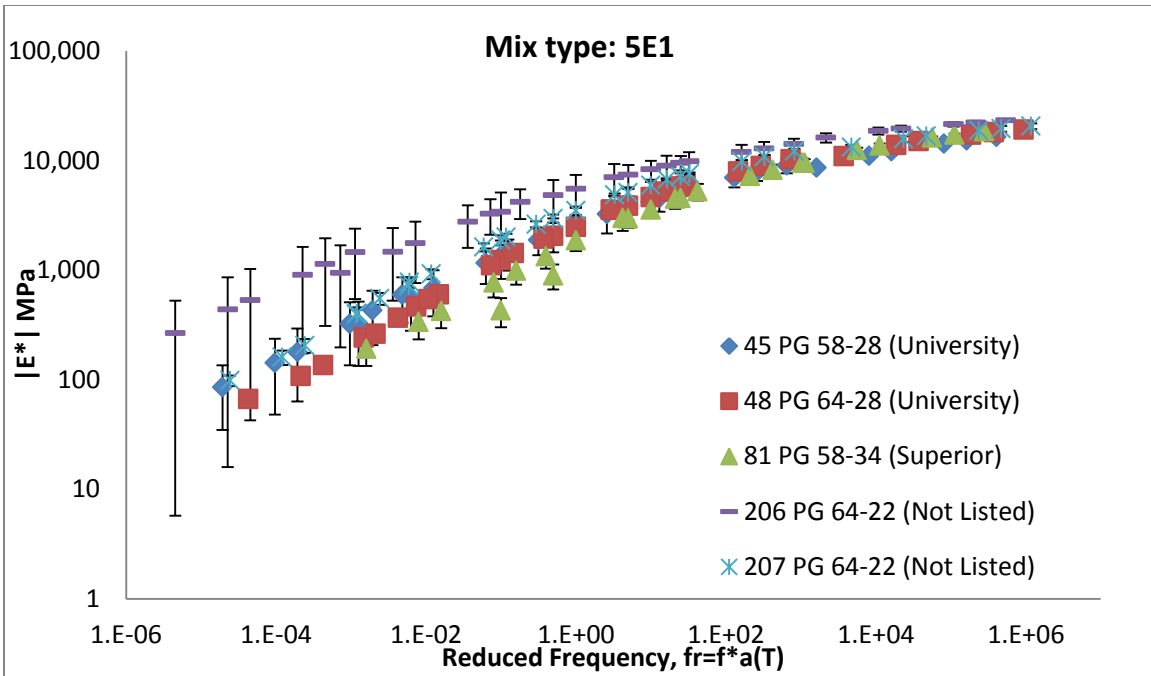


Figure D.11: Dynamic modulus $|E^*|$ master curves for 5E1 mixes

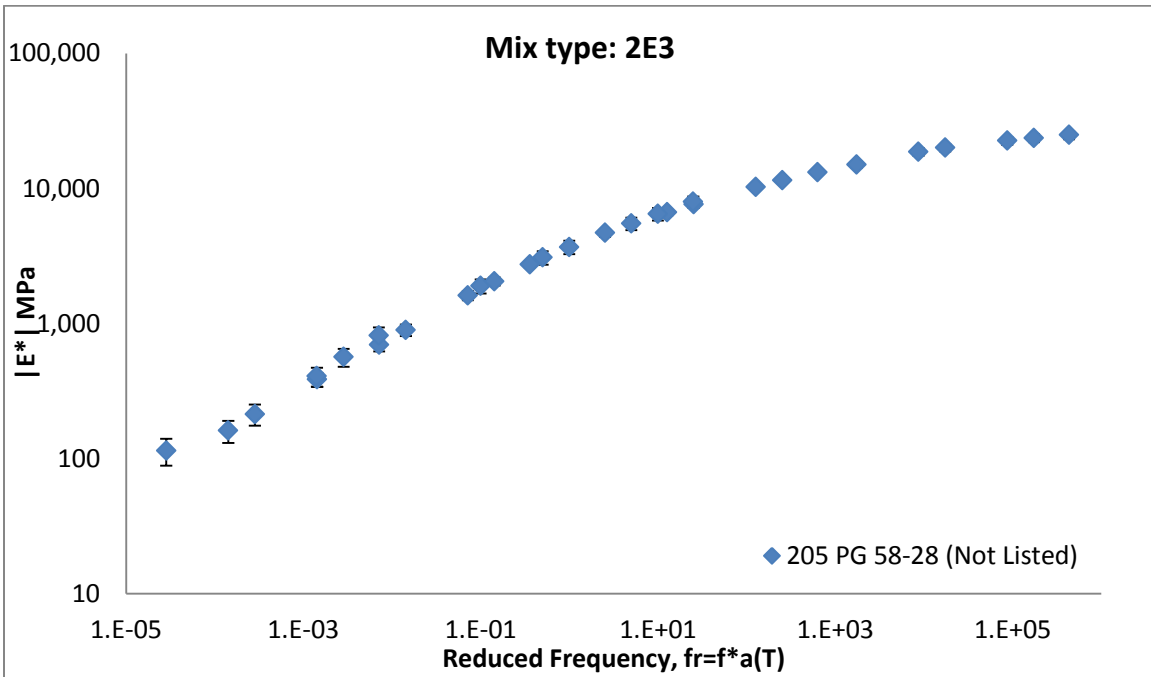


Figure D.12: Dynamic modulus $|E^*|$ master curves for 2E3 mixes

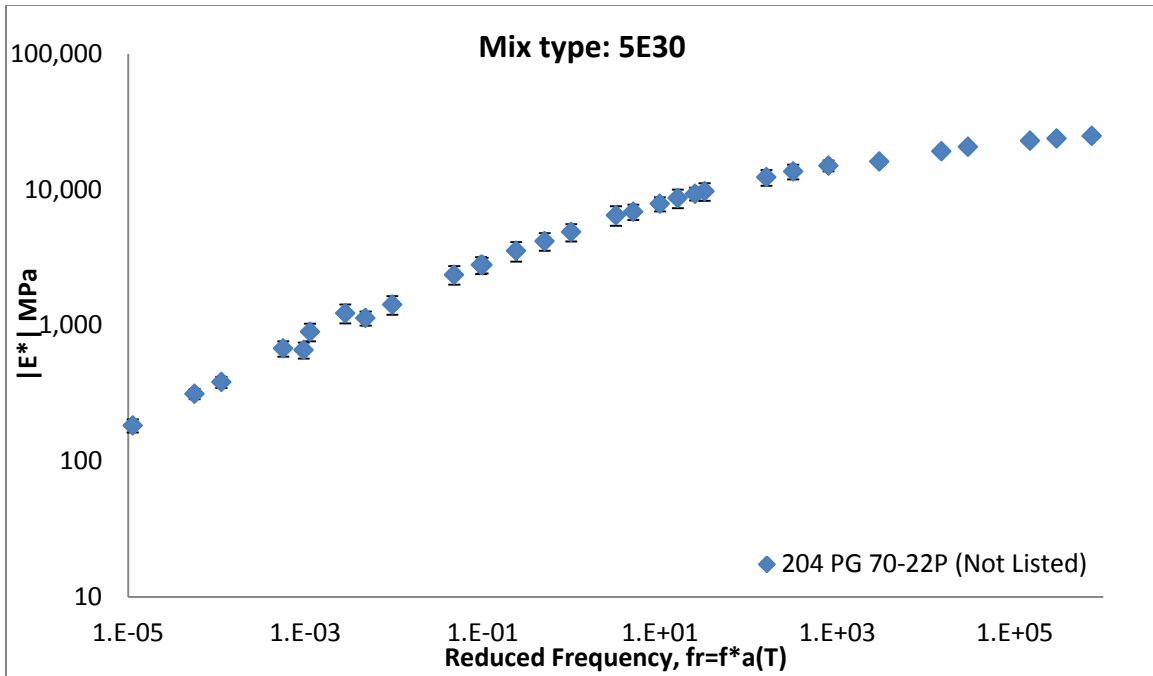


Figure D.13: Dynamic modulus $|E^*|$ master curves for 5E30 mixes

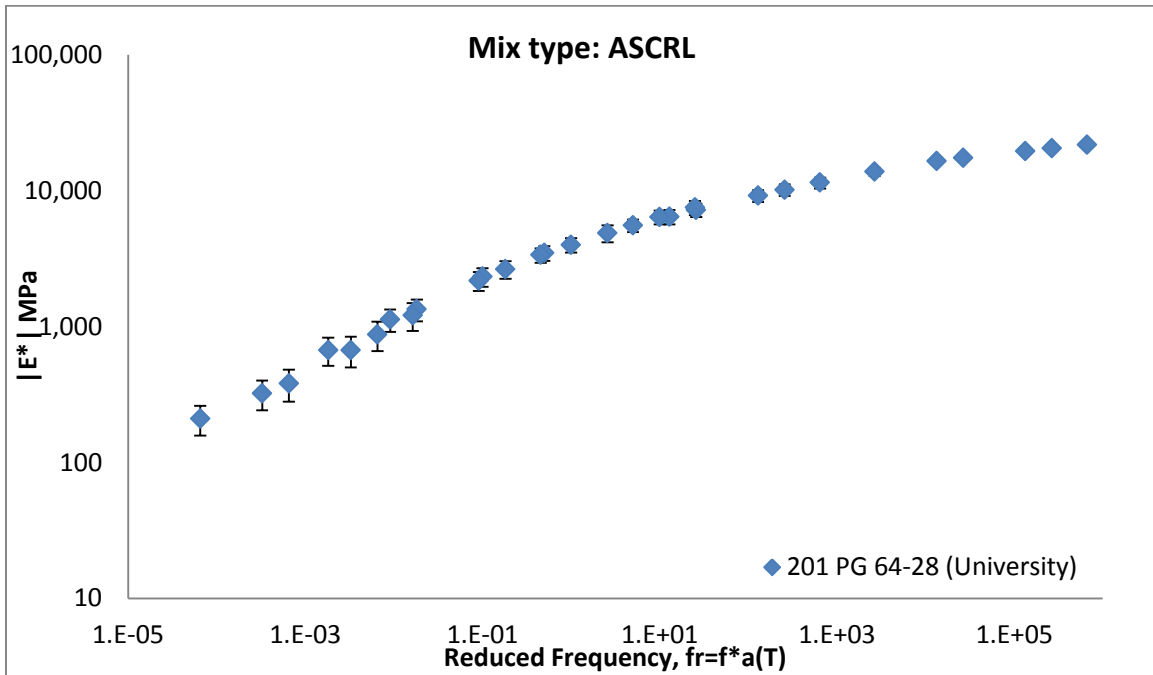


Figure D.14: Dynamic modulus $|E^*|$ master curves for ASCRL mixes

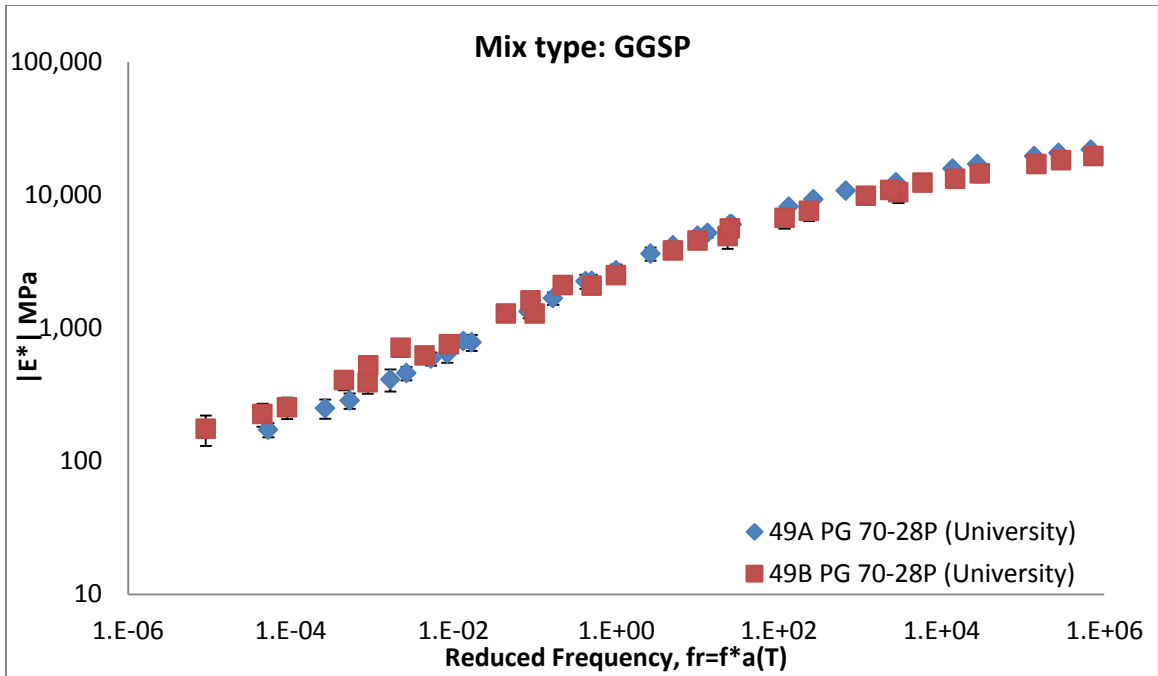


Figure D.15: Dynamic modulus $|E^*|$ master curves for GGSP mixes

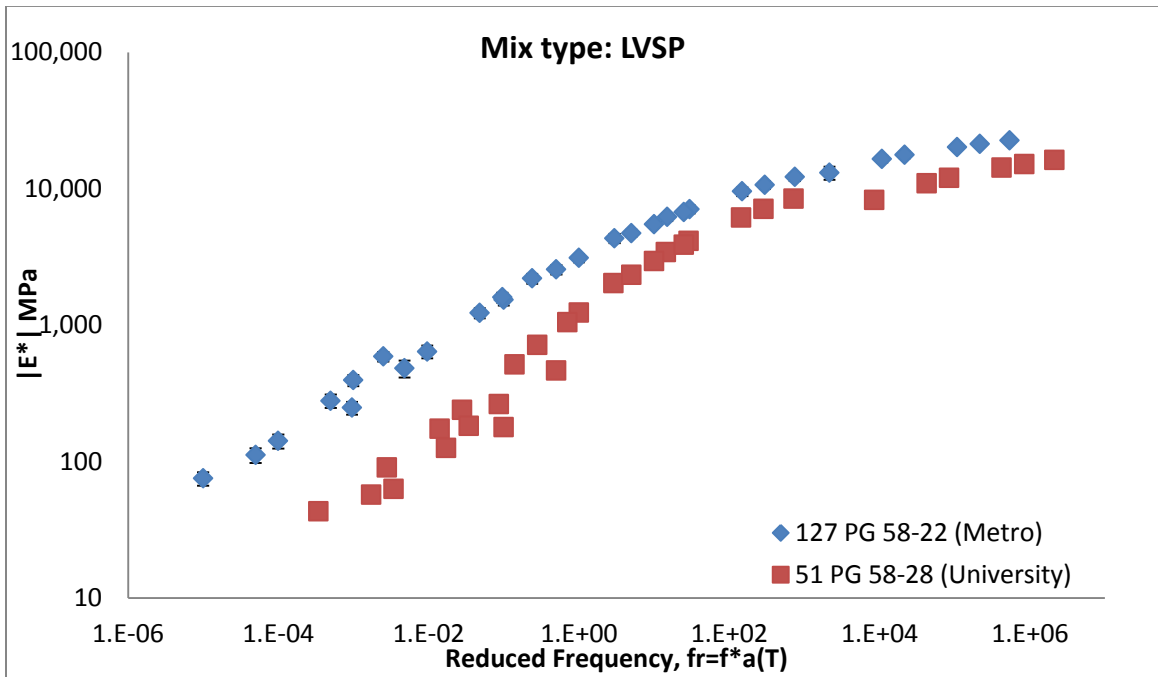


Figure D.16: Dynamic modulus $|E^*|$ master curves for LVSP mixes

APPENDIX E: $|G^*|$ MASTER CURVES GROUPED BASED ON THE PG

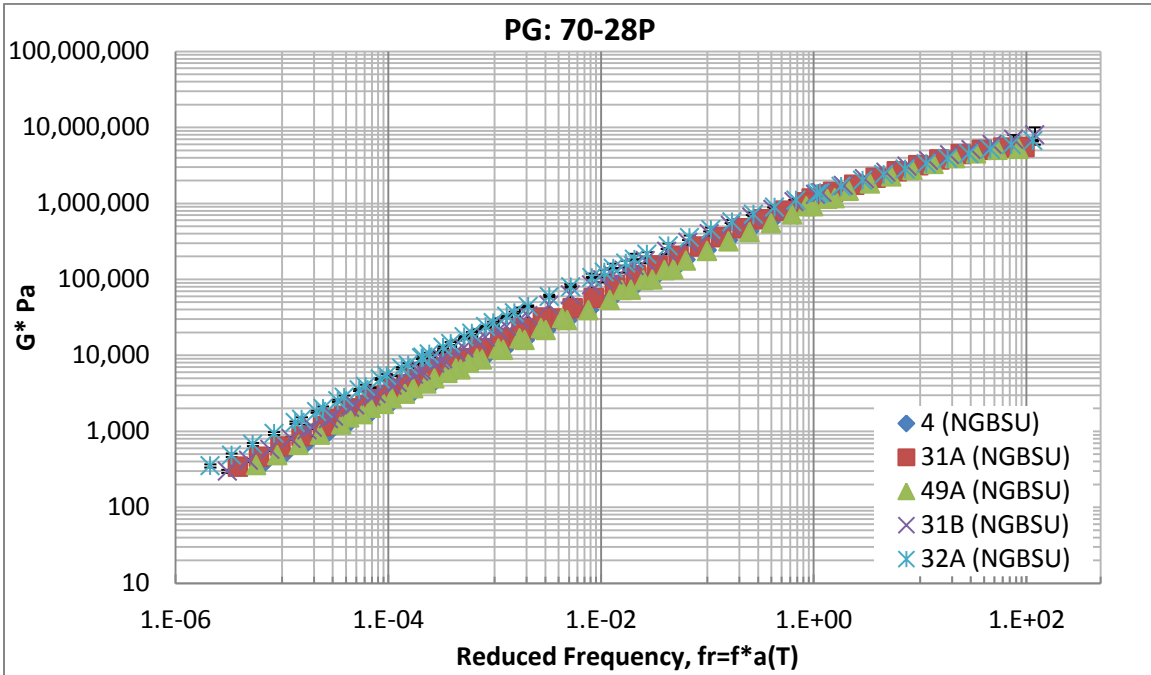


Figure E.1: $|G^*|$ mastercurves of different PG70-28P binders. NGBSU = North, Grand, Bay, Southwest and University Regions

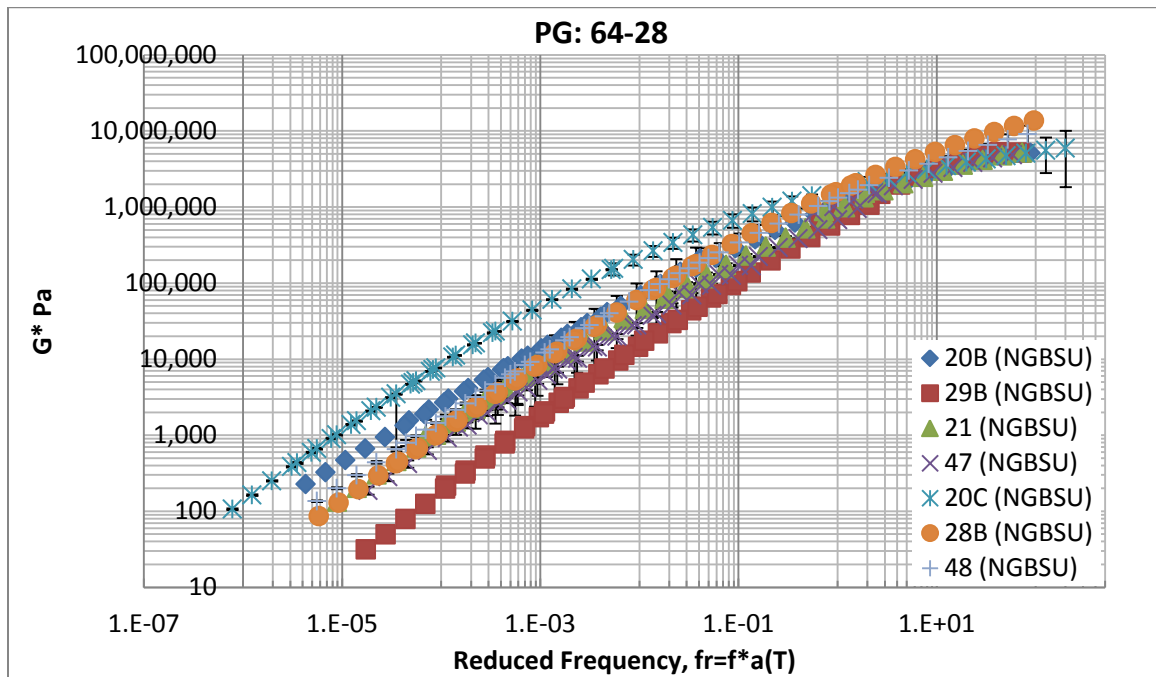


Figure E.2: $|G^*|$ mastercurves of different PG64-28 binders. NGBSU = North, Grand, Bay, Southwest and University Regions

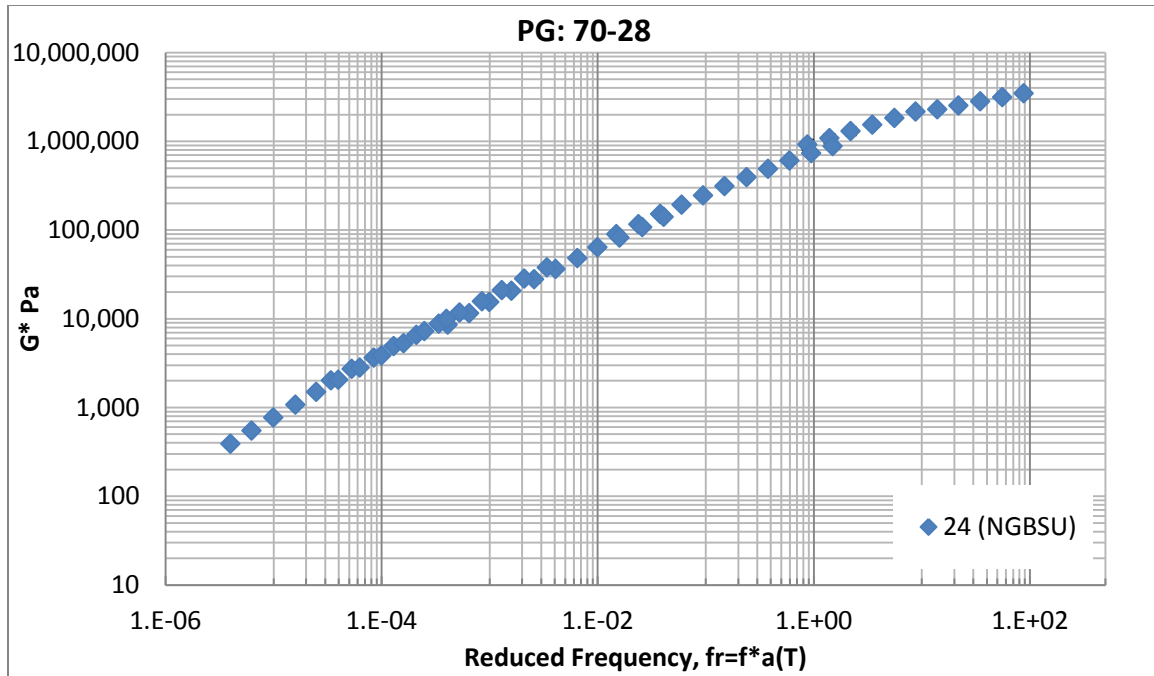


Figure E.3: $|G^*|$ mastercurves of different PG70-28 binders. NGBSU = North, Grand, Bay, Southwest and University Regions

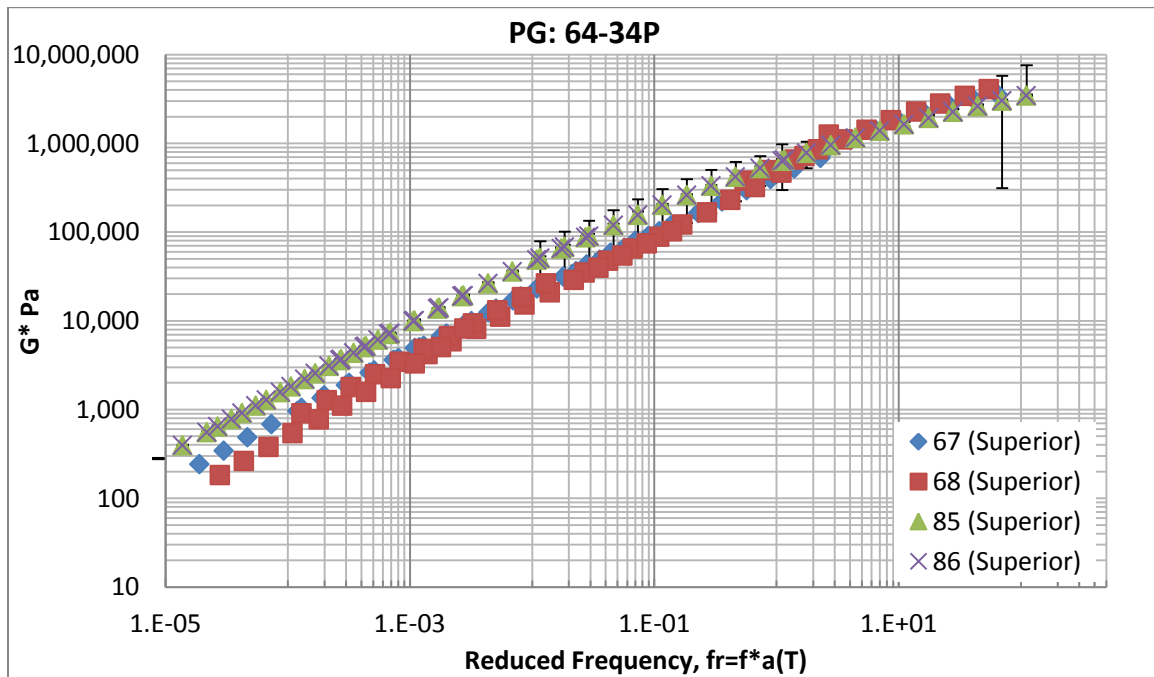


Figure E.4: $|G^*|$ mastercurves of different PG64-34P binders. NGBSU = North, Grand, Bay, Southwest and University Regions

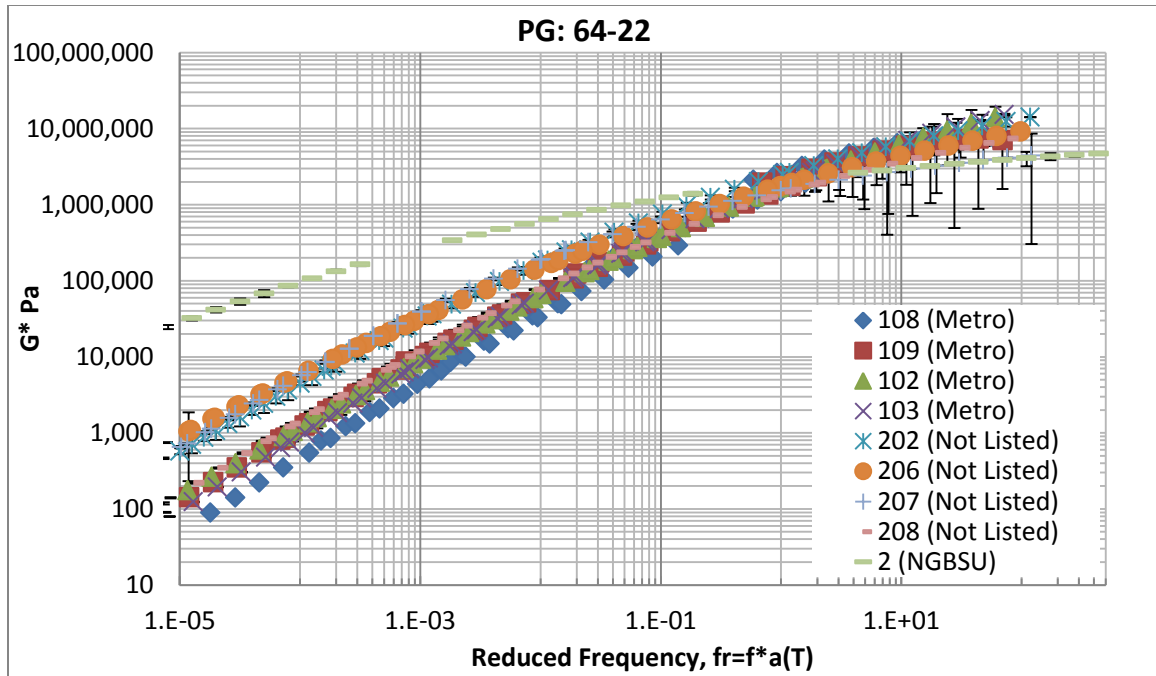


Figure E.5: $|G^*|$ mastercurves of different PG64-22 binders. NGBSU = North, Grand, Bay, Southwest and University Regions

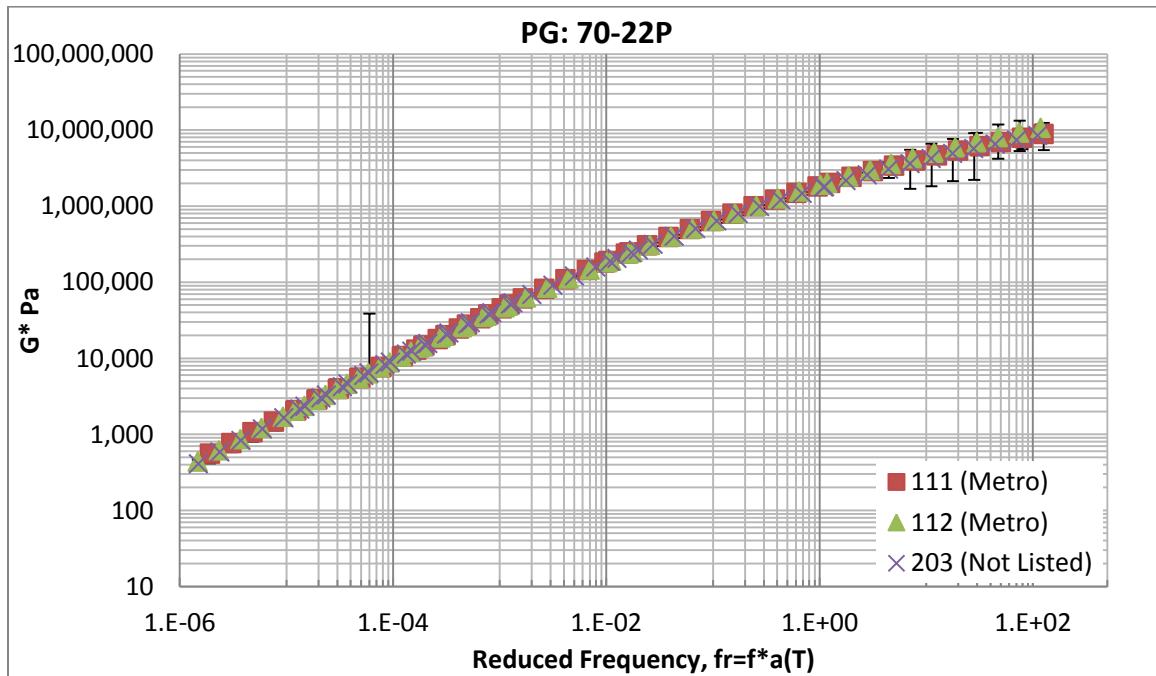


Figure E.6: $|G^*|$ mastercurves of different PG70-22P binders.

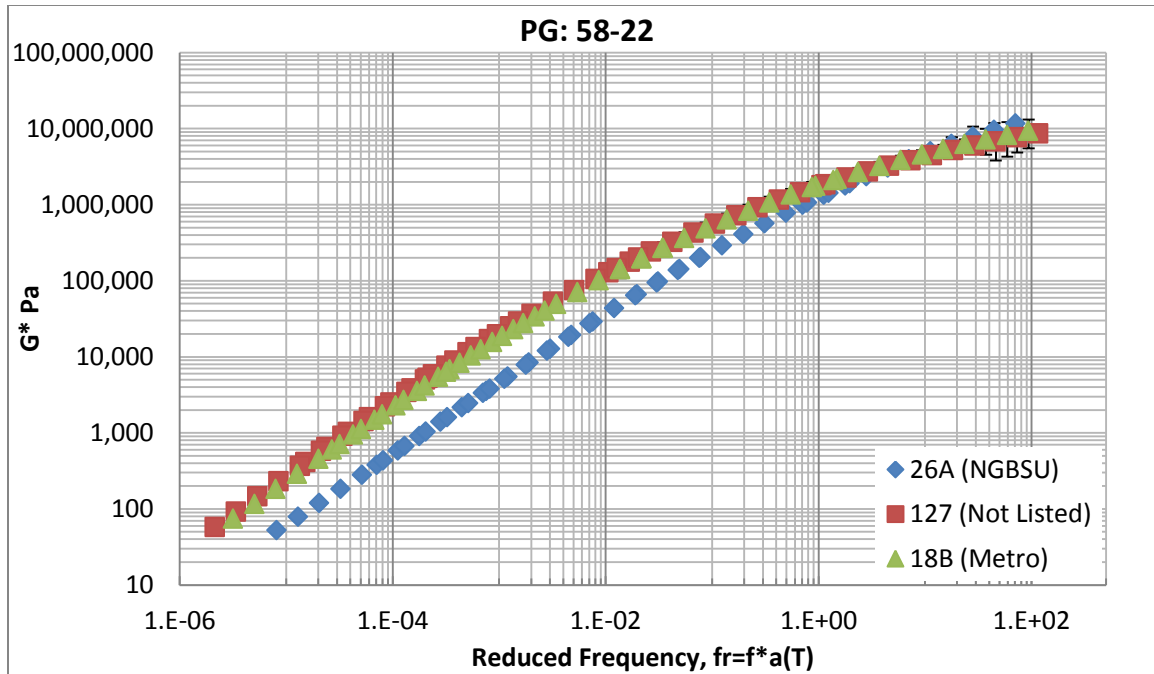


Figure E.7: $|G^*|$ mastercurves of different PG58-22 binders. NGBSU = North, Grand, Bay, Southwest and University Regions

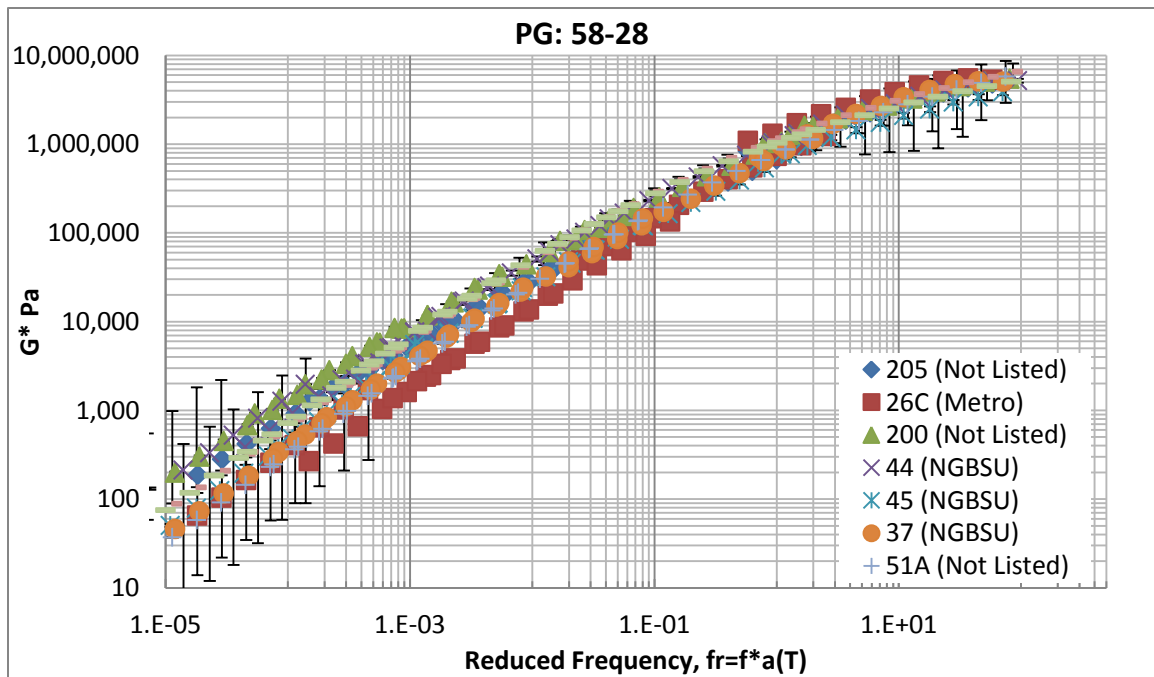


Figure E.8: $|G^*|$ mastercurves of different PG58-28 binders. NGBSU = North, Grand, Bay, Southwest and University Regions

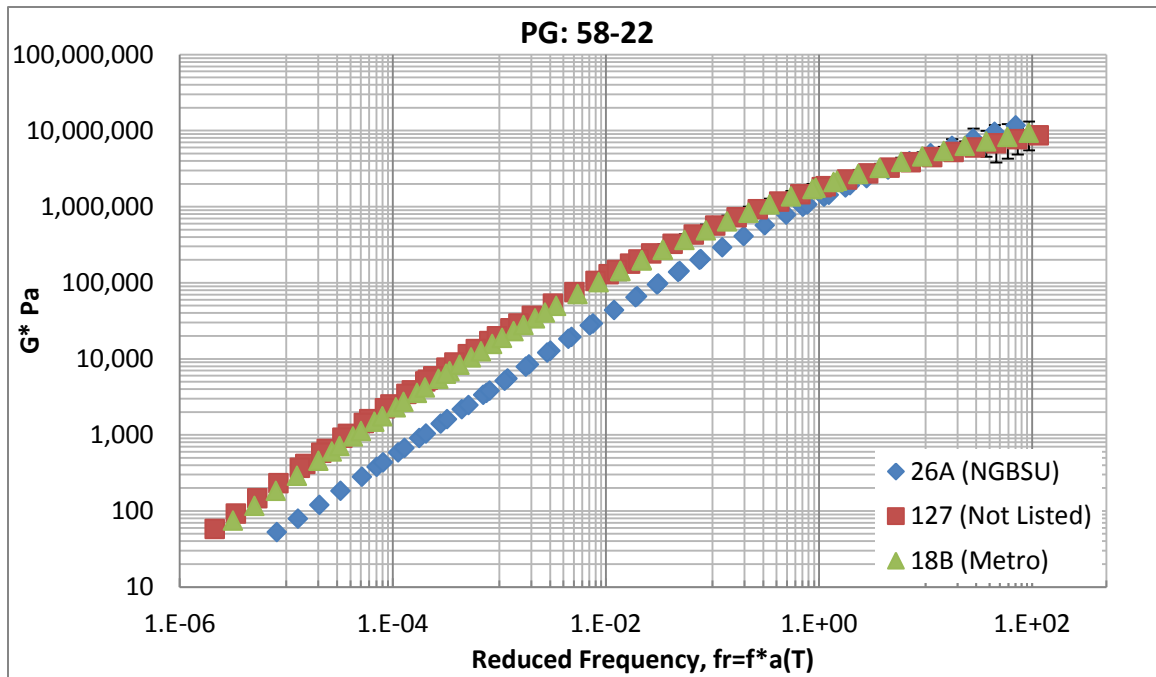


Figure E.9: $|G^*|$ mastercurves of different PG58-22 binders. NGBSU = North, Grand, Bay, Southwest and University Regions

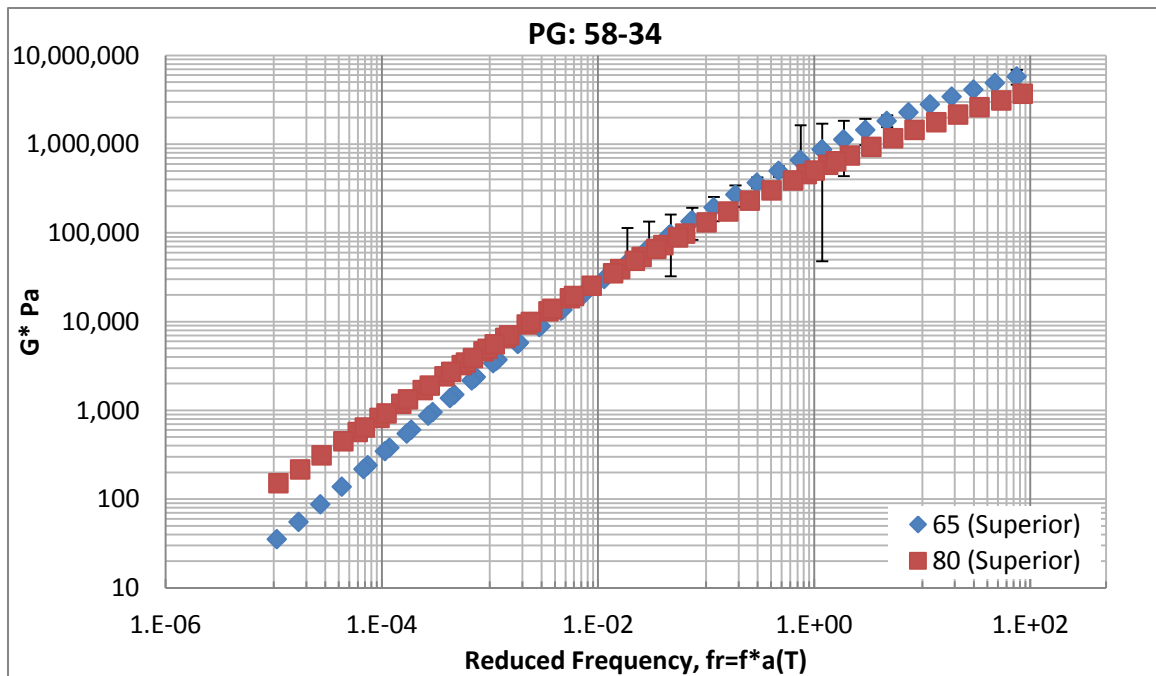


Figure E.10: $|G^*|$ mastercurves of different PG58-34 binders.

APPENDIX F: DYNAMOD SOFTWARE TUTORIAL

Step 1: Choose a Database

Start by choosing a database by clicking on one of the "|E*|Database", "|G*|Database", and "D(t) & |IDT| Database" tabs as shown in Figure (1) below.

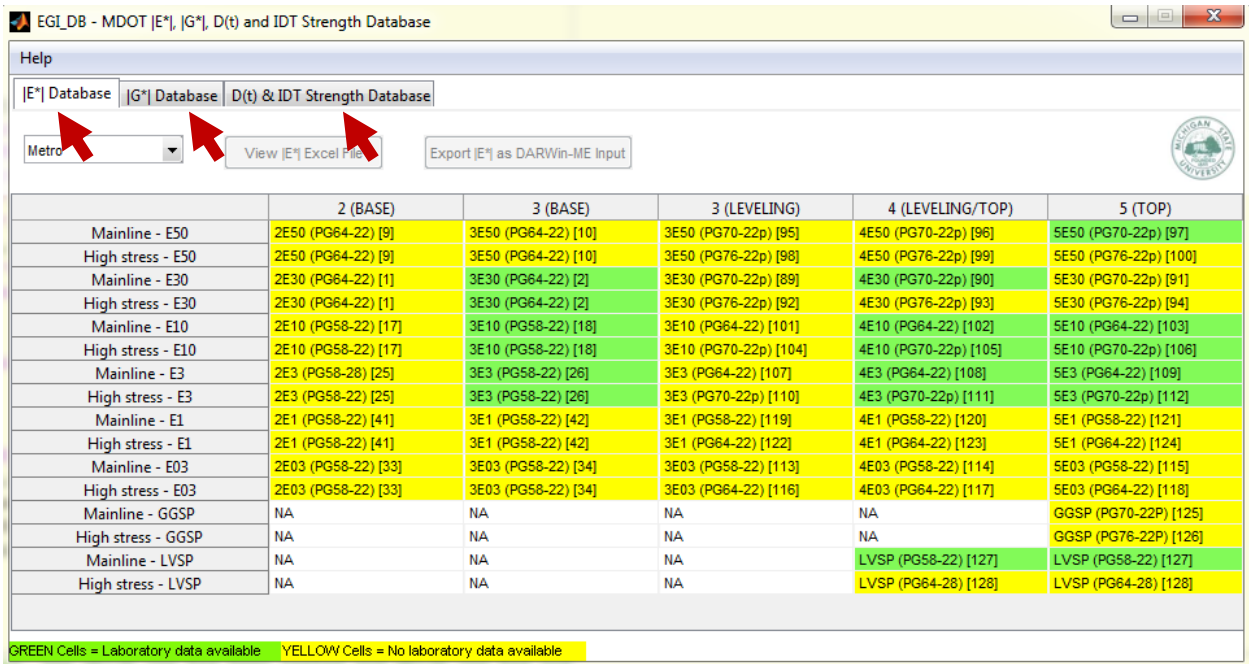


Figure (1): Snapshot of the software interface and how the user can switch between different test databases.

Step 2: Select a Region

1. To select the region which you would like to view the database for, or to switch from one region to another; click the scroll down button shown in Figure (2). A list of four regions namely; "Metro", "North, Grand, Bay, Southwest, and University", "Superior" and "Other" will display.

		3 (BASE)	3 (LEVELING)	4 (LEVELING/TOP)	5 (TOP)
Metro					
North, Grand, Bay, Southwest and University Regions					
Superior		3E50 (PG64-22) [10]	3E50 (PG70-22p) [95]	4E50 (PG70-22p) [96]	5E50 (PG70-22p) [97]
Other					
High stress - E0	2E30 (PG64-22) [9]	3E50 (PG64-22) [10]	3E50 (PG76-22p) [98]	4E50 (PG76-22p) [99]	5E50 (PG76-22p) [100]
Mainline - E50	2E30 (PG64-22) [1]	3E30 (PG64-22) [2]	3E30 (PG70-22p) [89]	4E30 (PG70-22p) [90]	5E30 (PG70-22p) [91]
High stress - E30	2E30 (PG64-22) [1]	3E30 (PG64-22) [2]	3E30 (PG76-22p) [92]	4E30 (PG76-22p) [93]	5E30 (PG76-22p) [94]
Mainline - E10	2E10 (PG58-22) [17]	3E10 (PG58-22) [18]	3E10 (PG64-22) [101]	4E10 (PG64-22) [102]	5E10 (PG64-22) [103]
High stress - E10	2E10 (PG58-22) [17]	3E10 (PG58-22) [18]	3E10 (PG70-22p) [104]	4E10 (PG70-22p) [105]	5E10 (PG70-22p) [106]
Mainline - E3	2E3 (PG58-28) [25]	3E3 (PG58-22) [26]	3E3 (PG64-22) [107]	4E3 (PG64-22) [108]	5E3 (PG64-22) [109]
High stress - E3	2E3 (PG58-22) [25]	3E3 (PG58-22) [26]	3E3 (PG70-22p) [110]	4E3 (PG70-22p) [111]	5E3 (PG70-22p) [112]
Mainline - E1	2E1 (PG58-22) [41]	3E1 (PG58-22) [42]	3E1 (PG58-22) [119]	4E1 (PG58-22) [120]	5E1 (PG58-22) [121]
High stress - E1	2E1 (PG58-22) [41]	3E1 (PG58-22) [42]	3E1 (PG64-22) [122]	4E1 (PG64-22) [123]	5E1 (PG64-22) [124]
Mainline - E03	2E03 (PG58-22) [33]	3E03 (PG58-22) [34]	3E03 (PG58-22) [113]	4E03 (PG58-22) [114]	5E03 (PG58-22) [115]
High stress - E03	2E03 (PG58-22) [33]	3E03 (PG58-22) [34]	3E03 (PG64-22) [116]	4E03 (PG64-22) [117]	5E03 (PG64-22) [118]
Mainline - GGSP	NA	NA	NA	NA	GGSP (PG70-22p) [125]
High stress - GGSP	NA	NA	NA	NA	GGSP (PG76-22p) [126]
Mainline - LVSP	NA	NA	NA	LVSP (PG58-22) [127]	LVSP (PG58-22) [127]
High stress - LVSP	NA	NA	NA	LVSP (PG64-28) [128]	LVSP (PG64-28) [128]

GREEN Cells = Laboratory data available YELLOW Cells = No laboratory data available

Figure (2): Snapshot of how the user can switch between regions

2. Once the region is selected, a corresponding table with types of asphalt mixtures will automatically display. Columns represent the layers of which a mixture is used (i.e., BASE, LEVELING or TOP). The rows describe the traffic level (i.e., Mainline - E3, and High stress - E3). In each table there will be three different colors; yellow, green and white. A yellow cell indicates a mixture with no available laboratory data. A green cell indicates a mixture

with available laboratory test data. The white cell indicates that mix is not specified for the selected region.

|E*| Database:

Step 1: Select Mixture and View Corresponding Excel File

1. The selected mixture cell will immediately turn red as shown in Figure (3).
2. By simply clicking on the “View |E*| Excel File” button also shown in Figure (3); the Excel spreadsheet of the selected mixture type and the particular test database will pop up.

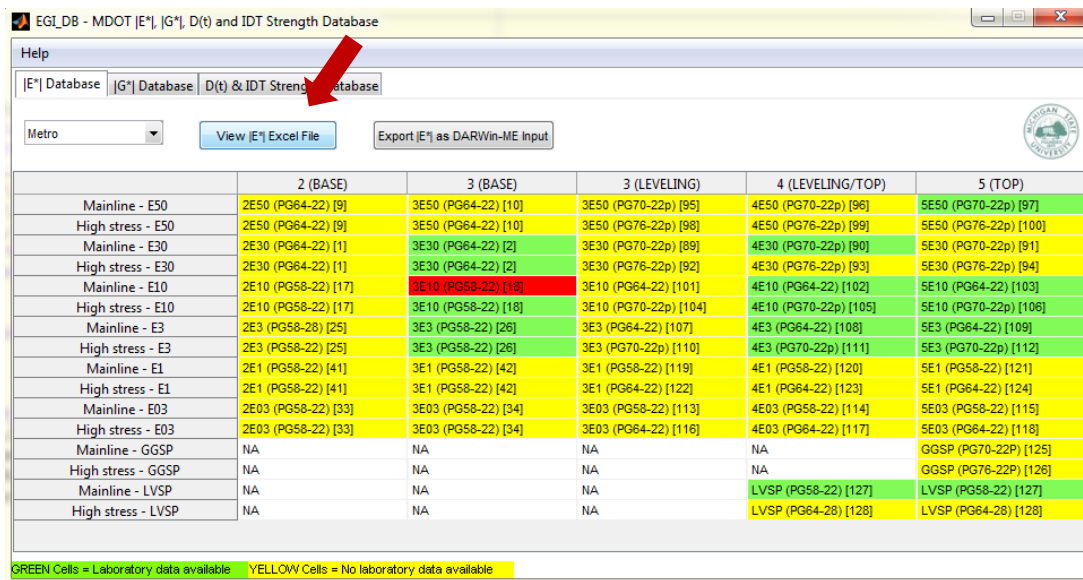


Figure (3): Snapshot of how to select a mixture and view the corresponding Excel file.

3. If there is more than one corresponding Excel spreadsheet for the same mix design, another window will pop up asking for the specific mixture the user would like to view as shown in Figure (4).

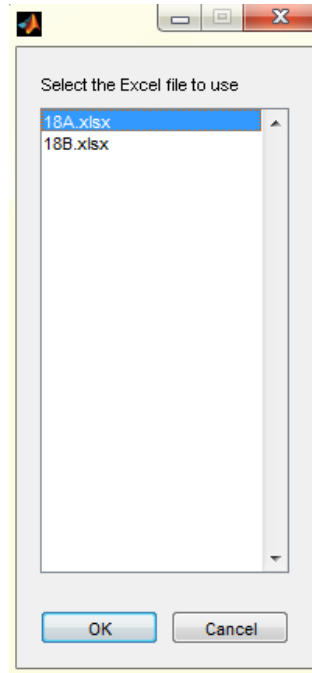


Figure (4): Snapshot of how to choose a particular file for mixtures with more than one Excel file.

4. The "View |E*| Excel File" button will automatically freeze if a yellow cell is selected since there is no laboratory data under yellow cells as shown in Figure (5).

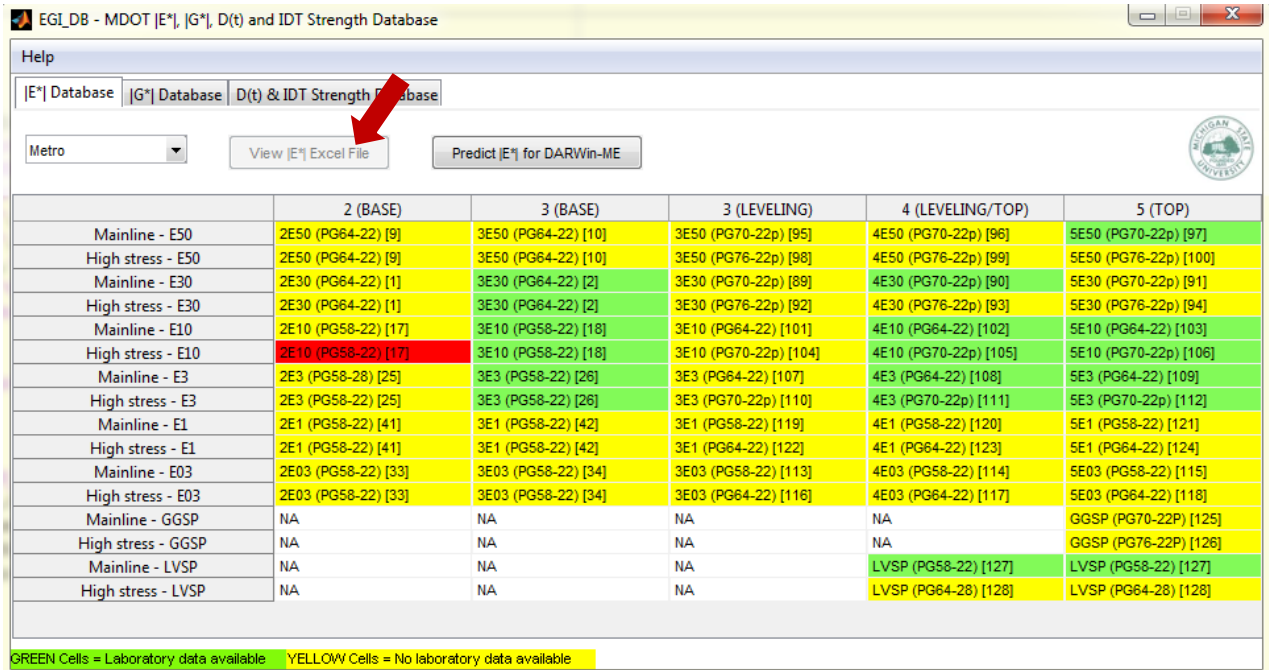


Figure (5): Snapshot of how the "View |E*| Excel File" button will automatically freeze if a yellow cell is selected.

Step 2: Export Data as DARWin-ME Input

1. Once a cell is selected, corresponding data can be exported by simply clicking on the "Export |E*| as DARWin-ME Input" button shown in Figure (6).

2. If there is more than one corresponding Excel spreadsheet for the same mix design, another window will pop up asking for the specific mixture the user would like to export as shown in Figure (7).

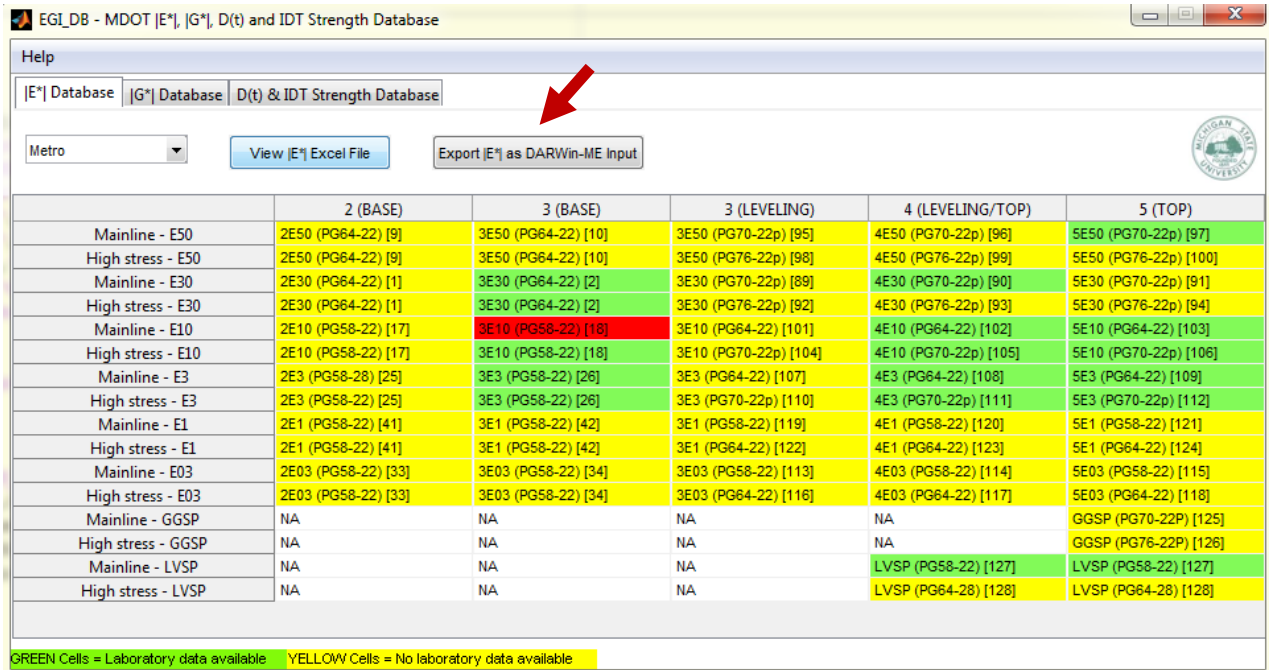


Figure (6): Snapshot of how to select a mixture and export the data as DARWin-ME input.

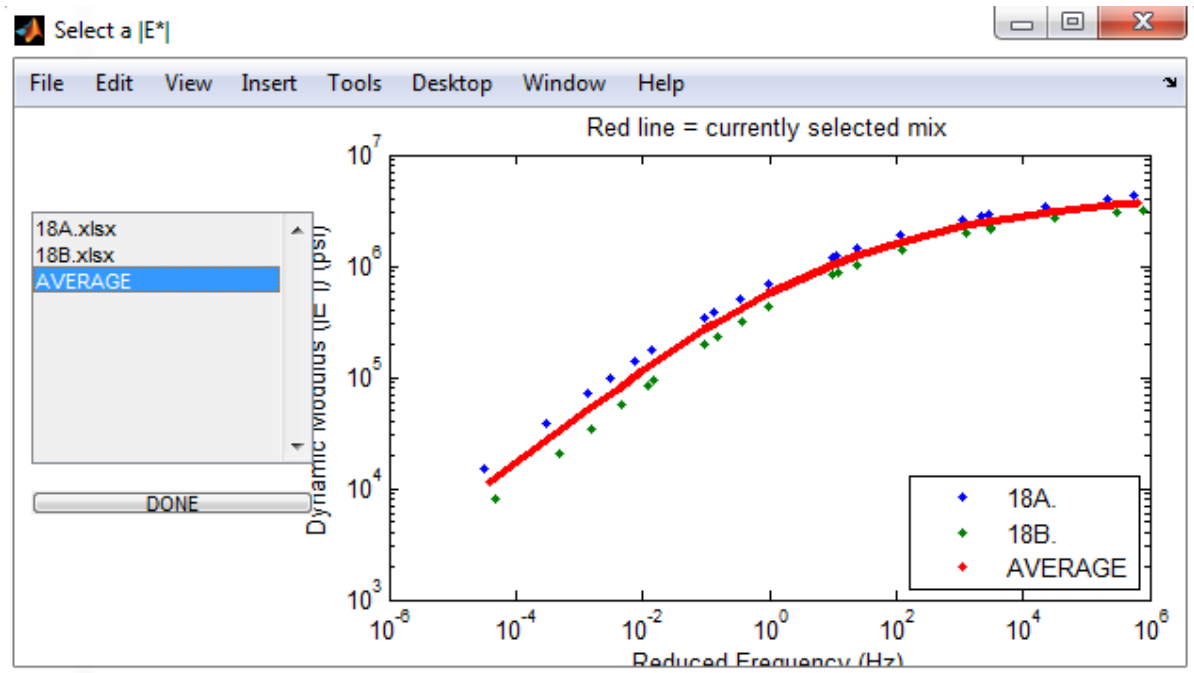


Figure (7): Snapshot of how to choose a particular file to export as DARWin-ME input.

3. After choosing the specific mixture the user would like to export, another browse window will show up asking where to save the Export (*.dwn) file as shown in Figure (8).

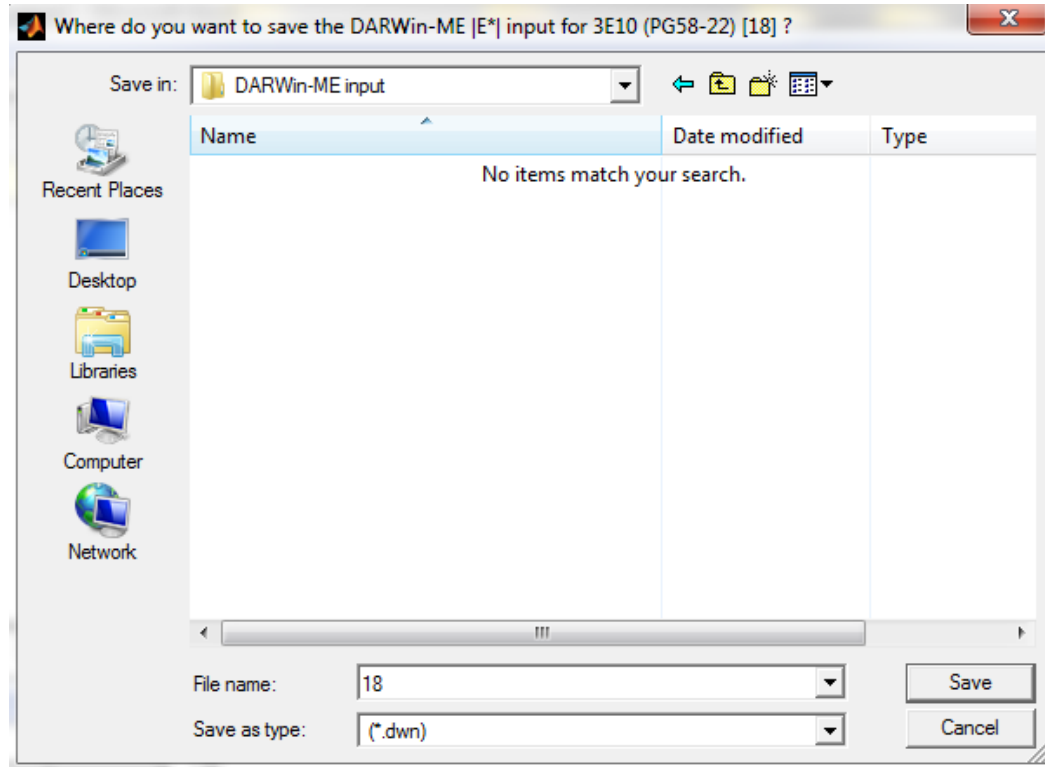


Figure (8): Snapshot of the browse window that asks where the user wants to save the Export (*.dwn) file

4. A dialog box describing the location of the saved file and the corresponding units displays as shown in Figure (9).

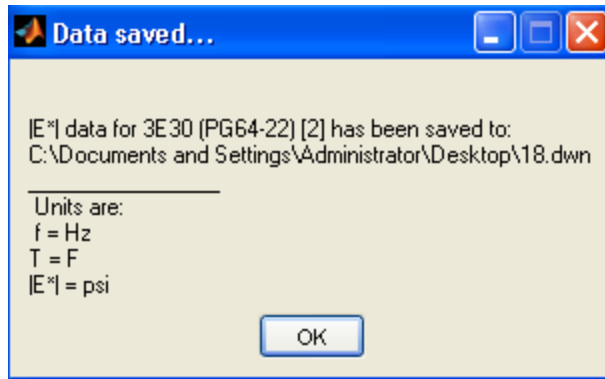


Figure (9): Snapshot of the dialog box showing the location of the saved file and the corresponding units.

5. The exported file should be in the following form as shown in Figure (10). The first column represents the temperature ($^{\circ}\text{F}$), and the first row represents the frequency (Hz). The remaining cells are the exported $|E^*|$ data of the asphalt mixture.

#	0.1	1.0	10.0	25.0
10.0	2490039.5	3076815.9	3572926.6	3741766.0
40.0	1052736.3	1640293.0	2278667.4	2528668.6
70.0	270163.0	559499.5	1008063.0	1226372.8
100.0	52910.0	133579.0	307655.7	414301.5
130.0	11497.6	29890.4	77973.5	112646.7

Figure (10): Snapshot of the exported data file format.

Step 3: $|E^*|$ Prediction

1. Material properties of all mix designs presented in the yellow cells without any available laboratory test data can be predicted. Once the cell is selected, data can be predicted by simply clicking on the "Predict $|E^*|$ for DARWin-ME" button shown in Figure (11).

EGI_DB - MDOT |E*|, |G*|, D(t) and IDT Strength Database

Help

|E*| Database |G*| Database |D(t) & IDT Strength Database

Metro

	2 (BASE)	3 (BASE)	3 (LEVELING)	4 (LEVELING/TOP)	5 (TOP)
Mainline - E50	2E50 (PG64-22) [9]	3E50 (PG64-22) [10]	3E50 (PG70-22p) [95]	4E50 (PG70-22p) [96]	5E50 (PG70-22p) [97]
High stress - E50	2E50 (PG64-22) [9]	3E50 (PG64-22) [10]	3E50 (PG76-22p) [98]	4E50 (PG76-22p) [99]	5E50 (PG76-22p) [100]
Mainline - E30	2E30 (PG64-22) [1]	3E30 (PG64-22) [2]	3E30 (PG70-22p) [89]	4E30 (PG70-22p) [90]	5E30 (PG70-22p) [91]
High stress - E30	2E30 (PG64-22) [1]	3E30 (PG64-22) [2]	3E30 (PG76-22p) [92]	4E30 (PG76-22p) [93]	5E30 (PG76-22p) [94]
Mainline - E10	2E10 (PG58-22) [17]	3E10 (PG58-22) [18]	3E10 (PG64-22) [101]	4E10 (PG64-22) [102]	5E10 (PG64-22) [103]
High stress - E10	2E10 (PG58-22) [17]	3E10 (PG58-22) [18]	3E10 (PG70-22p) [104]	4E10 (PG70-22p) [105]	5E10 (PG70-22p) [106]
Mainline - E3	2E3 (PG58-28) [25]	3E3 (PG58-22) [26]	3E3 (PG64-22) [107]	4E3 (PG64-22) [108]	5E3 (PG64-22) [109]
High stress - E3	2E3 (PG58-22) [25]	3E3 (PG58-22) [26]	3E3 (PG70-22p) [110]	4E3 (PG70-22p) [111]	5E3 (PG70-22p) [112]
Mainline - E1	2E1 (PG58-22) [41]	3E1 (PG58-22) [42]	3E1 (PG58-22) [119]	4E1 (PG58-22) [120]	5E1 (PG58-22) [121]
High stress - E1	2E1 (PG58-22) [41]	3E1 (PG58-22) [42]	3E1 (PG64-22) [122]	4E1 (PG64-22) [123]	5E1 (PG64-22) [124]
Mainline - E03	2E03 (PG58-22) [33]	3E03 (PG58-22) [34]	3E03 (PG58-22) [113]	4E03 (PG58-22) [114]	5E03 (PG58-22) [115]
High stress - E03	2E03 (PG58-22) [33]	3E03 (PG58-22) [34]	3E03 (PG64-22) [116]	4E03 (PG64-22) [117]	5E03 (PG64-22) [118]
Mainline - GGSP	NA	NA	NA	NA	GGSP (PG70-22p) [125]
High stress - GGSP	NA	NA	NA	NA	GGSP (PG76-22p) [126]
Mainline - LVSP	NA	NA	NA	LVSP (PG58-22) [127]	LVSP (PG58-22) [127]
High stress - LVSP	NA	NA	NA	LVSP (PG64-28) [128]	LVSP (PG64-28) [128]

GREEN Cells = Laboratory data available YELLOW Cells = No laboratory data available

Figure (11): Snapshot of how to predict |E*| for DARWin-ME for mixtures that do not have available laboratory test data.

2. Once the "Predict |E*| for DARWin-ME" button is clicked; the window shown in Figure (12) will be displayed. The user will be asked to enter the asphalt mixture properties (i.e., aggregate gradation and volumetric properties), as well as the asphalt binder properties which can be directly loaded from the MDOT test database.

| E* | prediction - Witczak and MSU-ANN models

Asphalt mixture properties

Aggregate blend: % passing 3/4" sieve =

Aggregate blend: % passing 3/8" sieve =

Aggregate blend: % passing #4 sieve =

Aggregate blend: % passing #200 sieve =

Pb (%) (Binder content) =

Gb (Binder specific gravity) =

Va (%) (Air void content) =

Gsb (Bulk specific gravity of aggregate blend) =

Gmm (Maximum specific gravity of the mix) =

Binder properties

Load |G*| & phase angle from MDOT binder test database

Binder |G*| (Pa)

	0.1 Hz	1 Hz	10 Hz	25Hz
10F				
40F				
70F				
100F				
1000F				

Binder phase angle (degrees)

	0.1 Hz	1 Hz	10 Hz	25Hz
10F				
40F				
70F				
100F				
1000F				

Figure (12): Snapshot of the |E*| prediction window using Witczak's equation or the MSU's ANN model.

3. To load the asphalt binder properties from the test database, the user will have to click the "Load | G* | & phase angle from MDOT binder test database" button. Once clicked, the window shown in Figure (13) will pop up asking for the specific binder properties the user wants to load based on the binder PG.

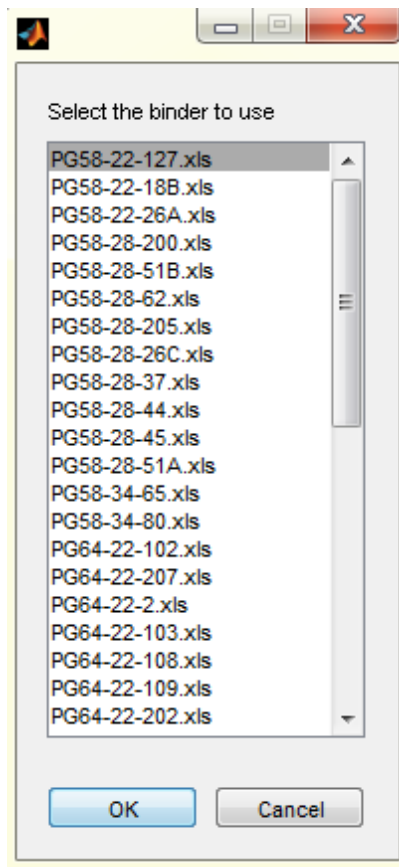


Figure (13): Snapshot of the window that asks which specific binder properties the user wants to load.

|G*| Database:

1. In the |G*| database; the first row represents the high end of a binder PG grade, and the first column represents the low end of a binder PG grade as shown in Figure (14). Similar to the |E*| database; there will be two different cell colors; yellow, and green. A yellow cell indicates an asphalt binder with no available laboratory test data, and a green cell indicates an asphalt binder with available laboratory test data.

	PG 58	PG 64	PG 70	PG 76
-22	PG 58-22	PG 64-22	PG 70-22	PG 76-22
-22P	PG 58-22P	PG 64-22P	PG 70-22P	PG 76-22P
-28	PG 58-28	PG 64-28	PG 70-28	PG 76-28
-28P	PG 58-28P	PG 64-28P	PG 70-28P	PG 76-28P
-34	PG 58-34	PG 64-34	PG 70-34	PG 76-34
-34P	PG 58-34P	PG 64-34P	PG 70-34P	PG 76-34P

GREEN Cells = Laboratory data available YELLOW Cells = No laboratory data available

Figure (14): Snapshot of the |G*| test database.

Step 1: Select Asphalt Binder and View Corresponding Excel File

1. Similar to |E*| database; the selected asphalt binder cell will immediately turn red. By simply clicking on the “View |G*| Excel File” button, another window will pop up asking for the specific asphalt binder the user would like to view as shown in Figure (15).

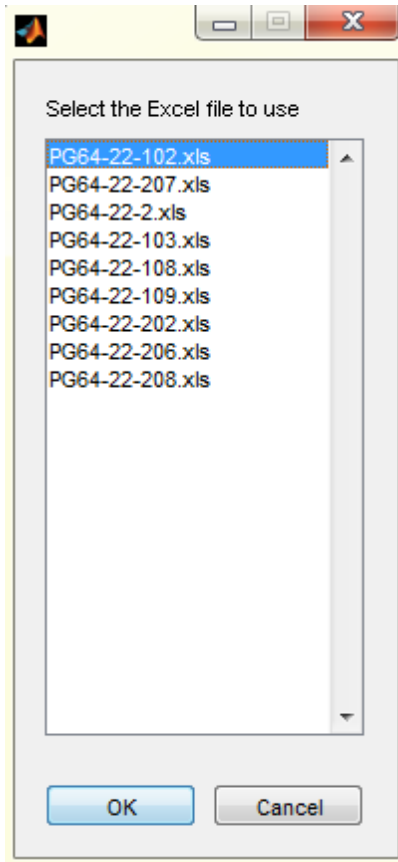


Figure (15): Snapshot of how to select a specific asphalt binder and view the corresponding Excel file

Step 2: Export Data as DARWin-ME Input

1. Similar to the |E*| database; once a cell is selected, corresponding data can be exported by simply clicking on the "Export |E*| as DARWin-ME Input" button shown in Figure (14).
2. If there is more than one corresponding Excel spreadsheet for the same asphalt binder, another window will pop up asking for the specific binder the user would like to export as shown in Figure (16).
3. After choosing the specific binder the user would like to export, another browse window will show up asking where to save the Export (*.bif) file.

4. The exported file should be in the following form as shown in Figure (17). The first column represents the temperature ($^{\circ}\text{F}$), and the other two columns represent the $|G^*|$ (Pa) at 10 rad/sec and Delta (degree) at 10rad/sec as needed by DARWin-ME.

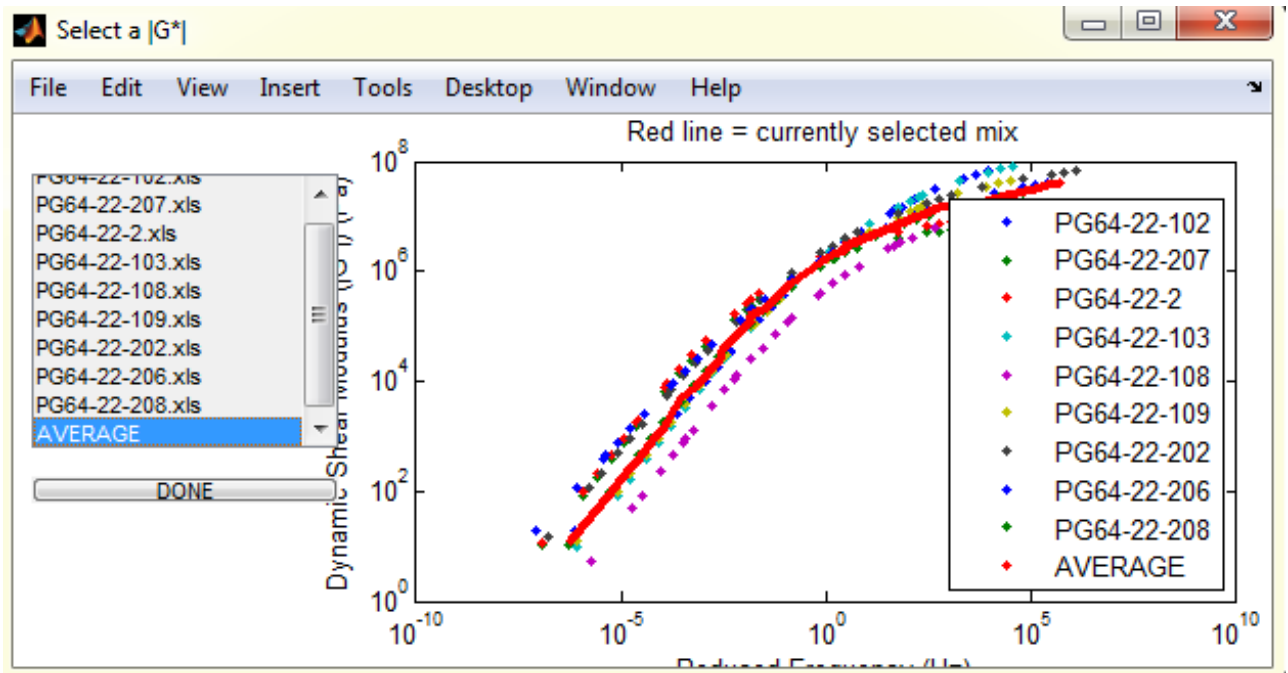


Figure (16): Snapshot of how to select an asphalt binder and export the data as DARWin-ME input.

	G^* (Pa) at 10rad/s	Delta (degree) at 10rad/s
10.0	24132887.5	46.9
40.0	9004524.2	52.8
70.0	1739867.3	58.1
100.0	183992.7	62.5
130.0	15076.5	66.2
168.0	891.2	69.6

Figure (17): Snapshot of the exported data file format.

5. The "View |G*| Excel File" and "Export |G*| as DARWin-ME Input" buttons automatically freeze if a yellow cell is selected just like the |E*| database.

D(t) & IDT Strength Database:

1. Similar to the |E*| database; once the region is selected, a corresponding table with types of asphalt mixtures will automatically display as shown in Figure (18). Columns represent the layers of which a mixture is used for (i.e., BASE, LEVELING or TOP). And the rows describe the traffic level (i.e., Mainline - E3, and High stress - E3). In each table there will be three different colors; yellow, green and white. A yellow cell indicates a mixture with no available laboratory data. A green cell indicates a mixture with available laboratory test data. And a white cell indicates no mixture designs under this condition.

2. Once a mixture cell is selected, it will immediately turn red. By simply clicking on the "View D(t) & IDT Strength" button; the Excel spreadsheet of the selected mixture type will directly pop up.

3. The "View D(t) & IDT Strength" button will automatically freeze if a yellow cell is selected since there is no laboratory data under yellow cells.

EGL_DB - MDOT |E*, |G*, D(t) and IDT Strength Database

Help

|E*| Database |G*| Database D(t) & IDT Strength Database

Metro View D(t) & IDT Strength

	2 (BASE)	3 (BASE)	3 (LEVELING)	4 (LEVELING/TOP)	5 (TOP)
Mainline - E50	2E50 (PG64-22) [9]	3E50 (PG64-22) [10]	3E50 (PG70-22p) [95]	4E50 (PG70-22p) [96]	5E50 (PG70-22p) [97]
High stress - E50	2E50 (PG64-22) [9]	3E50 (PG64-22) [10]	3E50 (PG76-22p) [98]	4E50 (PG76-22p) [99]	5E50 (PG76-22p) [100]
Mainline - E30	2E30 (PG64-22) [1]	3E30 (PG64-22) [2]	3E30 (PG70-22p) [89]	4E30 (PG70-22p) [90]	5E30 (PG70-22p) [91]
High stress - E30	2E30 (PG64-22) [1]	3E30 (PG64-22) [2]	3E30 (PG76-22p) [92]	4E30 (PG76-22p) [93]	5E30 (PG76-22p) [94]
Mainline - E10	2E10 (PG58-22) [17]	3E10 (PG58-22) [18]	3E10 (PG64-22) [101]	4E10 (PG64-22) [102]	5E10 (PG64-22) [103]
High stress - E10	2E10 (PG58-22) [17]	3E10 (PG58-22) [18]	3E10 (PG70-22p) [104]	4E10 (PG70-22p) [105]	5E10 (PG70-22p) [106]
Mainline - E3	2E3 (PG58-28) [25]	3E3 (PG58-22) [26]	3E3 (PG64-22) [107]	4E3 (PG64-22) [108]	5E3 (PG64-22) [109]
High stress - E3	2E3 (PG58-22) [25]	3E3 (PG58-22) [26]	3E3 (PG70-22p) [110]	4E3 (PG70-22p) [111]	5E3 (PG70-22p) [112]
Mainline - E1	2E1 (PG58-22) [41]	3E1 (PG58-22) [42]	3E1 (PG58-22) [119]	4E1 (PG58-22) [120]	5E1 (PG58-22) [121]
High stress - E1	2E1 (PG58-22) [41]	3E1 (PG58-22) [42]	3E1 (PG64-22) [122]	4E1 (PG64-22) [123]	5E1 (PG64-22) [124]
Mainline - E03	2E03 (PG58-22) [33]	3E03 (PG58-22) [34]	3E03 (PG58-22) [113]	4E03 (PG58-22) [114]	5E03 (PG58-22) [115]
High stress - E03	2E03 (PG58-22) [33]	3E03 (PG58-22) [34]	3E03 (PG64-22) [116]	4E03 (PG64-22) [117]	5E03 (PG64-22) [118]
Mainline - GGSP	NA	NA	NA	NA	GGSP (PG70-22p) [125]
High stress - GGSP	NA	NA	NA	NA	GGSP (PG76-22p) [126]
Mainline - LVSP	NA	NA	NA	LVSP (PG58-22) [127]	LVSP (PG58-22) [127]
High stress - LVSP	NA	NA	NA	LVSP (PG64-28) [128]	LVSP (PG64-28) [128]

GREEN Cells = Laboratory data available YELLOW Cells = No laboratory data available

Figure (18): Snapshot of D(t) & IDT Database.